A Numerical Investigation on the Laminar Flame Speed of Methane/Air and Iso-octane/Air Mixtures with Ozone Addition

Marco D'Amato [1,*], Annarita Viggiano [1,*], Vinicio Magi [1,2]

[1] School of Engineering, University of Basilicata, 85100 Potenza, Italy;

marco.damato@unibas.it (M.D.)

annarita.viggiano@unibas.it, ORCID: 0000-0002-7874-6377 (A.V.)

vinicio.magi@unibas.it, ORCID: 0000-0003-1724-2121 (V.M.)

[2] Department of Mechanical Engineering, San Diego State University, San Diego, CA 92182, USA

[*] Correspondence: marco.damato@unibas.it (M.D.); annarita.viggiano@unibas.it (A.V.)

ACCEPTED MANUSCRIPT

Cite as: M. D'Amato, A. Viggiano, V. Magi, A numerical investigation on the laminar flame speed of methane/air and iso-octane/air mixtures with ozone addition, Combust. Flame 241 (2022) 112145. https://doi.org/10.1016/j.combustflame.2022.112145

A Numerical Investigation on the Laminar Flame Speed of Methane/Air and Iso-octane/Air Mixtures with Ozone Addition

Marco D'Amato [1,*], Annarita Viggiano [1,*] and Vinicio Magi [1,2]

[1] School of Engineering, University of Basilicata, 85100 Potenza, Italy; marco.damato@unibas.it (M.D.); annarita.viggiano@unibas.it, ORCID: 0000-0002-7874-6377 (A.V.); vinicio.magi@unibas.it, ORCID: 0000-0003-1724-2121 (V.M.)
[2] Department of Mechanical Engineering, San Diego State University, San Diego, CA 92182, USA
* Correspondence: marco.damato@unibas.it (M.D.); annarita.viggiano@unibas.it (A.V.)

Received: date; Accepted: date; Published: date

Abstract: A numerical study has been carried out to evaluate the influence of ozone addition on the laminar flame speed for both methane/air and iso-octane/air mixtures under thermodynamic conditions typical of internal combustion engines. Ozone is a highly oxidising chemical species and modifies the fuel oxidation reaction pathways, mainly in the initial stages of combustion. In the case of alkanes, such as methane and iso-octane, ozone enhances the laminar flame speed. This study aims to analyse similarities and differences of the flame structure of methane and iso-octane for different values of ozone concentration and equivalence ratio and for a wide range of pressure and temperature conditions. A 1-D numerical model, validated against several experimental data taken from the scientific literature, has been employed and simulations have been carried out by using a chemical kinetic reaction mechanism for methane and three different mechanisms for iso-octane. The results show that the laminar flame speed increases with ozone concentration in the range 0-7000 ppm. At 1 bar, the percentage enhancement in terms of LFS with the addition of 7000 ppm of ozone, compared to the case without ozone, is about 4% for both fuels, under stoichiometric conditions, as long as temperature is lower than about 540 K. On the other hand, at higher temperatures ozone addition enables the formation of a cool flame for iso-octane/air mixtures, and the reactions follow a different path compared to the case with methane. This leads to a greater influence of ozone on the iso-octane laminar flame speed. Besides, for iso-octane/air stoichiometric mixtures, at 560 K with 7000 ppm ozone, LFS shows a non-monotonic behaviour with pressure, being higher at 20 bar than at 15 bar, which is somehow unexpected. If the reactants temperature increases, the non-monotonic trend appears at lower pressures and lower ozone concentrations and is due to the fast ozone decomposition, promoted by the pressure increase. Such a decomposition enables fuel oxidation reactions by OH radicals in the cool flame region. This phenomenon does not occur for the methane case.

Keywords: Laminar Flame Speed; Ozone Assisted Combustion; Cool Flame; Methane; Iso-octane

1. Introduction

The Laminar Flame Speed (LFS) of a fuel/air mixture plays a key role in combustion systems, such as gas turbines, furnaces and Internal Combustion Engines (ICEs), since it has a direct impact on combustion efficiency and pollutant emissions. The estimate of LFS of a large variety of fuel-oxidizer mixtures under different thermodynamic conditions has led, over the years, to many experimental and theoretical works in the literature [1] and to the development of several experimental techniques [2-5]. Based on experimental evidence, various correlations for the LFS have been developed for different mixtures [6-8]. From the numerical point of view, several one-dimensional models have been developed [9,10] to analyse the chemical progress of the mixture composition, the heat and mass diffusion and the influence of various parameters (pressure, temperature, equivalence ratio, dilution, etc.) on the LFS.

Among hydrocarbon fuels, the most widely investigated is methane [3,11,12]. However, due to their importance for many combustion systems, especially for ICEs, gasoline surrogates, such as iso-octane and Primary Reference Fuels (PRFs), have also been extensively taken into consideration [13]. Davis and Law [14] compared the LFS of hydrocarbons from C1 to C8, showing that the LFS of such alkanes was similar for all the equivalence ratios under consideration, with the exception of methane, which is characterized by lower values.

Recently, combustion research focuses on unconventional combustion strategies, with the aim of increasing combustion efficiency and of reducing pollutant emissions. For instance, the fuel combustion in air enriched with oxidising chemical species is an interesting strategy. One of the most promising species is ozone, which, due to its relatively long lifetime, could be transported to the combustion region, thus promoting fuel oxidation. Ozone is able to modify ignition timing, accelerate and stabilise the flame and reduce pollutant emissions. The positive influence of ozone on combustion is mainly due to its chemical decomposition into atomic oxygen through the reaction $O_3 + M \rightleftarrows O_2 + O + M$. The influence of ozone on combustion has been extensively studied in the last decades [15]. Nomaguchi and Koda [16] employed methane and methanol as fuels and found that the ignition time, defined as the minimum spark time duration to ensure a stable kernel, was significantly reduced with partially ozonized air. Halter *et al.* [5] studied the influence of ozone on methane combustion by carrying out both experiments and simulations and proposed a mechanism for ozone chemical kinetics. Their experiments showed that, at room conditions, with 2369 ppm of ozone the LFS increased and the thermal flame thickness decreased, for all investigated equivalence ratios. Similar results were obtained by Wang *et al.* [17], who measured an LFS increase as the concentration of ozone increases in a mixture of methane and ozonized air. Gao *et al.* [18] examined the effect of

ozone on three different fuels: methane, propane and ethylene. The results showed different behaviours between alkanes and alkenes, due to the ozonolysis reactions of ethylene. Vu *et al.* [19] carried out experiments with methane/air and propane/air mixtures, thus showing that the addition of ozone was able to stabilise an initially unstable flame.

Ozone was also used in unconventional combustion engines in order to have a better control on combustion. Several studies focused on the use of ozone in HCCI engines [20-23]. Masurier *et al.* [21] considered different PRFs, from PRF0 to PRF100, and carried out experiments on a single cylinder of an HCCI engine powered with a mixture of PRF and ozonized air. The results showed that ozone promotes the formation of the cool flame and advances the entire combustion process. Masurier *et al.* [22] evaluated the effect of different oxidising species, i.e. nitric oxide, nitrogen dioxide and ozone, within an iso-octane fuelled HCCI engine and found that ozone was the species that most advanced and accelerated combustion. Pinazzi *et al.* [24,25] used ozone in a GCI direct injection engine to enable low load engine operations. They found that ozone had a greater impact on the engine performance if fuel injection was advanced. However, the influence of ozone was limited by the presence of nitrogen oxides due to direct reactions between such species. Such an interaction was also found by Masurier *et al.* [22].

On the other hand, the use of ozone in engines has been less taken into consideration for Spark Ignition (SI) engines. Gong *et al.* [26] carried out a numerical study on a methanol fuelled SI engine, and found that ozone was able to reduce emissions of both formaldehyde and unburnt methanol with a stronger effect under cold engine start.

In this scenario, the aim of this work is to provide a comprehensive analysis of the influence of ozonized air on the LFS of iso-octane and to highlight differences and similarities of such a fuel with respect to methane by using one-dimensional numerical simulations. Indeed, no experiments on iso-octane LFS in ozonized air have been found in the scientific literature. Ozone plays its role starting from the beginning of the oxidation process, so it has an influence on the low-temperature chemistry by changing the main reaction paths, with a possibility to induce the formation of a cool flame [27,28]. For this reason, ozone may have potentially different effects on the methane and iso-octane oxidation. For iso-octane, for example, a cool flame was detected in some combustion systems [29,30] but not in ICEs, because iso-octane needs very high temperatures to auto-ignite and the residence time in ICEs is not long enough for the cool flame to develop. However, some works in the literature [21,31] show that ozone may also promote the formation of a cool flame for iso-octane under typical thermodynamic conditions of an HCCI engine since it strongly advances the ignition timing. Combustion with ozone is investigated in the present work for different equivalence ratios and for a

wide range of temperatures and pressures, since ozone may have a different impact on the combustion process depending on the chemical composition of the fuel/air mixture and on the thermodynamic conditions. In addition, three iso-octane reaction mechanisms have been considered, in order to assess if, with ozone addition, they provide the same response.

This work is organised as follows: first, the mathematical and numerical model is described; then the model is validated on the basis of various data from the scientific literature, both with and without ozone; then the influence of temperature and pressure on both the chemical pathway of ozone and the LFS is analysed; finally, the results are summarised in the conclusions.

2. The Simulation Model

2.1 Governing Equations

Numerical simulations are performed by using the premixed LFS solver Chemkin-Pro by ANSYS [32]. Chemkin-Pro solves the system of differential governing equations of a one-dimensional, freely propagating flame under steady-state conditions, and returns the value of the LFS. The governing equations read

Continuity equation: $$\dot{M} = \rho u A, \tag{1}$$

Energy equation: $$\dot{M}\frac{dT}{dx} - \frac{1}{c_p}\frac{d}{dx}\left(\lambda A \frac{dT}{dx}\right) + \frac{A}{c_p}\sum_{i=1}^{N_s}\rho Y_i V_i c_{pi}\frac{dT}{dx} + \frac{A}{c_p}\sum_{i=1}^{N_s}\dot{\omega}_i h_i W_i = 0, \tag{2}$$

Chemical species equation: $$\dot{M}\frac{dY_i}{dx} + \frac{d}{dx}(\rho A Y_i V_i) - A\dot{\omega}_i W_i = 0, \quad i = 1, \dots, N_s, \tag{3}$$

Equation of State: $$\rho = \frac{P\bar{W}}{RT}, \tag{4}$$

where x is the spatial coordinate, $\dot{M}$ is the mass flow rate, ρ is the mass density, u is the fluid mixture velocity, A is the cross-sectional area of the stream tube enclosing the flame, T is the temperature, c_p and c_{pi} are the constant-pressure heat capacity of the mixture and of the i-th chemical species, respectively, λ is the thermal conductivity of the mixture, N_s is the number of gas species, Y_i is the mass fraction of the species i in the mixture, V_i is the diffusion velocity of the species i, $\dot{\omega}_i$ is the molar rate of production/consumption by chemical reactions of the i-th species per unit volume, h_i is the specific enthalpy of the i-th species, W_i is the molecular weight of the i-th species and $\bar{W}$ is the mean molecular weight of the mixture, P is the pressure and R is the universal gas constant.

The net chemical production/consumption rate depends on all reactions involving the i-*th* species and is computed by assuming that each reaction rate obeys to the law of mass action with the forward rate coefficients, k_f, given by the Arrhenius equation as:

$$k_f = CT^{\beta} e^{\frac{-E_a}{RT}}, \tag{5}$$

where C is the pre-exponential factor, β is the temperature exponent and E_a is the activation energy.

The transport properties of each species are evaluated by using the mixture-averaged formulation. This model assumes that the diffusion rate has three contributions:

$$V_i = V_i' + V_i'' + V_c\ . \tag{6}$$

V_i' is the ordinary diffusion velocity and is computed by the Curtiss-Hirschfelder approximation [33], V_i'' is the thermal diffusion velocity [34], and V_c is the correction velocity [35], which ensures that the mass fractions sum is unity.

The inlet conditions are given in terms of temperature, pressure and mixture composition. No heat losses are considered.

Four different reaction mechanisms are employed. The first one refers to the oxidation of methane [36], whereas the other mechanisms refer to the oxidation of iso-octane [37-39]. The reaction mechanism of Cai & Pitsch [38] also accounts for NO_x formation, whereas the Saxena sub-mechanism for NO_x [40] is added to the remaining mechanisms. Moreover, all the mechanisms are modified by adding the ozone sub-mechanism proposed by Halter *et al.* [5] and given in Table S1 in the supplementary material. This ozone sub-mechanism is the most commonly used coupled to hydrocarbon mechanisms, with at most minor modifications [15,17,18,20-22]. The resulting mechanisms are:

- "CurranModif" for iso-octane with 889 species and 3866 reactions;
- "Cai&PitschModif" for iso-octane with 340 species and 1707 reactions;
- "YooModif" for iso-octane with 187 species and 931 reactions;
- "GRI3.0Modif" for methane with 54 species and 342 reactions.

Both detailed and reduced mechanisms are used for iso-octane oxidation. The most detailed mechanism [39] is used to infer the chemical phenomena involved in combustion with ozone addition. However, this mechanism may not be adequate for the analysis of multi-dimensional fluid-dynamic

problems within a practical computational time. Hence, it is also important to test the accuracy of skeletal [37] and reduced [38] mechanisms to predict the main features of ozone-assisted combustion.

2.2 Numerical Method

A one-dimensional domain of length 10 cm is considered. As regards boundary conditions, the pressure, temperature and composition of the mixture are given at the cold boundary, whereas, at the hot boundary, all gradients vanish. A first-guess value for the position of the flame, i.e. an initial temperature profile, and for either the mass flow rate or the inlet velocity is set. The governing equations are discretized by using first order and second order finite differences for the convective and diffusive terms, respectively, and iteratively solved.

The computational grid is dynamically adaptive. The numerical domain is discretized into a number of grid points and this number increases till specific criteria on the flow gradients and curvature of the numerical solution are satisfied. In particular, the criteria for each point *j* of the mesh are

$$\left|\phi_{n,j} - \phi_{n,j-1}\right| \leq \delta(\max\phi_n - \min\phi_n)\,, \tag{7}$$

$$\left|\left(\frac{d\phi_n}{dx}\right)_j - \left(\frac{d\phi_n}{dx}\right)_{j-1}\right| \leq \gamma\left(\max\frac{d\phi_n}{dx} - \min\frac{d\phi_n}{dx}\right), \tag{8}$$

where ϕ_n is the n-*th* component of the unknowns vector and δ and γ are user-specified parameters.

If Eqs. (7) and (8) are not satisfied between two subsequent grid points, then a new grid point is added at the midpoint of such subinterval, and a new iteration is carried out. Absolute and relative tolerance values of 1.0×10^{-9} and 1.0×10^{-4}, respectively, are chosen for the converged solution. The computation is carried out with several successive continuations: starting with fairly high values of δ and γ, the solution of a previous continuation was assumed to be the starting condition for a new continuation with smaller values of δ and γ and so on.

The computational time is strongly dependent on the values of δ and γ, and on the number of species and chemical reactions of the mechanism. For the mechanism of methane, with a relatively low number of species and reactions, the minimum values of δ and γ are set to 0.01 and 0.05, respectively. For the iso-octane mechanisms, in order to reduce the computational time, the values of δ and γ are slightly increased compared to the methane case and are set to 0.035 and 0.075, respectively. Finally, for all computations, the minimum timestep is $1.0 \times 10^{-10} s$.

With these settings, the numerical method converged for all cases. The difference between the converged solution, in terms of LFS, and the solution of the previous continuation is within 1% and 1.5% for the simulations with methane and iso-octane, respectively, for all the selected thermodynamic conditions.

3. Results and Discussion

At first the model has been validated against experimental data, then several simulations have been performed, for both methane and iso-octane as fuels, by varying ozone concentrations, temperature, pressure and equivalence ratio of the fresh mixtures from 2330 to 7000 ppm referred to oxygen, from 300 K to 700 K, from 1 bar to 20 bar, and from 0.6 to 1.4, respectively.

3.1 Model Validation

For methane as a fuel, the validation has been carried out against experimental data, both in absence of ozone [2,3,5,11,12 ,17,18] and with the addition of ozone [17]. On the other hand, for iso-octane as a fuel, the model has been validated against available data obtained in absence of ozone [4,41-48], since, in the literature, there are no data in terms LFS for $C_8H_{18}/Air/O_3$ mixtures.

3.1.1 Methane

Fig. 1 shows the numerical results obtained in terms of LFS for methane/air mixtures as a function of the equivalence ratio under ambient conditions (1 bar, 300 K), compared with several measurements. The figure shows that the model is able to reproduce the experimental data with a very good accuracy in the entire range of equivalence ratio from 0.6 to 1.4.

The model validation with ozone addition has been carried out against the data of Wang *et al.* [17], who measured, at ambient conditions, the LFS of a mixture of methane, air and ozone with different concentrations of ozone in oxygen, i.e. 2330, 3730, 5130 and 7000 ppm. The comparison between the numerical results and measurements is shown in Fig. 2 as a function of the equivalence ratio. Fig. 3 shows the comparison in terms of the LFS relative enhancement defined as:

$$\epsilon = \frac{S_L' - S_L^0}{S_L^0}, \tag{9}$$

where S_L^0 is the LFS in absence of O_3, and S_L' is the LFS with ozone addition.

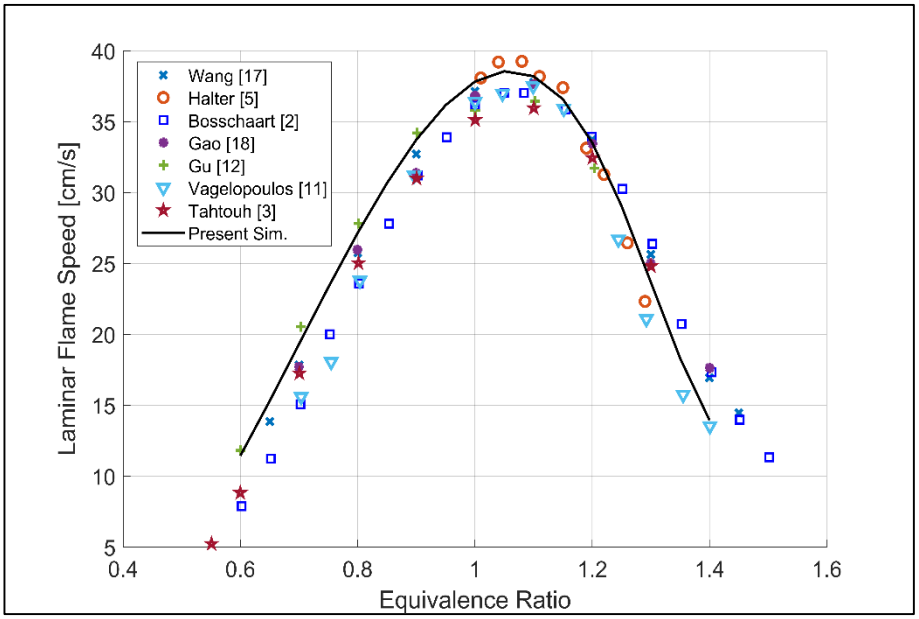

Figure 1. Comparison between experimental and numerical results in terms of LFS vs equivalence ratio for CH_4/Air mixtures at ambient conditions (1 bar, 300 K).

Fig. 2 shows that the simulations are able to provide the trends observed in the experiments. The maximum measurement uncertainty in the experiments in Fig. 2a is about 0.8 cm/s and occurs at $\phi = 0.65$ for the case without ozone. As the ozone concentration increases, there is an increase of the LFS for all the equivalence ratios. The LFS enhancement is mostly within the range of the measurement uncertainty for all equivalence ratios. The simulations under-predict the LFS enhancement for both 2330 and 3730 ppm cases with $\phi = 1.4$ and for 3730 ppm case with $\phi = 0.65$.

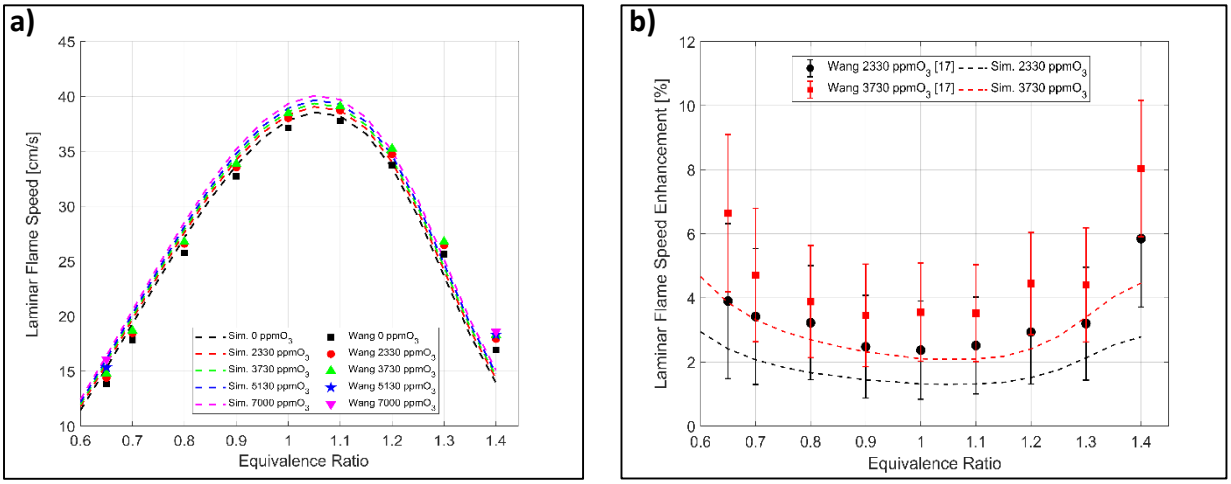

Figure 2. Comparison between experimental and numerical results in terms of: a) LFS vs equivalence ratio; b) LFS relative enhancement vs equivalence ratio for $CH_4/Air/O_3$ mixtures at ambient conditions (1 bar, 300 K) with different O_3 concentrations.

The differences between the simulations and the measurements are likely due to the kinetic mechanism. A similar trend is also found by Wang *et al.* [17].

3.1.2 Iso-Octane

The three reaction mechanisms for iso-octane are validated by comparing the numerical results, in terms of LFS, with measurements available in the scientific literature for mixtures of iso-octane and air with different equivalence ratios, since experimental results with mixtures of iso-octane and ozonized air are not available in the literature.

Fig. 3 shows the comparison between the numerical results in terms of LFS and the experimental data available in the literature [4,41-48], as a function of equivalence ratio, both at ambient conditions and considering higher values of pressure and temperature. The results show that the three mechanisms are able to accurately reproduce the experimental data at ambient conditions for all the equivalence ratios. The results at $p = 5\ bar$ fall in the experimental data range for $\phi < 1.1$, but for higher equivalence ratios, the simulations underestimate the LFS measured by Mandilas *et al.* [48]. Besides, compared to ambient conditions, a larger dispersion of the numerical results is observed, depending on the specific reaction mechanism. Under stoichiometric conditions, at $p = 1\ bar$ and $T = 300\ K$ a LFS between 34.34 and 34.89 cm/s is obtained for all the three mechanisms, whereas at $5\ bar$ and $355\ K$ the LFS varies from 27.45 cm/s, with the modified Yoo mechanism, to 31.49 cm/s, with the modified Cai&Pitsch mechanism.

The numerical results at 25 bar and 373 K are compared with the experimental data of Jerzembeck *et al.* [4] and are shown in Fig. 3c. A good match of the simulated results with the experimental data is observed, except for rich mixtures. Specifically, for $\phi < 0.8$ all the three mechanisms provide values of the LFS within the uncertainty range of the measurements. For higher equivalence ratios, the modified Yoo mechanism underestimates the LFS and for $\phi = 1.2$ all the three mechanisms underestimate the LFS between 11% and 27%.

In summary, the modified mechanisms are able to provide a LFS which is comparable to that observed in the measurements, even under high pressure conditions, for lean and stoichiometric mixtures, which are the conditions of interest for SI engines.

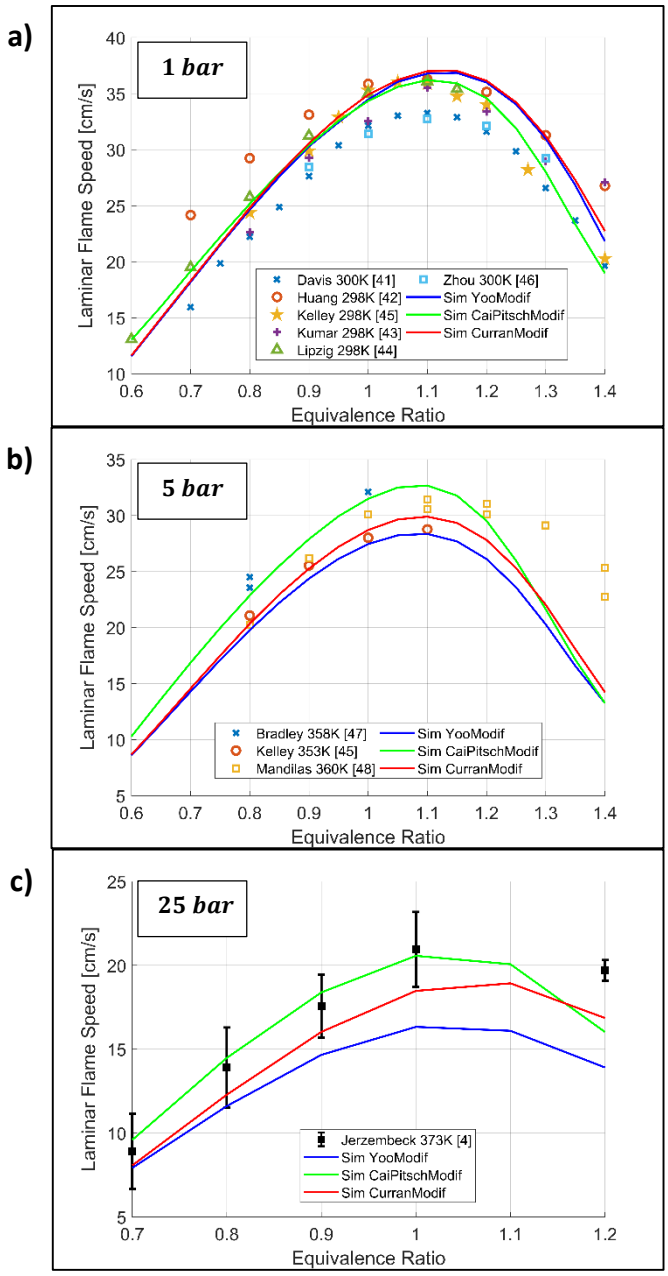

Figure 3. Comparison between experimental and numerical results in terms of LFS vs equivalence ratio for C_8H_{18}/Air mixtures at: a) 1bar, 300 K; b) 5 bar, 355 K; c) 25 bar, 373 K. For the experimental data, the mixture temperature is given in the legend.

LFS sensitivity analyses have also been carried out for the three mechanisms at room conditions (1 bar, 300 K) for lean, stoichiometric and rich mixtures without ozone addition. Fig. 4 shows the main LFS sensitivity coefficients, for each mechanism and equivalence ratio. The sensitivity analysis shows very similar results for the modified Curran and Yoo mechanisms for each equivalence ratio. On the other hand, for the modified Cai&Pitsch mechanism, LFS is more affected by reactions that are less important for the other two mechanisms. However, for all the three mechanisms, LFS shows large sensitivity to the kinetics of the main chain-branching reaction, $H +$

$O_2 \rightleftarrows O + OH$. The reactions $H + O_2\ (+M) \rightleftarrows HO_2\ (+M)$, $CO + OH \rightleftarrows CO_2 + H$ and $CH_3 + H\ (+M) \rightleftarrows CH_4\ (+M)$ also have a significant role for all the three mechanisms.

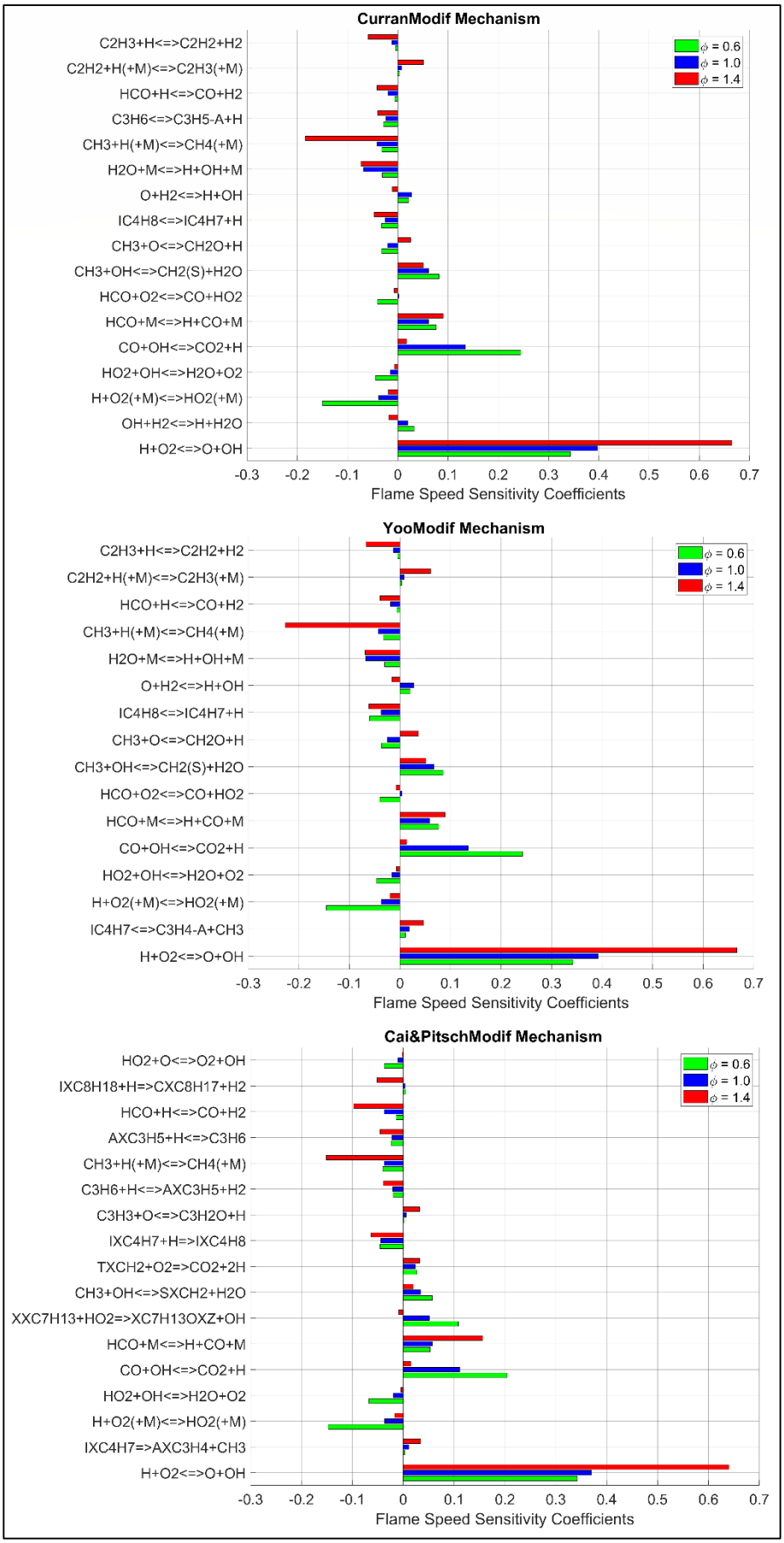

Figure 4. LFS sensitivity coefficients for the modified Curran, Yoo and Cai&Pitsch mechanisms at 1 bar, 300 K and for three different equivalence ratios.

3.2 LFS for Iso-Octane/Air/Ozone Mixtures

The same thermodynamic conditions used for methane in section 3.1.1 are considered for iso-octane/air/ozone mixtures, such that a direct comparison between the two fuels can be carried out. Fig. 5a shows the LFS, obtained with the modified Curran mechanism, as a function of equivalence ratio. With increasing ozone concentrations, an increase in the LFS is observed for all investigated equivalence ratios. This trend is also observed by the other two reaction mechanisms and, for the sake of conciseness, is not shown.

The relative enhancement of the LFS obtained with 2330 and 7000 ppm O_3 is shown in Fig. 5b for both iso-octane and methane by using all the selected kinetic mechanisms. The results show that the trends are the same for both methane and iso-octane, and are in agreement with the experimental data [17], available only for methane (Fig. 2b). LFS increases with ozone concentration, especially for lean and rich mixtures, whereas a lower benefit is observed under near-stoichiometric conditions.

As regards iso-octane, the three reaction mechanisms give similar results, especially for lean mixtures and with lower ozone concentration. With the addition of 2330 ppm O_3, for all equivalence ratios, the values of the LFS enhancement with the three iso-octane reaction mechanisms differ by less than 0.4%. For 7000 ppm O_3 concentrations, the maximum difference is less than 0.5% for $\phi < 1.3$, while at $\phi = 1.4$ the relative enhancement ranges from about 6% with the modified Curran mechanism to about 8% with the modified Cai&Pitsch mechanism.

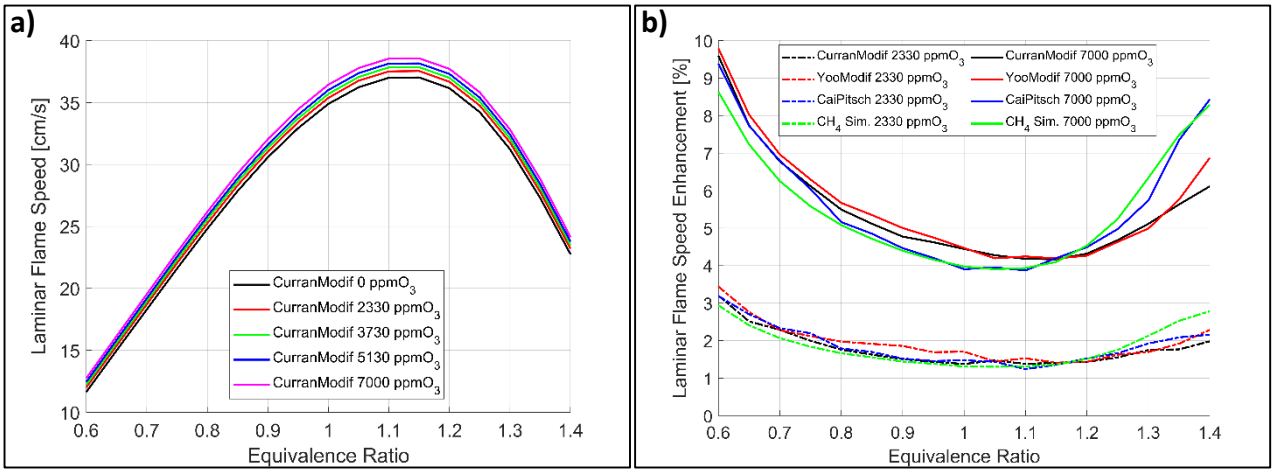

Figure 5. Numerical results in terms of LFS vs equivalence ratio at ambient conditions (1 bar, 300 K): a) LFS (with the modified Curran mechanism) for $C_8H_{18}/Air/O_3$ mixture; b) LFS relative enhancement for $C_8H_{18}/Air/O_3$ and for CH_4Air/O_3 mixtures.

Moreover, for 2330 ppm ozone concentration, the results show that for $\phi < 1.1$ the LFS enhancement for methane is comparable to that for iso-octane, whereas, for higher equivalence ratios,

the maximum enhancement is obtained with methane. For higher ozone concentrations, the LFS enhancement obtained for methane is very close to that obtained with the modified Cai&Pitsch mechanism for iso-octane, except for low equivalence ratios.

LFS increases linearly with ozone concentration for both methane and iso-octane mixtures, as shown in Fig. 6, where three equivalence ratios, i.e. 0.6, 1 and 1.4, are considered. By using a linear fit, the following expression can be written:

$$SL_{x_{O_3}} = SL_0 + \alpha x_{O_3} \,, \tag{10}$$

where $SL_{x_{O_3}}$ is the LFS of the mixture with *x* ppm of ozone, SL_0 is the LFS without ozone addition, and $x_{O_3}$is the ozone concentration. The α coefficients for all cases are also given in Fig. 6, with LFS given in cm/s and ozone concentration in thousands of ppm. The highest value of α is obtained under stoichiometric conditions for all mechanisms except for the modified Cai&Pitsch mechanism, which predicts a maximum value at $\phi = 1.4$. The lowest α values are observed in the case of methane for both lean and rich mixtures, whereas under stoichiometric conditions α values are comparable for the two fuels. For iso-octane mixtures, the influence of the addition of ozone on the absolute speed enhancement is significantly lower for lean mixtures with respect to stoichiometric and rich mixtures.

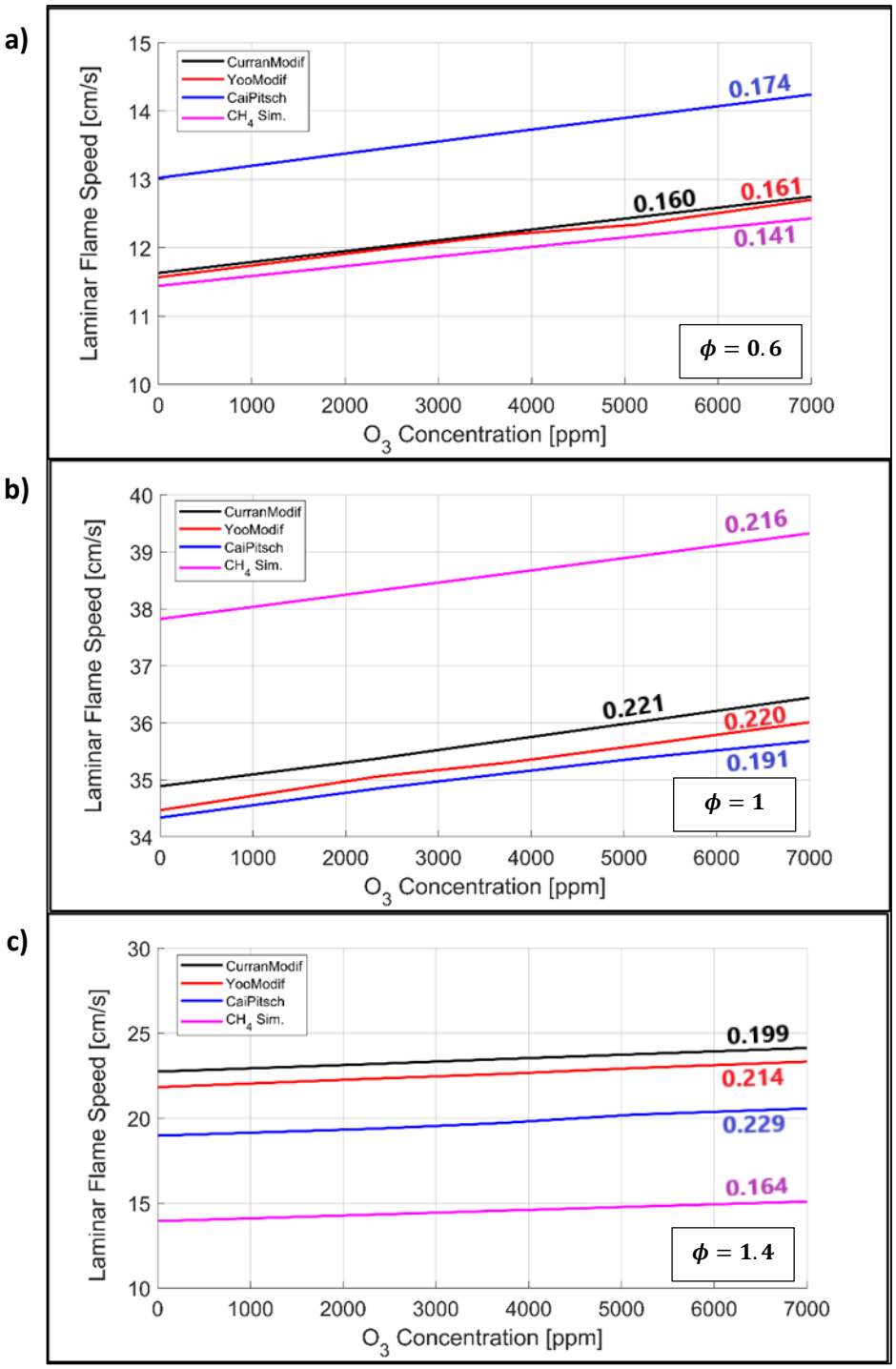

Figure 6. Numerical results in terms of LFS vs ozone concentration for $C_8H_{18}/Air/O_3$ and $CH_4/Air/O_3$ mixtures at ambient conditions (P=1 bar, T=300 K) and for different equivalence ratios, with α coefficients expressed in cm/(s*1000ppm_{O_3}): a) $\phi = 0.6$; b) $\phi = 1$; c) $\phi = 1.4$.

3.3 Influence of Mixture Temperature

Simulations are carried out by varying by 20 K the temperature of the reactant mixture, in the range 300 - 700 K, with the aim of investigating the case of ozonized air at higher temperatures, which are of interest for SI engines. Such simulations have been carried out by setting the equivalence ratio to 1 and the pressure to 1 bar.

Fig. 7a shows the LFS of $CH_4/Air/O_3$ mixtures as a function of reactants temperature for different ozone concentrations. Fig. 7b and Fig. 7c show the absolute and relative LFS enhancement, respectively. As expected, the results show that the LFS increases with temperature for all cases, and that this trend is enhanced by adding ozone to the mixture. By increasing the temperature in the range 300-540 K, the absolute value of the LFS enhancement for the cases with ozone (Fig. 7b) increases linearly with a slope that is proportional to the ozone concentration; above 540 K ozone addition has a stronger effect and the slope of the profiles increases the greater the ozone concentration.

As regards the relative LFS enhancement (Fig. 7c), in the range 300-520 K, for a given ozone concentration, the relative LFS enhancement slightly decreases with increasing temperature, whereas for temperatures in the range 520-680 K the relative enhancement increases with temperature and, finally, over about 680 K it approaches a constant, temperature-independent value. This trend indicates that, as long as the temperature is relatively low, ozone addition has a minor effect with respect to the increase of temperature; starting from about 520 K, instead, ozone has a major influence and an opposite trend is achieved.

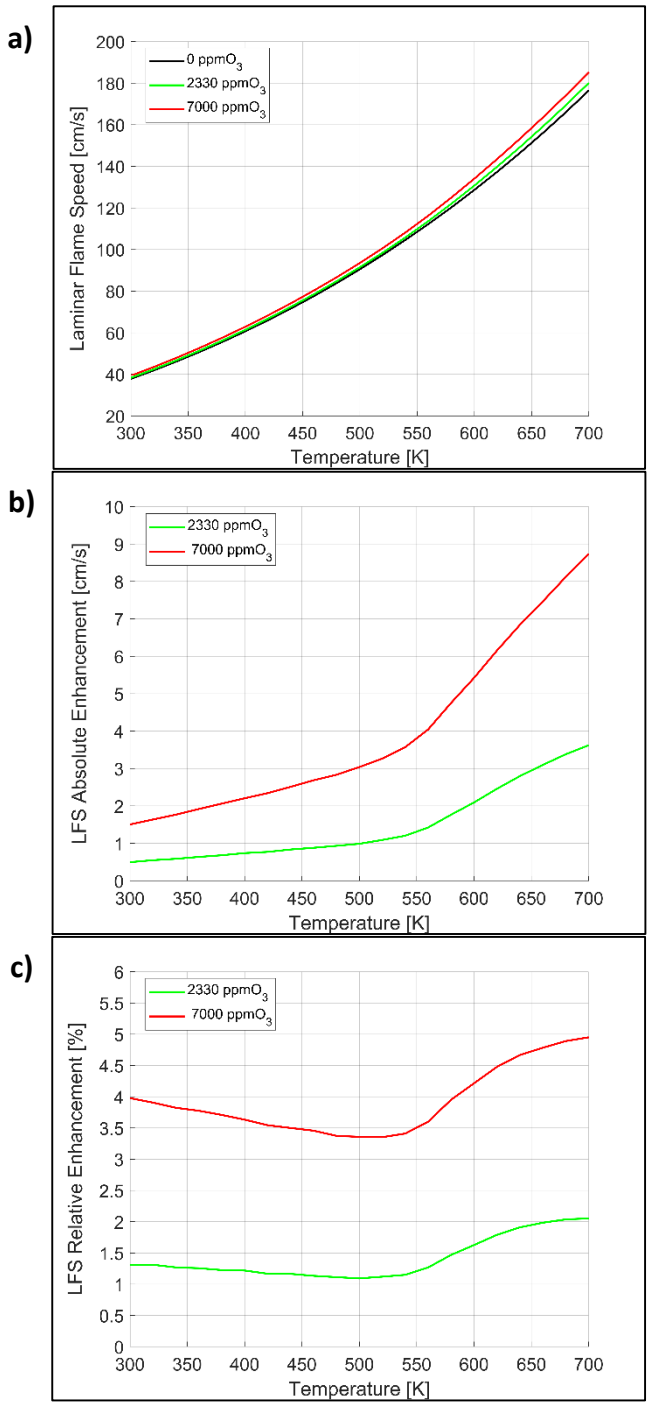

Figure 7. Numerical results in terms of LFS vs mixture temperature for $CH_4/Air/O_3$ for different ozone concentrations at P=1 bar and $\phi = 1$: a) LFS; b) absolute enhancement; c) relative enhancement.

The same analysis has also been performed for a mixture of iso-octane/air/ozone. Fig. 8a shows the LFS as a function of mixture temperature for different ozone concentrations by using the modified Yoo mechanism, whereas Fig. 8b shows the derivative of the LFS with respect to temperature, i.e. $\frac{dS_L(T)}{dT}$, obtained with 0, 2330 and 7000 ppm of ozone. Similar trends have been found by using both the modified Curran and the modified Cai&Pitsch mechanisms.

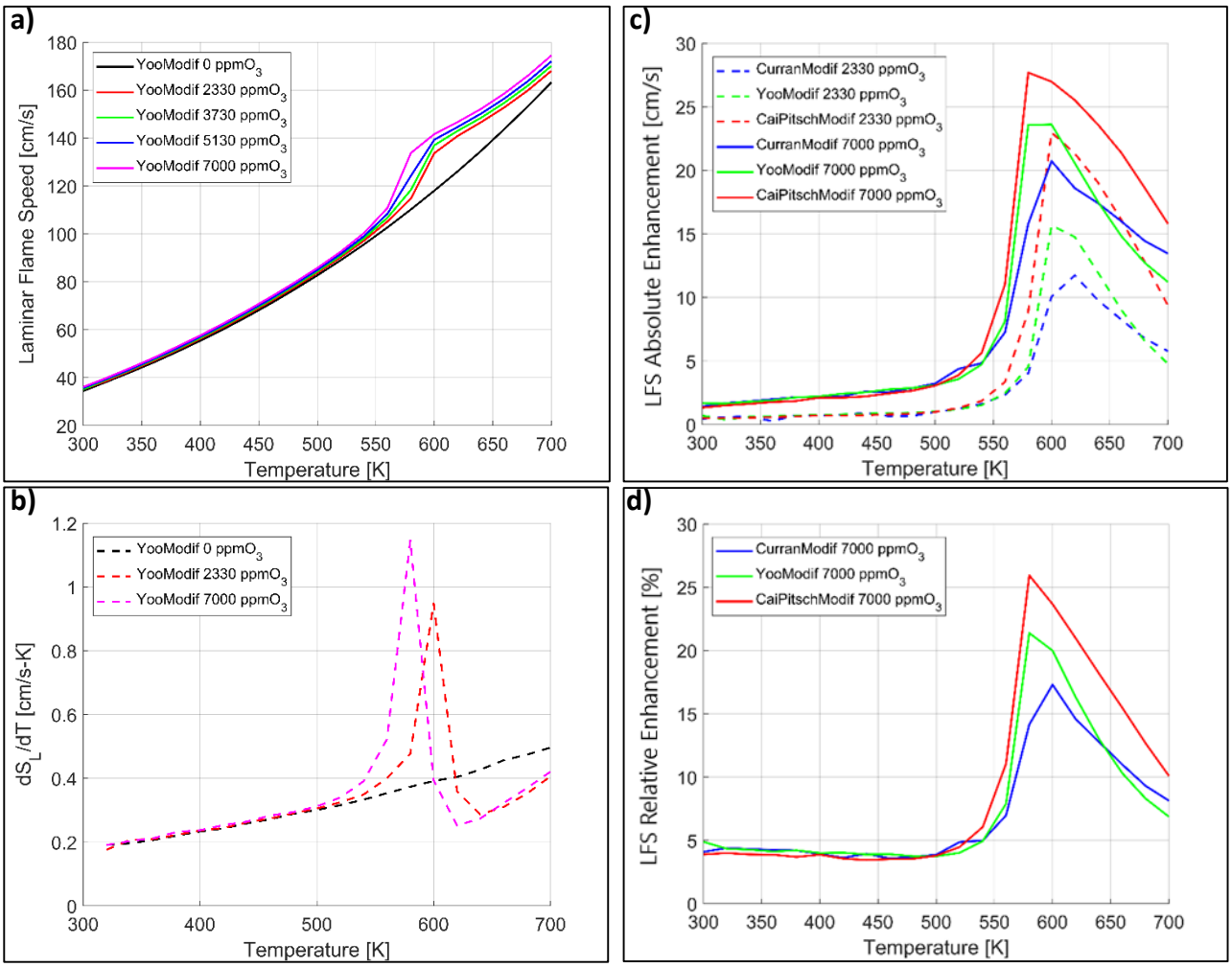

Figure 8. Numerical results for $C_8H_{18}/Air/O_3$ mixtures with different reaction mechanisms and ozone concentrations at P=1 bar and $\phi = 1$: a) LFS; b) derivative of LFS with respect to temperature; c) absolute enhancement of LFS; d) relative enhancement of LFS vs mixture temperature.

The results show that, in absence of ozone, the LFS as a function of temperature has a similar trend with respect to the case of methane given in Fig. 7a: specifically, S_L increases more than linearly with temperature. With ozone addition, a similar behaviour has been obtained up to about 520 K. Above this value the LFS increases with temperature much faster. Indeed, Fig. 8b shows that with 7000 ppm of ozone, in the temperature range 520-580 K, the slope of the $S_L(T)$ profile considerably increases, reaching a maximum value of 1.15 $\frac{cm}{s\,K}$ at 580 K, against 0.37 $\frac{cm}{s\,K}$ for the case in absence of ozone at the same temperature. With a decrease of the ozone concentrations, the peak of the $\frac{dS_L(T)}{dT}$ profile drops and moves towards higher temperatures, as shown in Fig. 8b. After the peak, a sharp decrease of the LFS derivative is observed with lower values than those obtained in absence of ozone are reached, and then it slowly increases.

The results obtained by using the other two mechanisms for iso-octane are qualitatively similar and a comparison is shown in Fig. 8c and Fig. 8d in terms of absolute and relative LFS enhancements with respect to the case in absence of ozone.

The results show that in the temperature range 300-520 K all the three mechanisms give approximately the same results. In this range, both the relative and the absolute LFS enhancements are quantitatively similar to those obtained for methane; besides, similar trends are achieved as a function of temperature, with a linear increase of the absolute value of the LFS enhancement. Instead, for higher temperatures a different behaviour with respect to methane is obtained, since with iso-octane the enhancements are much greater in the 540-640 K range. All the three mechanisms give the same trends, even if the results quantitatively differ in this temperature range. The maximum values of both relative and absolute enhancements are different and occur at different temperatures, depending on the reaction mechanism, for each ozone concentration. Similar to Fig. 8b, after the peak value, the influence of ozone is reduced and the relative LFS enhancement approaches the values obtained at lower temperatures.

In order to investigate the behaviour of iso-octane/air/ozone mixtures at temperature higher than 540 K with respect to the case of methane/air/ozone mixtures, the profiles of specific quantities across the flame, i.e. temperature, ozone mole fraction and OH mole fraction, are analysed and given in Fig. 9 for the case with 7000 ppm of ozone under stoichiometric condition and for two different reactants temperatures, i.e. 500 and 620 K. The results show that, for iso-octane with ozone addition and reactants temperature of 620 K, a cool flame occurs, in agreement with other works available in the literature [21,29-31].

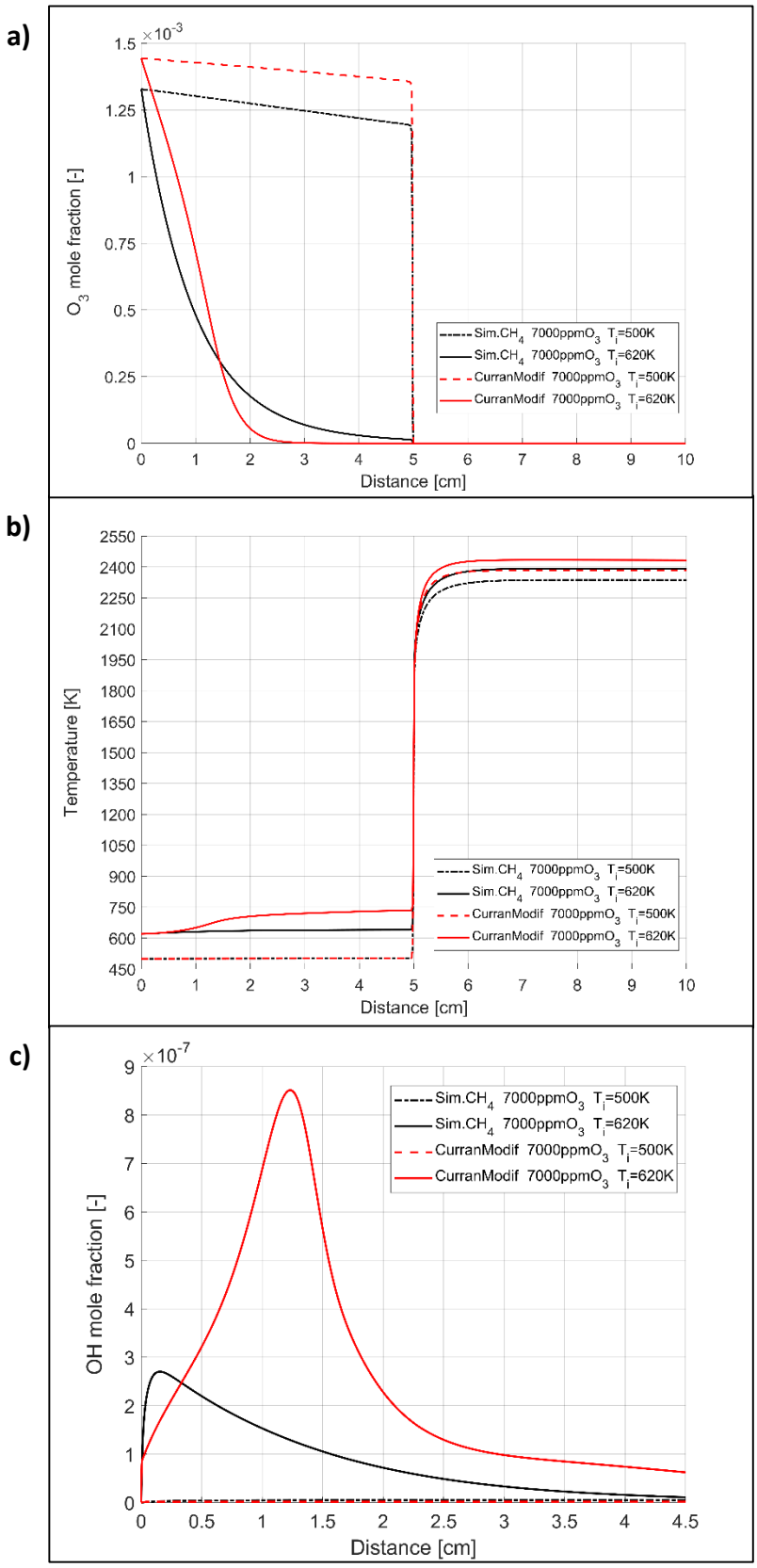

Figure 9. Profiles across the flame for stoichiometric $CH_4/Air/O_3$ and $C_8H_{18}/Air/O_3$ mixtures with 7000 ppm of O_3 at P=1 bar, $T_i = 500\ K$ and $T_i = 620\ K$: a) O_3 mole fraction; b) temperature; c) OH mole fraction as a function of distance across the flame.

Fig. 9a shows that ozone decomposition depends on both the inlet temperature and the specific fuel. With a reactants temperature of 500 K, ozone is partially decomposed ahead of the high temperature flame: at the flame location, i.e. 4.94 cm, 6.2% and 10.2% of the initial amount of ozone is decomposed for the iso-octane and methane mixtures, respectively. On the other hand, with a reactants temperature of 620 K, ozone is almost completely decomposed ahead of the high-temperature flame, i.e. 98.9% and 100% of the initial amount of ozone is decomposed for methane and iso-octane mixtures, respectively.

The much faster ozone decomposition for the iso-octane mixture with an initial temperature of 620 K is due to the different temperature profile, shown in Fig. 9b. With a temperature of the reactants of 500 K, the flame is located approximately at 4.94 cm for both methane and iso-octane. Upstream of the flame, the temperature remains nearly the same to the initial value. On the other hand, when the temperature of the reactants is 620 K, a cool flame is established for iso-octane, therefore the fuel is consumed ahead of the high-temperature flame. At 2 cm the temperature is already 706 K (+86 K) and 38.5% of the initial amount of iso-octane is consumed. Just upstream of the high-temperature flame 47.2% of the initial amount of fuel is consumed and the temperature is 734 K. This phenomenon for methane is less evident and more gradual, so just upstream of the high temperature flame 98.4% of the fuel is present and the temperature is increased by only 20 K. Fig. 9c shows the OH mole fraction in the 0 - 4.5 cm region. With a temperature of the reactants of 500 K, the OH mole fraction is of the order of 10^{-9} for both methane and iso-octane and increases very slowly with distance. On the other hand, with an initial temperature of 620 K, OH radicals are produced and, then, consumed, with a maximum in the case of iso-octane at 1.22 cm.

The trend shown in Fig. 9 occurs with the entire set of iso-octane reaction mechanisms and with lower ozone concentrations. The cool flame location depends on the reactant temperature, on the reaction mechanism and on the ozone concentration, in agreement with the previous discussion on the increase of the LFS. In the case of methane, on the other hand, the cool flame does not occur in any of the conditions, even when the temperature of the reactants is 700 K.

As previously stated, ozone is able to activate the cool flame for iso-octane/air/ozone mixture at temperature above 560 K. To identify which reactions are involved in the cool-flame process, additional analyses have been carried out. Fig. 10 shows the chemical reactions characterized by the highest values of the Absolute Rate of Production (ARP) of iso-octane, ozone, and atomic oxygen for the case with 7000 ppm of ozone and a temperature of the inlet mixture of 620 K, by using the modified Curran mechanism, at the distance x^* defined as:

$$x^* = x : \max\left\{\frac{dX_{OH}(x)}{dx}\right\},\ 0 < x < 4.95\ cm, \quad (11)$$

where x is the distance from the inlet and $X_{OH}(x)$ is the molar fraction of OH. x^* is the distance corresponding to the maximum OH increase in the region ahead of the high-temperature flame. In the case under consideration, x^* is about $1\ cm$. The corresponding temperature is $T_{x^*} = 650\ K$, i.e. 30 K higher than the temperature of the mixture at the inlet. By definition, the ARP is negative if the specific chemical species is consumed, otherwise it is positive. Fig. 10 also shows the main reaction pathways leading to the formation of OH, together with the ARP values. As regards ozone decomposition, Fig. 10 shows the reaction pathways with the Relative Rate of Production (RRP) greater than 0.1% and the reactants or products involved in the reaction.

Fig. 10a shows the ARPs of the 10 main reactions of the ozone reaction pathways. Specifically, from the figure, it can be observed that the faster reactions are:

R1) $O_3 + N_2 \rightarrow O_2 + O + N_2$,

R2) $O_3 + H \rightarrow O_2 + OH$.

Those two reactions account together for 84.1% of the total ozone decomposition, i.e. R1 is responsible for 71.9% and R2 for 12.2%, as shown in Fig. 10e.

Fig. 10b shows the 10 fastest reactions for the fuels. These reactions are of three types:

R3) $C_8H_{18} + OH \rightarrow C_8H_{17} + H_2O$,

R4) $C_8H_{18} + O \rightarrow C_8H_{17} + OH$,

R5) $C_8H_{18} + H \rightarrow C_8H_{17} + H_2$.

Specifically, the sum of R3-type reactions is responsible for 88.7% of the total C_8H_{18} consumption, whereas R4-type reactions are responsible for 10.6%.

Finally, Fig. 10c shows the fastest reactions that involve atomic oxygen. Some of these reactions produce O and others consume it. The production of atomic oxygen is primarily due to two reactions involving ozone: R1 and $O_3 + O_2 \rightarrow 2O_2 + O$. R1 is the fastest reaction for atomic oxygen production, followed by R4-type reactions.

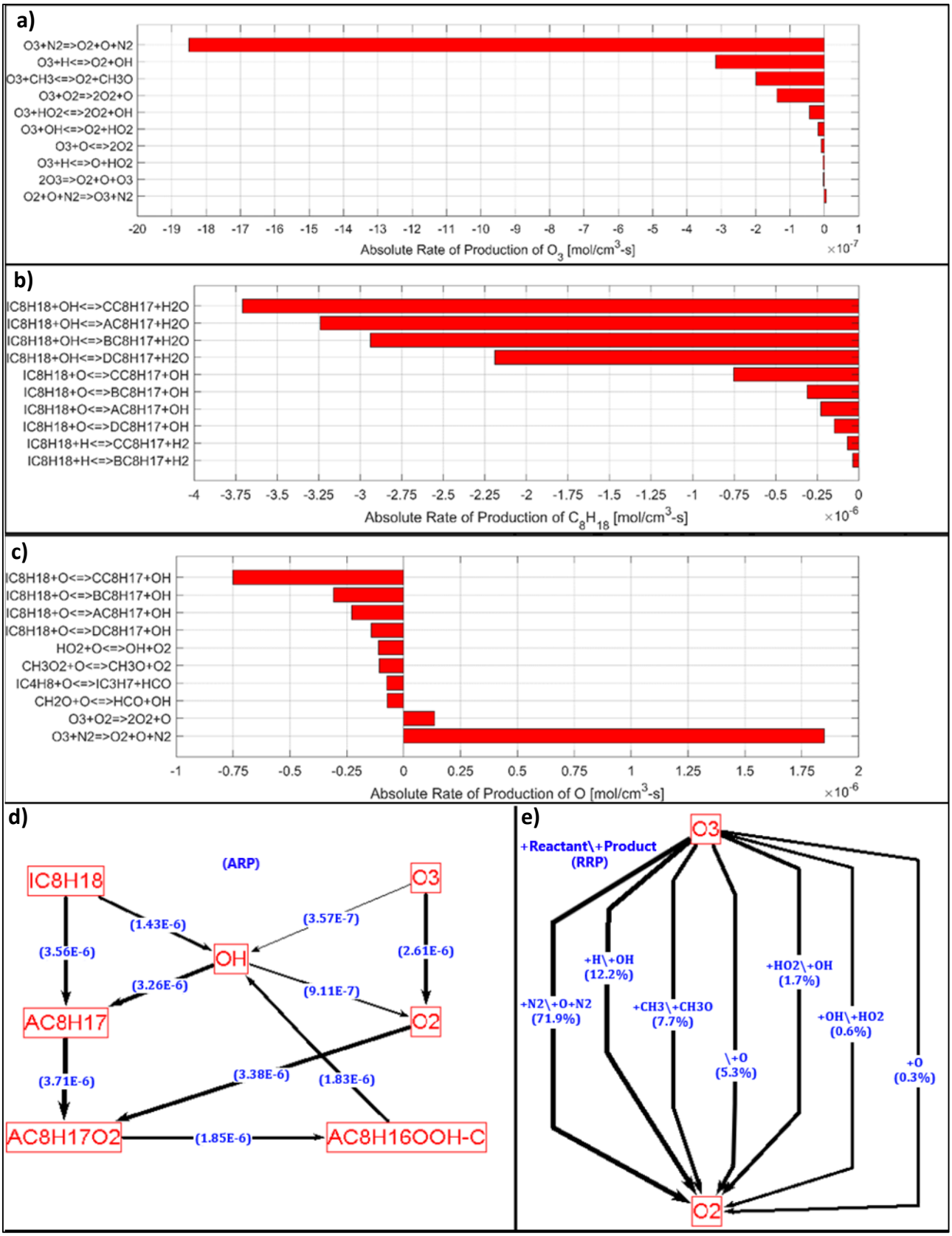

Figure 10. Absolute Rates of Production (ARP) and reaction paths at $x^* = 1\ cm$ for a stoichiometric $C_8H_{18}/Air/O_3$ mixture with 7000 ppm of O_3 with the modified Curran mechanism, P=1 bar, $T_i = 620\ K$. Highest ten ARPs for a) O_3; b) C_8H_{18} ; c) *O*. Main reaction paths for d) production of *OH*; e) O_3decomposition.

Therefore, ozone is decomposed very fast by R1 reaction producing atomic oxygen. The atomic oxygen, being highly reactive, attacks the C_8H_{18} molecules by R4 reaction producing OH radicals that advance the oxidation, as shown in Fig. 10d. As a matter of fact, at the pipe inlet ($x = 0\ cm$) with $T_i = 620\ K$ the R1 reaction already occurs with an ARP of $-1.73 \times 10^{-6}\ \frac{mol}{cm^3 s}$, i.e. with about the same rate that occurs at x^* with $T_{x^*} = 650\ K$, which is shown in Fig. 10a. The reactions involving iso-octane also occur very fast just after the pipe inlet. For instance, at $x = 10^{-3}\ cm$ the reaction $IC_8H_{18} + O \rightarrow CC_8H_{17} + OH$ occurs with an ARP of $-0.41 \times 10^{-6}\ \frac{mol}{cm^3 s}$, i.e. with the same order of magnitude corresponding to x^* and shown in Fig. 10c. On the other hand, for a mixture temperature equal to 500 K, ozone decomposes very slowly up to the high-temperature flame, as also shown in Fig. 9a. At $x = 4.95\ cm$ the R1 reaction proceeds with an ARP of $-3 \times 10^{-8}\ \frac{mol}{cm^3 s}$, i.e. about 100 times lower than the 620 K case, thus not allowing the oxidation reactions of iso-octane by atomic oxygen and OH radicals to be efficiently initiated to start the cool flame.

3.4 Influence of Mixture Pressure

In this section, the influence of the mixture pressure on the chemical kinetics of ozone and on the LFS of iso-octane/air/ozone and methane/air/ozone stoichiometric mixtures is investigated. The modified Cai&Pitsch mechanism is used for iso-octane, since it is in better agreement with the experimental data at higher pressure (Fig. 3), especially at $\phi = 1$.

3.4.1 Influence of Mixture Pressure on Ozone Decomposition

The influence of pressure on the two main ozone reactions, i.e.

R1) $O_3 + N_2 \rightarrow O_2 + O + N_2$,

R2) $O_3 + H \rightarrow O_2 + OH$,

is analysed in Fig. 11, which shows the total ozone ARP together with the ozone ARP in R1 and R2 reactions as a function of distance from the inlet of the stream tube. Three different pressures, i.e. 1, 2 and 3 bar, and two inlet temperatures, i.e. 300 K and 600 K, are considered for an iso-octane/air/ozone mixture with 2330 ppm O_3. For the case with an initial temperature of 300 K, the x-axis shows the region near the flame, whereas for the case with an initial temperature of 600 K, the region upstream the flame is also of interest since a cool flame occurs.

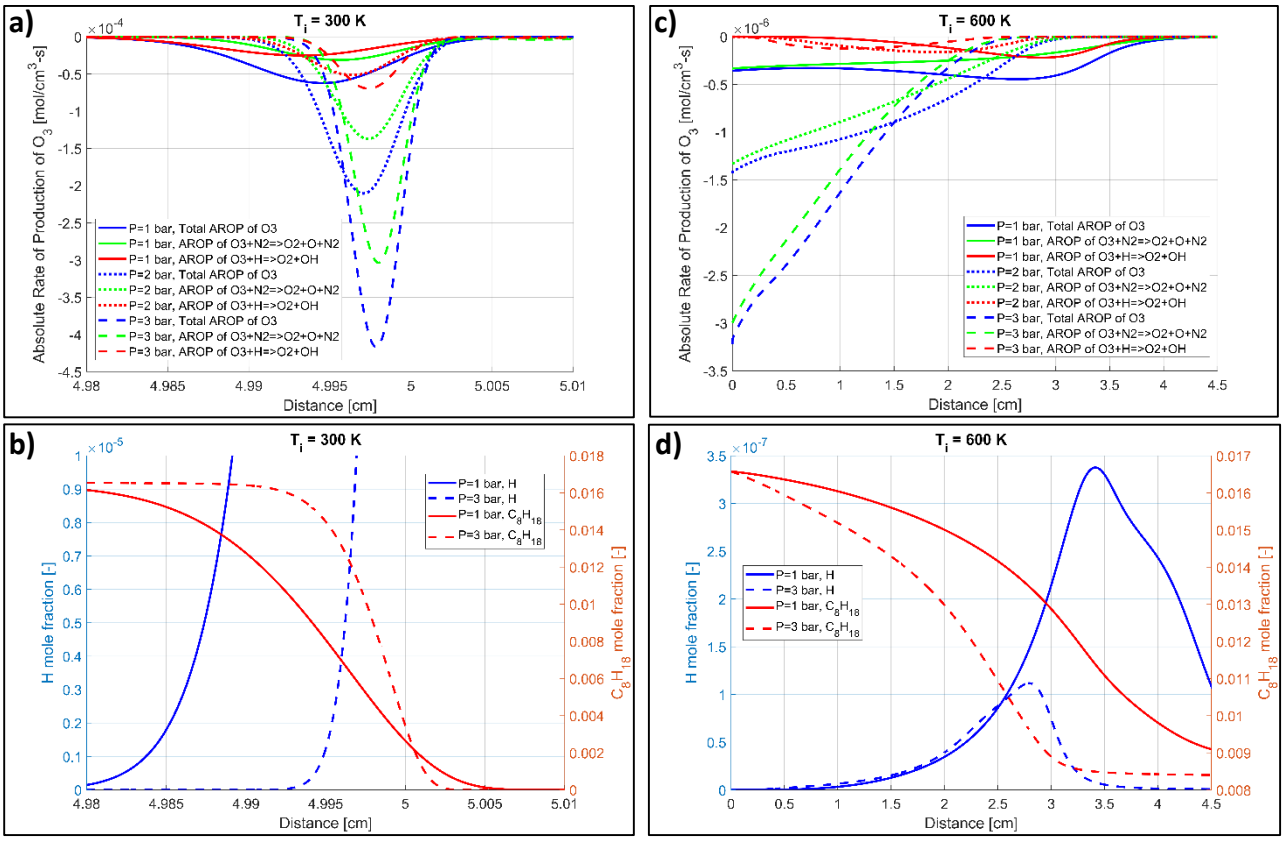

Figure 11. Simulations of stoichiometric $C_8H_{18}/Air/O_3$ mixtures with 2330 ppm of ozone for different values of pressure by using the modified Cai&Pitsch mechanism: a) O_3 ARPs at $T_i = 300\ K$; b) H and C_8H_{18} mole fractions at $T_i = 300\ K$; c) O_3 ARPs at $T_i = 600\ K$; d) H and C_8H_{18} mole fractions at $T_i = 600\ K$.

Fig. 11 shows that the decomposition of ozone is very different depending on the inlet temperature of the mixture. With a temperature of 300 K, as previously discussed, only the high temperature flame is established and ozone decomposes very close to the flame. Ozone decomposition occurs earlier and is slower when the pressure is low. Specifically, the peak value of the total amount of ARP of O_3 increases by 240% and 570% for pressures of 2 bar and 3 bar, respectively, with respect to 1 bar case.

At the location where the total ozone ARP is maximum, reactions R1 and R2 contributes 88% to the total consumption of O_3 regardless of pressure. Despite this, the contribution of each reaction changes considerably as a function of pressure. When the pressure is 1 bar, the ozone starts to mainly decompose by the R2 reaction, which occurs due to the diffusion of hydrogen atoms from the flame region to the preheating zone, as shown in Fig. 11b. Furthermore, the ARP peak value of R1 and R2 reactions are similar and, at the point where the ozone ARP is maximum, R1 contributes 48% and R2 39%.

As the mixture pressure increases, the contribution of R1 increases and that of R2 decreases. Specifically, at the point where the ozone consumption rate is maximum, R1 contributes 65% and 72% at 2 bar and 3 bar, respectively, whereas the contribution of R2 decreases to 23% and 16% at 2 and 3 bar, respectively. The increase in pressure, in fact, leads to a decrease in the diffusivity of the chemical species, so the amount of H in the preheating zone is lower: for instance, where the mole fraction of C_8H_{18} is 0.014, i.e. 84.6% of the initial amount, at 1 bar the mole fraction of H is 6.28×10^{-6}, whereas at 3 bar it is only 1.93×10^{-6}, i.e. more than three times less. On the other hand, R1, being a third body reaction, is favoured by increasing pressure.

With a temperature of the reactants of 600 K a cool flame takes place, and, as shown in Fig. 11c, the ozone ARP has a very different route. Regardless of the pressure, the decomposition of ozone starts at the inlet of the tube, mainly due to R1 reaction, whose ARP represents 93% of the total. In agreement with Fig. 9a for the 620 K case, ozone is completely consumed before the high-temperature flame is established, as inferred by the total ARP. At this temperature, the sum of the ARP of R1 and R2 reactions is about 93% of the total amount and is independent of pressure and spatial location.

At 600 K, ozone decomposes much faster by increasing the pressure and this is more pronounced with respect to the case at 300 K. For instance, with a pressure of 3 bar, at 2.5 cm from the inlet the total ozone ARP is about 0, whereas at a pressure of 1 bar it is approximately equal to its maximum value. At 1 bar, the total ARP of ozone changes slightly from the pipe inlet to about 3 cm, and the maximum value is obtained at 2.64 cm, where the ARPs of R1 and R2 reactions are nearly the same and equal to 46%. On the other hand, at 2 and 3 bar the total ozone ARP monotonically decreases in the pipe, with a faster decrease in the case of high pressure. At the pipe inlet, the peak value of the total ARP of O_3, compared to the case with P =1 bar, increases by 300% and 800% with pressures of 2 and 3 bar, respectively.

Based on these results, it can be expected that for even higher pressures, with a temperature high enough to generate a cool flame, ozone should mainly decompose by means of R1 reaction and this will take place so fast that it will be ended in a very short distance. In this way, the reactions of fuel with atomic oxygen take place very fast, resulting in a higher LFS.

3.4.2 Influence of Mixture Pressure on LFS

In order to analyse the influence of pressure on the LFS for the two fuels, several simulations have been carried out with different operating conditions, in terms of temperature (from 500 to 600 K), pressure (from 1 to 20 bar) and ozone concentration (from 0 to 7000 ppm). Fig. 12 summarises the results in terms of LFS as a function of pressure. Without ozone LFS decreases as pressure increases, regardless of inlet temperature, for both methane and iso-octane mixtures. With ozone addition to the mixtures, the LFS dependence on pressure is different for the two fuels.

For methane, the LFS decreases by increasing pressure, with a trend similar to the case without ozone. As expected, if ozone concentration is higher, LFS is higher, but for a given ozone concentration and temperature of the reactants, pressure only slightly affects the benefit of adding ozone. Indeed, at 600 K with 7000 ppm of ozone, the increase of the LFS, compared to the case without ozone, is 4.2%, 5.4%, 5.9%, 6.2% and 6.4% with 1, 5, 10, 15 and 20 bar, respectively.

For iso-octane mixtures, pressure has a very different influence depending on both the ozone concentration and the temperature of the reactants. Indeed, Fig. 12 shows that, as long as the temperature of the reactant mixture is less than or equal to 540 K, the LFS decreases with increasing pressure for all the ozone concentrations. Furthermore, in this temperature range, it can be observed the influence of the cool flame on the widening of the beam of curves as the temperature increases: at 540 K the addition of ozone increases the LFS to a greater extent than in the case with 500 K. On the other hand, for higher temperatures, the trend is not monotonic as a function of pressure but, for pressures higher than a certain threshold, the LFS increases with pressure if air is ozonized. Such a threshold is lower if temperature and/or ozone concentration are higher. These results show that ozone is able to counterbalance the LFS decrease due to the increase in pressure if temperature is sufficiently high. The relative increases of the LFS, compared to the case without ozone, as a function of pressure are given in Table S2 in the supplementary material for selected cases.

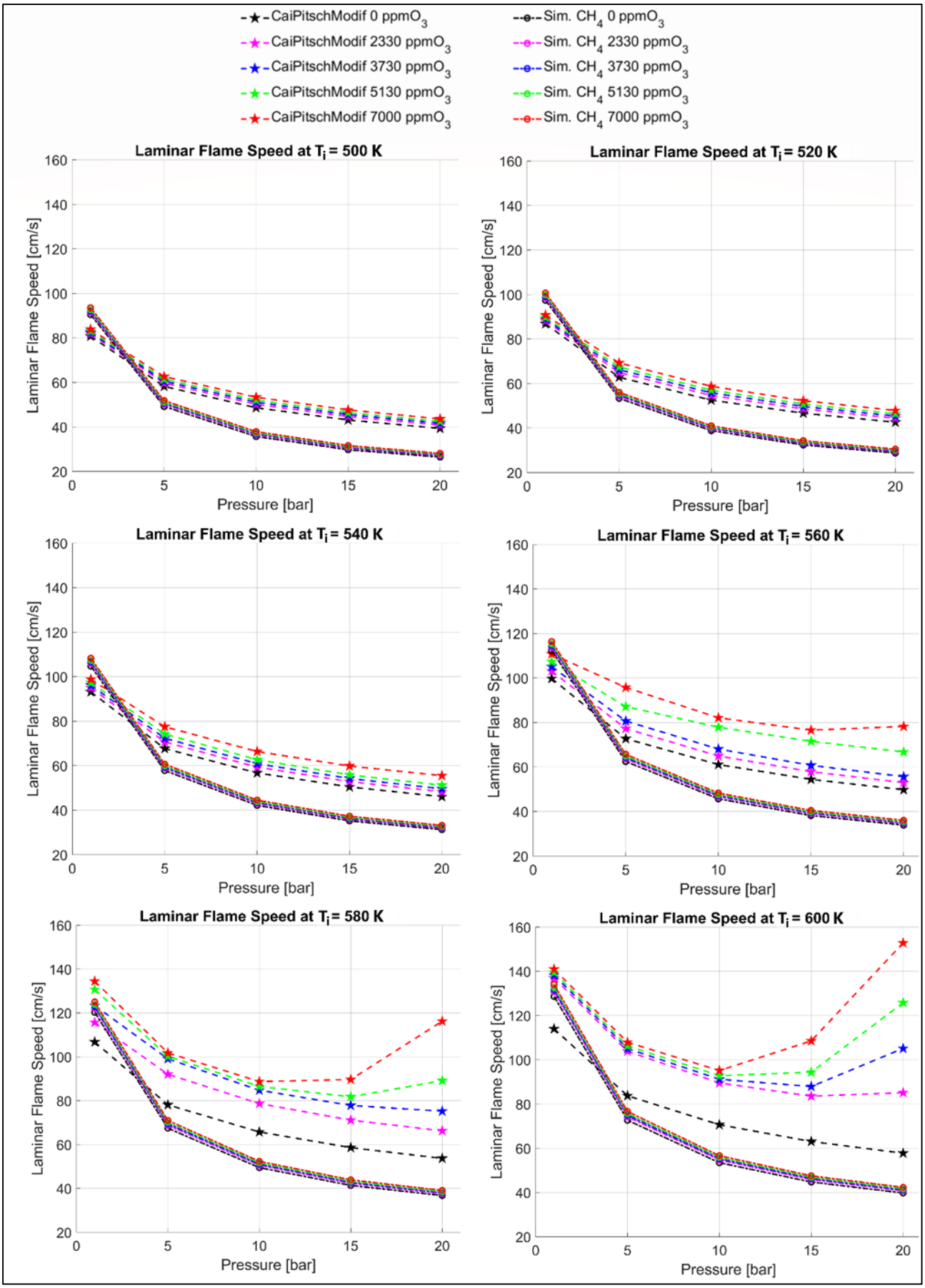

Figure 12. LFS as a function of pressure for stoichiometric $C_8H_{18}/Air/O_3$ and $CH_4/Air/O_3$ mixtures with different ozone concentrations and for different reactant temperatures.

In order to clarify the results shown in Fig. 12, sensitivity analyses have been carried out by using both the methane mechanism and the modified Cai&Pitsch mechanism for C_8H_{18} for three values of pressure, i.e. 1, 10 and 20 bar, both with 7000 ppm of O_3 and without ozone. The case with a reactants temperature of 600 K has been considered, since at this temperature a non-monotonic trend of LFS as a function of pressure for C_8H_{18} and ozonized air is found. Besides, this trend is more severe at 600 K with respect to the other cases at lower temperatures. The results of the sensitivity analyses are shown in Fig. 13 and Fig. 14. For each condition, the 10 reactions, to which the LFS is most sensitive, are given.

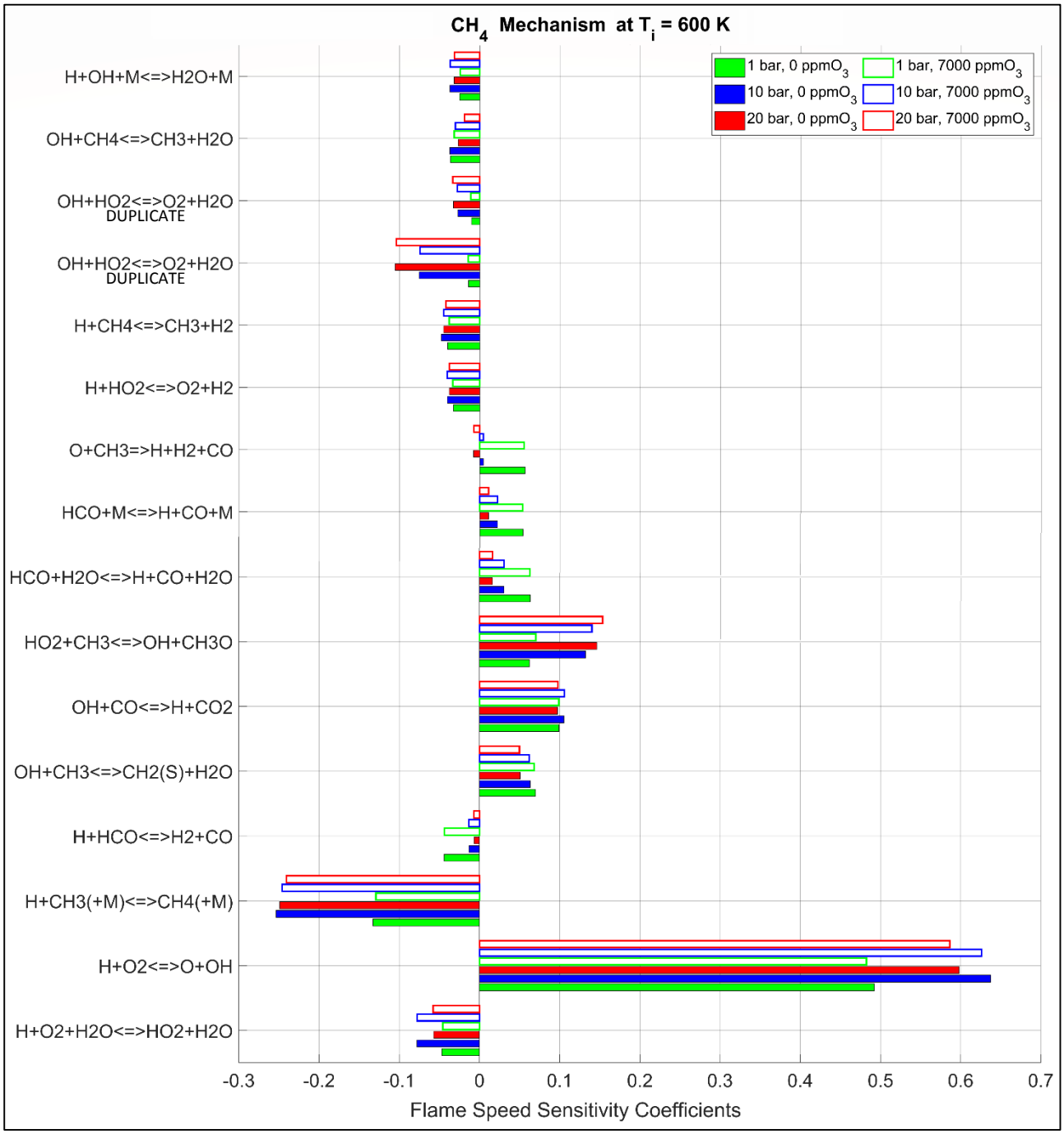

Figure 13. LFS sensitivity coefficients for CH_4 mechanism at $T_i = 600\ K$, with and without ozone and for different pressures.

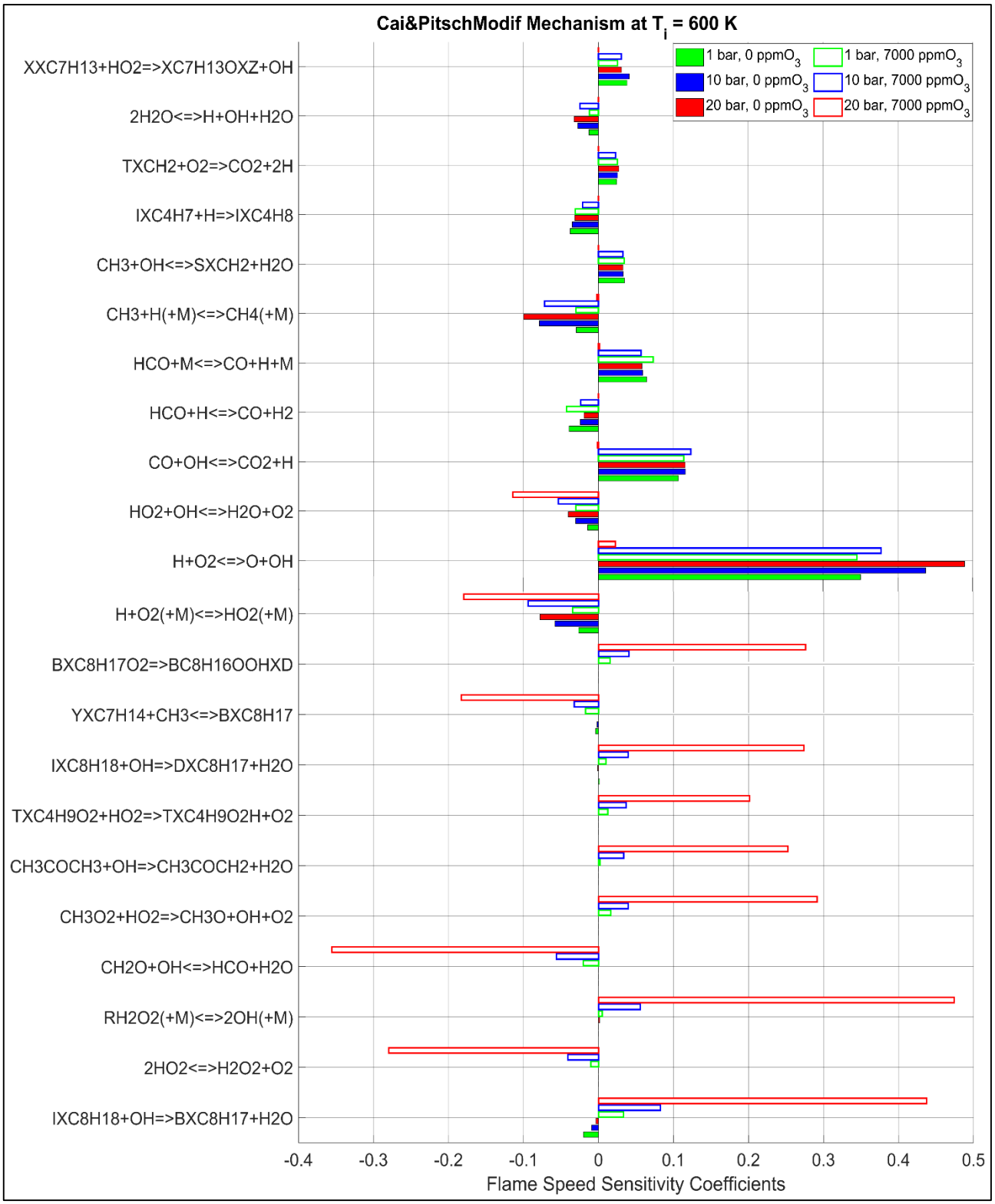

Figure 14. LFS sensitivity coefficients for C_8H_{18} modified Cai&Pitsch mechanism at $T_i = 600\ K$, with and without ozone and for different pressures.

As shown in Fig. 13, the main reactions for methane are the same with and without ozone, and a slight change of the corresponding sensitivity coefficients is observed for ozonized air. Specifically, the sensitivity of the reaction $H + O_2 \rightleftarrows O + OH$ decreases with the addition of ozone,

whereas the sensitivity of $HO_2 + CH_3 \rightleftarrows OH + CH_3O$ increases. This means that the increase of LFS with ozone is mainly due to the reaction pathway of HO_2. On the other hand, the reduction of LFS, as pressure increases, is mainly due to an increase of the negative sensitivity coefficients of the reactions $OH + HO_2 \rightleftarrows O_2 + H_2O$; $H + CH_3\ (+M) \rightleftarrows CH_4\ (+M)$.

As regards iso-octane, the sensitivity analysis shows large differences with and without ozone, as pressure increases (Fig. 14). In the absence of ozone, the main reactions remain the same, regardless of pressure. This is also observed for methane. Specifically, the main reaction is $H + O_2 \rightleftarrows O + OH$, whose sensitivity coefficient shows an increase with pressure. With the addition of 7000 ppm of ozone, at low pressure, i.e. 1 bar, the sensitivity coefficients of the important reactions $CO + OH \rightleftarrows CO_2 + H$ and $HCO + M \rightleftarrows CO + H + M$ show a slight increase with respect to the case without ozone. Furthermore, the importance of the following reactions $IXC_8H_{18} + OH \rightleftarrows BXC_8H_{17} + H_2O$; $BXC_8H_{17}O_2 \rightarrow BC_8H_{16}OOHXD$; $CH_3O_2 + HO_2 \rightleftarrows CH_3O + OH + O_2$, which are in the upper kinetic chain, increase as well. It can be observed that, as the pressure increases from 10 to 20 bar, the sensitivity coefficients of the above reactions increase such that they become the most important reactions with respect to the case without ozone. Specifically, the sensitivity coefficient of the reaction $IXC_8H_{18} + OH \rightleftarrows BXC_8H_{17} + H_2O$ changes from a negative value, in the absence of ozone, to a high positive value with ozone addition. Other relevant reactions for the LFS are: $RH_2O_2\ (+M) \rightleftarrows 2OH + M$; $IXC_8H_{18} + OH \rightleftarrows DXC_8H_{17} + H_2O$; $CH_3O_2 + HO_2 \rightleftarrows CH_3O + OH + O_2$. The analysis shows that the increase of LFS with ozone addition at high pressure and temperature is mainly due to the OH reaction pathway. As shown in Fig. 9, for the case with ozonized air, at relatively high temperatures, the production of OH radicals enables the formation of the cool flame. Fig. 10 shows that OH radicals are mainly produced by reactions $C_8H_{18} + O \rightleftarrows (A,B,C,D)C_8H_{17} + OH$. The atomic oxygen, which reacts with fuel molecules, is produced by ozone decomposition through the reaction $O_3 + N_2 \rightarrow O_2 + O + N_2$. Such a reaction is promoted and accelerated as pressure increases, especially at higher temperatures, as shown in Fig. 11. Hence, the increase of LFS at higher temperatures and pressures is a direct consequence of the speed up of ozone chemical kinetics in the cool flame region.

4. Conclusions

In this work, the influence of ozone addition on the combustion of methane and iso-octane in air has been investigated. Specifically, 1-D simulations have been carried out to compute the laminar flame speed by using a specific reaction mechanism for methane and three different mechanisms for

iso-octane. Each mechanism has been modified with the addition of an ozone sub-mechanism. The model has been validated against experimental data available in the literature under different conditions of pressure, temperature, equivalence ratio and ozone concentration. Final considerations are:

- the three modified mechanisms used for iso-octane provide similar results for all the simulations. The greatest discrepancies are found at high reactant temperatures (T>540 K) even if, qualitatively, the mechanisms are always in agreement;
- at ambient conditions (P = 1bar, T=300 K), ozone addition has the same impact on both mixtures with methane and iso-octane for all the equivalence ratios investigated;
- as the temperature of the reactants increases, ozone addition has a different influence on the two fuels. In the case of iso-octane, O_3 enables a cool flame, in agreement with other results in the literature. This phenomenon occurs at temperature equal to or higher than about 540 K when 7000 ppm ozone is added to the mixture, leading to an increase of the laminar flame speed;
- for mixture temperatures below 520-540 K, ozone mainly decomposes near the high-temperature flame. For higher temperatures, ozone is already almost completely consumed upstream the flame. In the case of iso-octane, the atomic oxygen, produced by the decomposition of ozone for temperatures higher than about 540 K, oxidises the fuel, thus producing OH-radicals, which advance the oxidation. These reactions are fast enough to generate the cool flame;
- for high mixture pressures, ozone decomposition by the reaction $O_3 + N_2 \rightarrow O_2 + O + N_2$ is greatly favoured and a different behaviour occurs for methane/air/ozone and for iso-octane/air/ozone mixtures. For methane, the laminar flame speed decreases as pressure increases, regardless of temperature. For iso-octane, the influence of ozone addition is the same as for methane with a temperature of the reactants below 540 K. For higher temperatures, i.e. in the presence of a cool flame, the laminar flame speed increases with pressure, to a greater extent for higher ozone concentrations and/or temperatures.
- as regards methane, LFS sensitivity analyses performed at 600 K show that, with and without ozone, the main reactions are the same regardless of pressure. Furthermore, the values of the sensitivity coefficients with and without ozone are comparable and present the same variations with pressure. As regards iso-octane, the sensitivity analyses at 600 K show that, in the presence of ozone, the laminar flame speed is

mainly influenced by reactions that do not correspond to those in the absence of ozone. Specifically, the most important reactions are those involved in the cool flame and activated by ozone kinetics. This is especially true at high pressure.

Acknowledgement

This research was funded by MIUR - "Ministero dell'Istruzione, dell'Università e della Ricerca" under project EXTREME - "Innovative technologies for EXTREMely Efficient spark ignited engines", ARS01_00849.

References

[1] A.A. Konnov, A. Mohammad, V.R. Kishore, N.I. Kim, C. Prathap, S. Kumar, A comprehensive review of measurements and data analysis of laminar burning velocities for various fuel+air mixtures, Prog. Energy Combust. Sci. 68 (2018) 197-267.

[2] K.J. Bosschaart, L.P.H. deGoey, The laminar burning velocity of flames propagating in mixtures of hydrocarbons and air measured with the heat flux method, Combust. Flame 136 (2004) 261–269.

[3] T. Tahtouh, F. Halter, C. Mounaïm-Rousselle, Measurement of laminar burning speeds and Markstein lengths using a novel methodology, Combust. Flame 156 (2009) 1735-1743.

[4] S. Jerzembeck, N. Peters, P. Pepiot-Desjardins, H. Pitsch, Laminar burning velocities at high pressure for primary reference fuels and gasoline: Experimental and numerical investigation, Combust. Flame 156 (2009) 292-301.

[5] F. Halter, P. Higelin, P. Dagaut, Experimental and Detailed Kinetic Modeling Study of the Effect of Ozone on the Combustion of Methane, Energy Fuels 25 (2011) 2909-2916.

[6] B. Galmiche, F. Halter, F. Foucher, Effects of high pressure, high temperature and dilution on laminar burning velocities and Markstein lengths of iso-octane/air mixtures, Combust. Flame 159 (2012) 3286–3299.

[7] E. Fanelli, A. Viggiano, G. Braccio, V. Magi, On laminar flame speed correlations for H2/CO combustion in premixed spark ignition engines, Applied Energy 130 (2014) 166-180.

[8] M. Metghalchi, J.C. Keck, Burning velocities of mixtures of air with methanol, isooctane, and indolene at high pressure and temperature, Combust. Flame 48 (1982) 191–210.

[9] R.J. Kee, J.F. Grcar, M.D. Smooke, J.A. Miller, E. Meeks, PREMIX: a fortran program for modelling steady laminar one-dimensional premixed flames, Report No. SAND85-8249, Sandia National Laboratories, CA, USA, 1985.

[10] D.G. Goodwin, H.K. Moffat, R.L. Speth, Cantera: An object-oriented software toolkit for chemical kinetics, thermodynamics, and transport processes, Pasadena, CA, Caltech, 2009.

[11] C.M. Vagelopoulos, F.N. Egolfopoulos, Direct experimental determination of laminar flame speeds, Symp. (Int.) Combust. 27 (1998) 513-519.

[12] X.J. Gu, M.Z. Haq, M. Lawes, R. Woolley, Laminar burning velocity and Markstein lengths of methane–air mixtures, Combust. Flame 121 (2000) 41-58.

[13] M. Reyes, F.V. Tinaut, A. Camaño, Experimental Study of Premixed Gasoline Surrogates Burning Velocities in a Spherical Combustion Bomb at Engine Like Conditions, Energies 13 (2020) 3430.

[14] S.G. Davis, C.K. Law, Determination of and fuel structure effects on laminar flame speeds of C1 to C8 hydrocarbons, Combust. Sci. Technol. 140 (1998) 427–449.

[15] W. Sun, X. Gao, B. Wu, T. Ombrello, The effect of ozone addition on combustion: Kinetics and dynamics, Prog. Energy Combust. Sci. 73 (2019) 1-25.

[16] T. Nomaguchi, S. Koda, Spark ignition of methane and methanol in ozonized air, Symp. (Int.) Combust. 22 (1989) 1677–1682.

[17] Z.H. Wang, L. Yang, B. Li, Z.S. Li, Z.W. Sun, M. Aldén, K.F. Cen, A.A. Konnov, Investigation of combustion enhancement by ozone additive in CH4/air flames using direct laminar burning velocity measurements and kinetic simulations, Combust. Flame 159 (2012) 120–129.

[18] X. Gao, Y. Zhang, S. Adusumilli, J. Seitzman, W. Sun, T. Ombrello, C. Carter, The effect of ozone addition on laminar flame speed, Combust. Flame 162 (2015) 3914-3924.

[19] T.M. Vu, S.H. Won, T. Ombrello, M.S. Cha, Stability enhancement of ozone-assisted laminar premixed Bunsen flames in nitrogen co-flow, Combust. Flame 161 (2014) 917-926.

[20] F. Foucher, P. Higelin, C. Mounaïm-Rousselle, P. Dagaut, Influence of ozone on the combustion of n-heptane in a HCCI engine, Proc. Combust. Inst. 34 (2013) 3005-3012.

[21] J-B Masurier, F. Foucher, G. Dayma, P. Dagaut, Homogeneous charge compression ignition combustion of primary reference fuels influenced by ozone addition, Energy Fuels 27 (2013) 5495-5505.

[22] J-B Masurier, F. Foucher, G. Dayma, P. Dagaut, Investigation of iso-octane combustion in a homogeneous charge compression ignition engine seeded by ozone, nitric oxide and nitrogen dioxide, Proc. Combust. Inst. 35 (2015) 3125-3132.

[23] J-B Masurier, F. Foucher, G. Dayma, C. Rousselle, P. Dagaut, Application of an Ozone Generator to Control the Homogeneous Charge Compression Ignition Combustion Process, SAE Technical Paper 2015-24-2456 (2015).

[24] P.M. Pinazzi, F. Foucher, Influence of Injection Parameters, ozone seeding and residual NO on a Gasoline Compression Ignition (GCI) engine at low load, Proc. Combust. Inst. 36 (2017) 3659-3668.

[25] P.M. Pinazzi, F. Foucher, Potential of Ozone to Enable Low Load Operations of a Gasoline Compression Ignition (GCI) Engine, SAE Technical Paper 2017-01-0746 (2017).

[26] C.M. Gong, J. Yu, K. Wang, J. Liu, W. Huang, X. Si, F. Wei, F. Liu, Y. Han, Numerical study of plasma produced ozone assisted combustion in a direct injection spark ignition methanol engine, Energy 153 (2018) 1028-1037.

[27] C.B. Reuter, S.H. Won, Y. Ju, Experimental study of the dynamics and structure of self-sustaining premixed cool flames using a counterflow burner, Combust. Flame 166 (2016) 125-132.

[28] S.H. Won, B. Jiang, P. Diévart, C.H. Sohn, Y. Ju, Self-sustaining n-heptane cool diffusion flames activated by ozone, Proc. Combust. Inst. 35 (2015) 881-888.

[29] K. Fieweger, R. Blumenthal, G. Adomeit, Self-ignition of S.I. engine model fuels: A shock tube investigation at high pressure, Combust. Flame 109 (1997) 599-619.

[30] R. Minetti, M. Carlier, M. Ribaucour, E. Therssen, L.R. Sochet, Comparison of oxidation and autoignition of the two primary reference fuels by rapid compression, Symp. (Int.) Combust. 26 (1996) 747-753.

[31] F. Contino, J-B Masurier, F. Foucher, T. Lucchini, G. D'Errico, P. Dagaut, CFD simulations using the TDAC method to model iso-octane combustion for a large range of ozone seeding and temperature conditions in a single cylinder HCCI engine, Fuel 137 (2014) 179-184.

[32] ANSYS Academic Chemkin-Pro, Release 20, ANSYS, Inc.

[33] J.O Hirschfelder, C.F. Curtiss, R.B. Bird, Molecular Theory of Gases and Liquids, John Wiley and Sons, New York, 1954.

[34] S. Chapman, T.G. Cowling, The Mathematical Theory of Non-Uniform Gases, Cambridge, University Press, Cambridge, 1970.

[35] T.P. Coffee, J.M. Heimerl, Transport algorithms for premixed, laminar steady-state flames, Combust. Flame 43 (1981) 273-289.

[36] G.P. Smith, D.M. Golden, M. Frenklach, N.W. Moriarty, B. Eiteneer, M. Goldenberg, C.T. Bowman, R.K. Hanson, S. Song, W.C. Gardiner Jr., V.V. Lissianski, Z. Qin. <http://www.me.berkeley.edu/gri_mech/>.

[37] M.B. Luong, Z. Luo, T.F. Lu, S.H. Chung, C.S. Yoo, Direct numerical simulations of the ignition of lean primary reference fuel/air mixtures with temperature inhomogeneities, Combust. Flame 160 (2013) 2038–2047.

[38] L. Cai, H. Pitsch, Optimized chemical mechanism for combustion of gasoline surrogate fuels, Combust. Flame 162 (2015) 1623-1637.

[39] H.J. Curran, P. Gaffuri, W.J. Pitz, C.K. Westbrook, A comprehensive modeling study of iso-octane oxidation, Combust. Flame 129 (2002) 253-280.

[40] P. Saxena, F.A. Williams, Numerical and Experimental Studies of Ethanol Flames, Proc. Combust. Inst. 31 (2007) 1149–1156.

[41] S.G. Davis, C.K. Law, Laminar flame speeds and oxidation kinetics of iso-octane-air and n-heptane-air flames, Symp. (Int.) Combust. 27 (1998) 521-527.

[42] Y. Huang, C.J. Sung, J.A. Eng, Laminar flame speeds of primary reference fuels and reformer gas mixtures, Combust. Flame 139 (2004) 239-251.

[43] K. Kumar, J.E. Freeh, C.J. Sung, Y. Huang, Laminar Flame Speeds of Preheated iso-Octane/O2/N2 and n-Heptane/O2/N2 Mixtures, J. Propuls. Power 23 (2007).

[44] J.PJ. Lipzig, E.J.K. Nilsson, L.P.H. de Goey, A.A. Konnov, Laminar burning velocities of n-heptane, iso-octane, ethanol and their binary and tertiary mixtures, Fuel 90 (2011) 2773-2781.

[45] A.P. Kelley, W. Liu, Y.X. Xin, A.J. Smallbone, C.K. Law, Laminar flame speeds, non-premixed stagnation ignition, and reduced mechanisms in the oxidation of iso-octane, Proc. Combust. Inst. 33 (2011) 501-508.

[46] J.X. Zhou, M. Cordier, C. Mounaïm-Rousselle, F. Foucher, Experimental estimate of the laminar burning velocity of iso-octane in oxygen-enriched and CO2-diluted air, Combust. Flame 158 (2011) 2375-2383.

[47] D. Bradley, R.A. Hicks, M. Lawes, C.G.W. Sheppard, R. Woolley, The Measurement of Laminar Burning Velocities and Markstein Numbers for Iso-octane–Air and Iso-octane–n-Heptane–Air Mixtures at Elevated Temperatures and Pressures in an Explosion Bomb, Combust. Flame 115 (1998) 126-144.

[48] C. Mandilas, M.P. Ormsby, C.G.W. Sheppard, R. Woolley, Effects of hydrogen addition on laminar and turbulent premixed methane and iso-octane–air flames. Proc. Combust. Inst 31 (2007) 1443-1450.

Figure 1

Click here to access/download;Figure;Fig.1.png

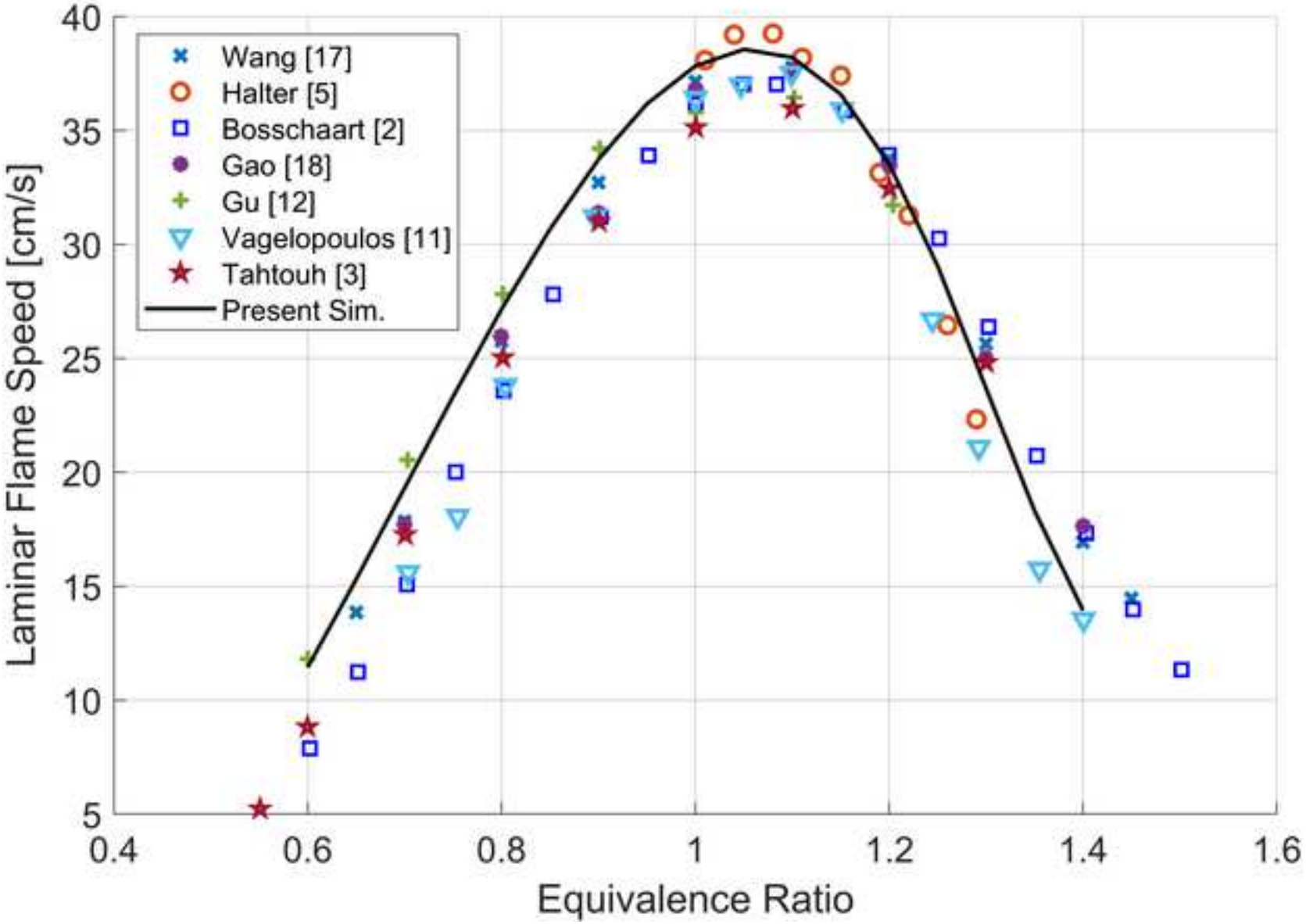

Figure 2a

Click here to access/download;Figure;Fig.2a.png

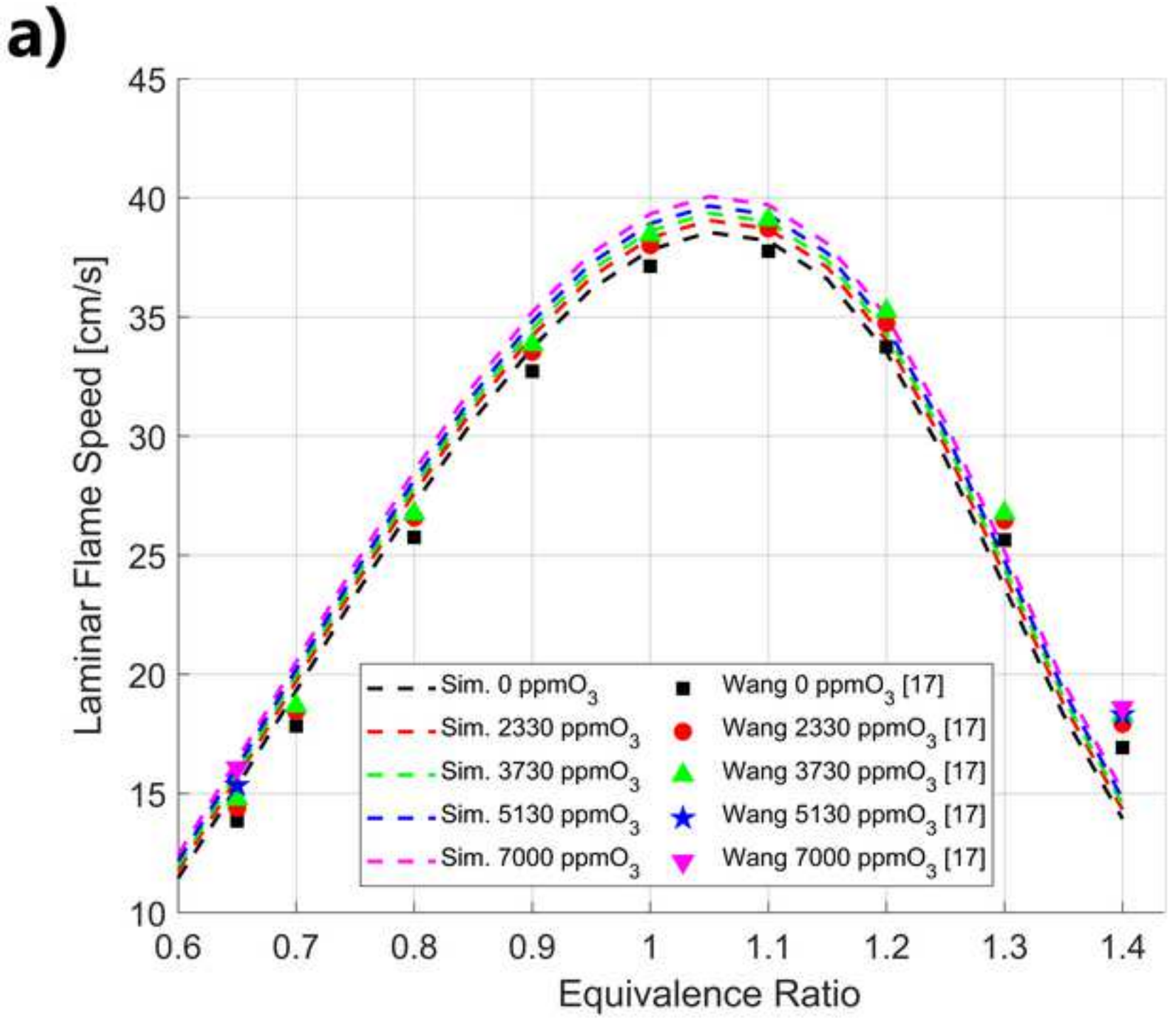

Figure 2b

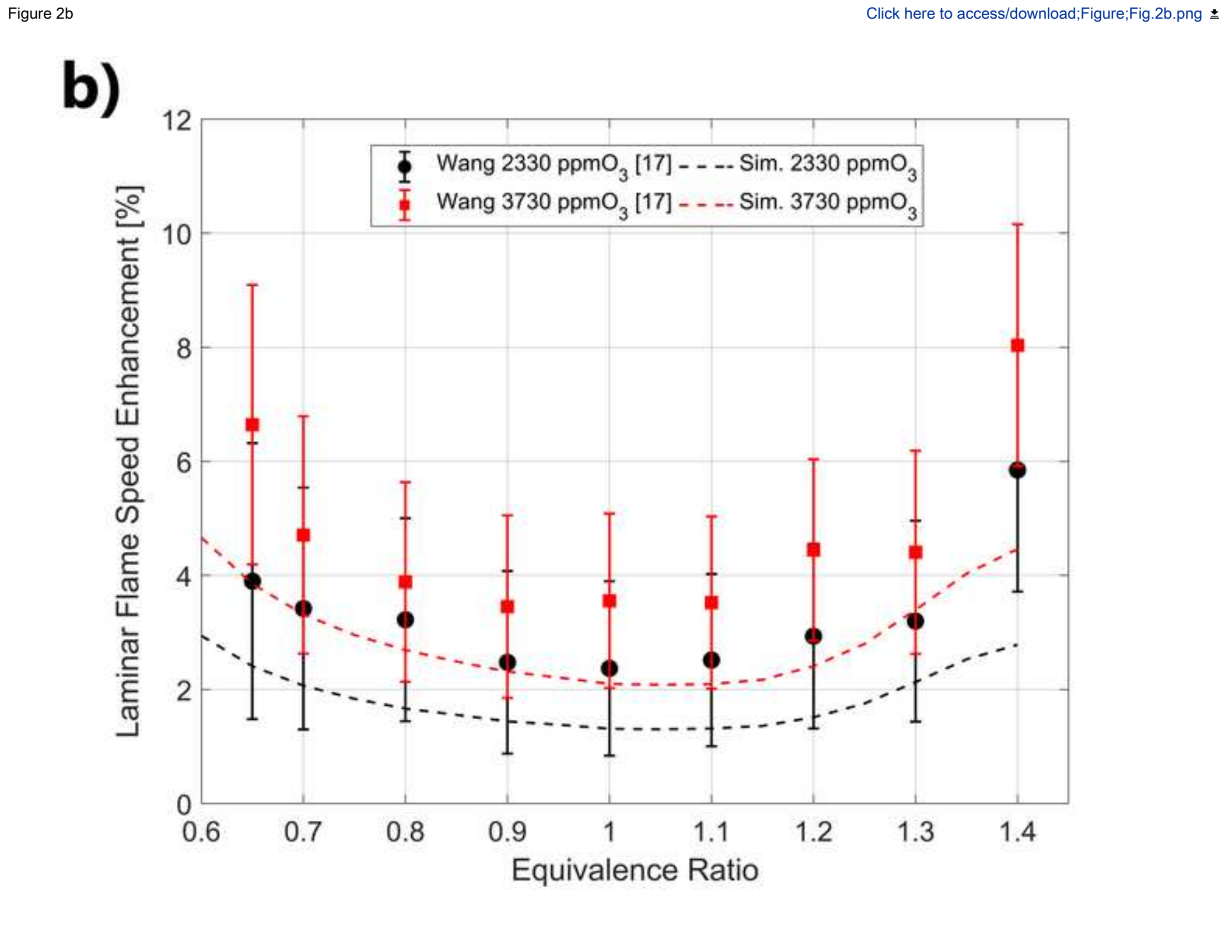

Figure 3a

Click here to access/download;Figure;Fig.3a.png

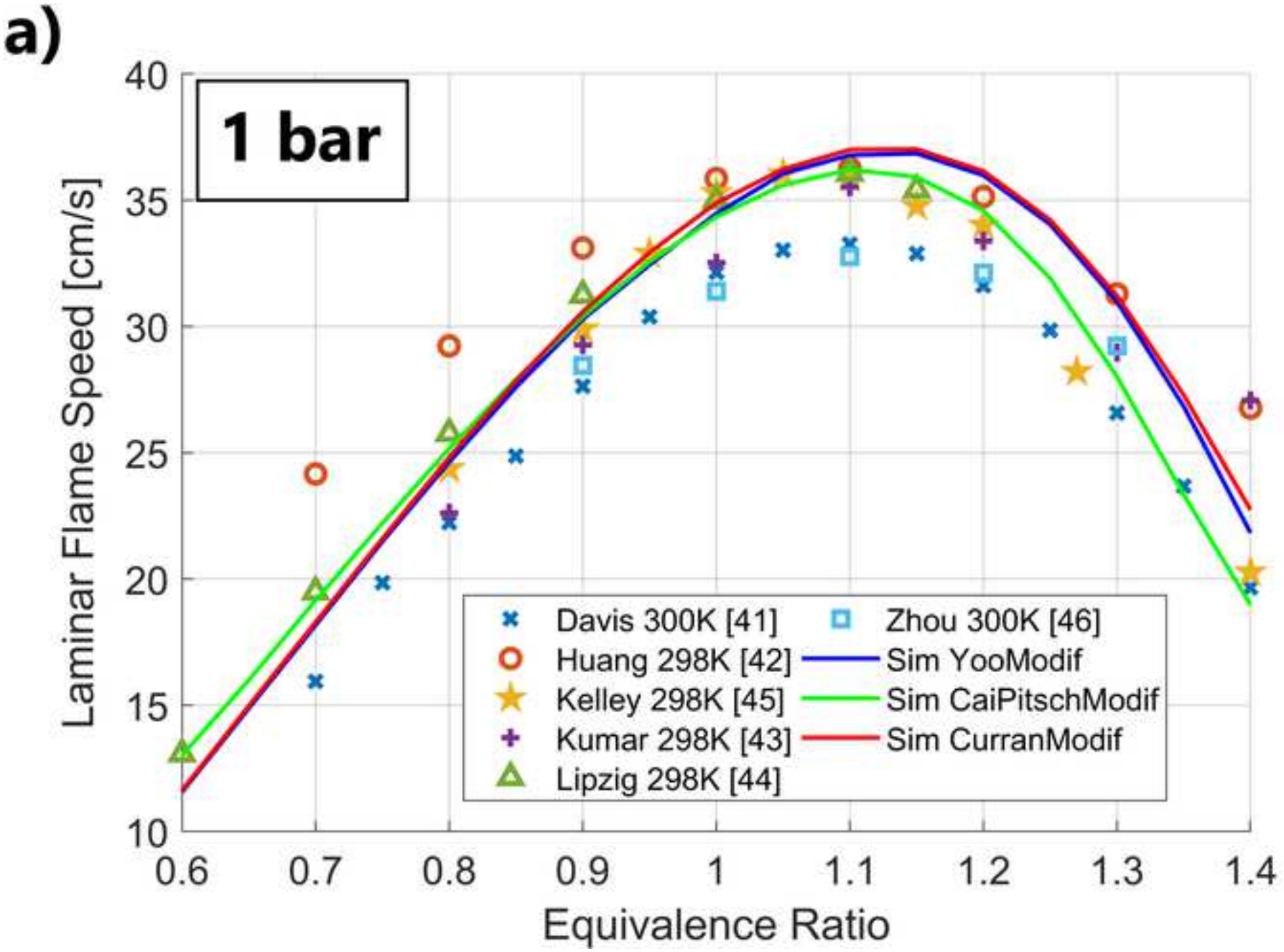

Figure 3b

Click here to access/download;Figure;Fig.3b.png

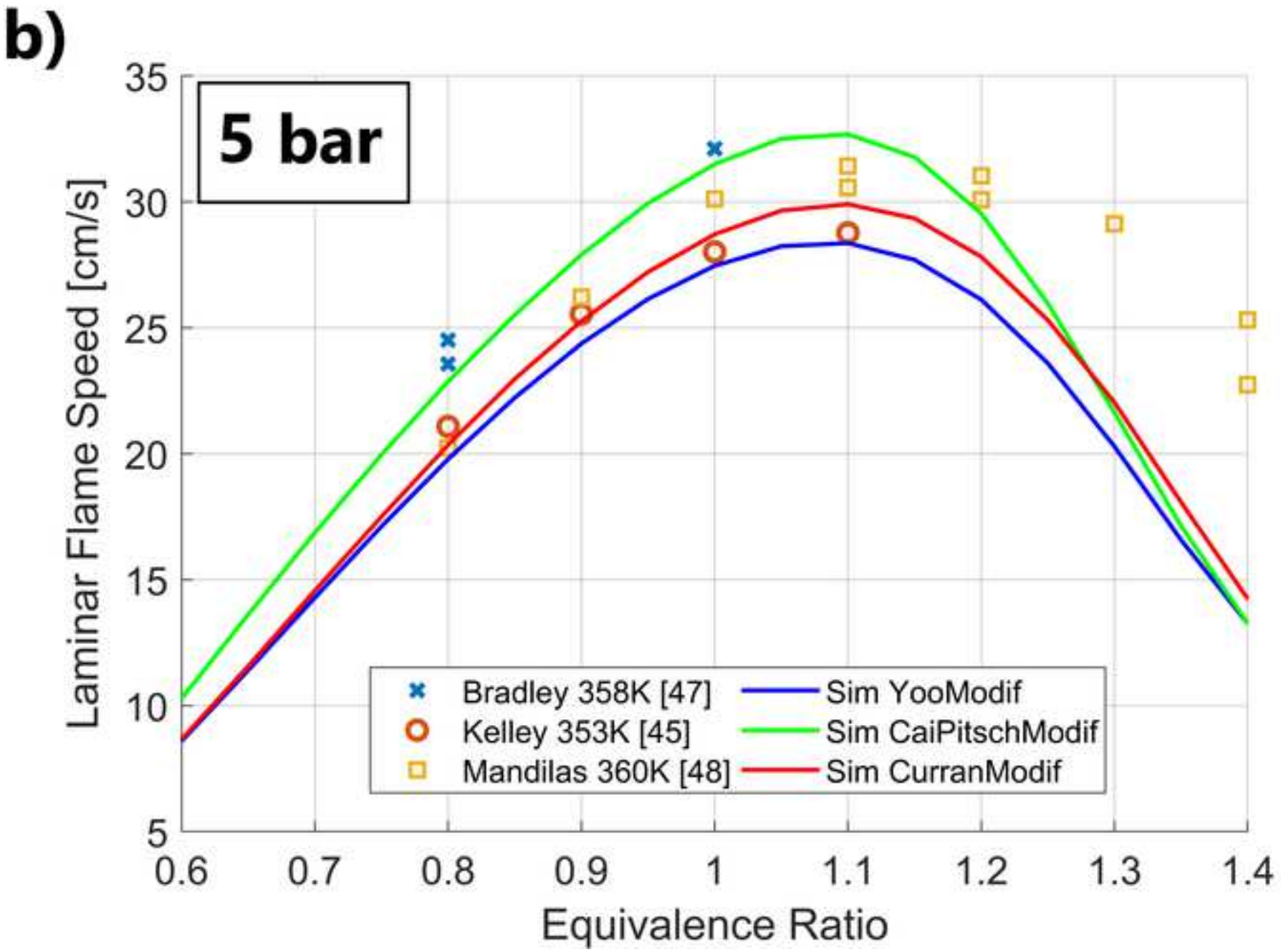

Figure 3c

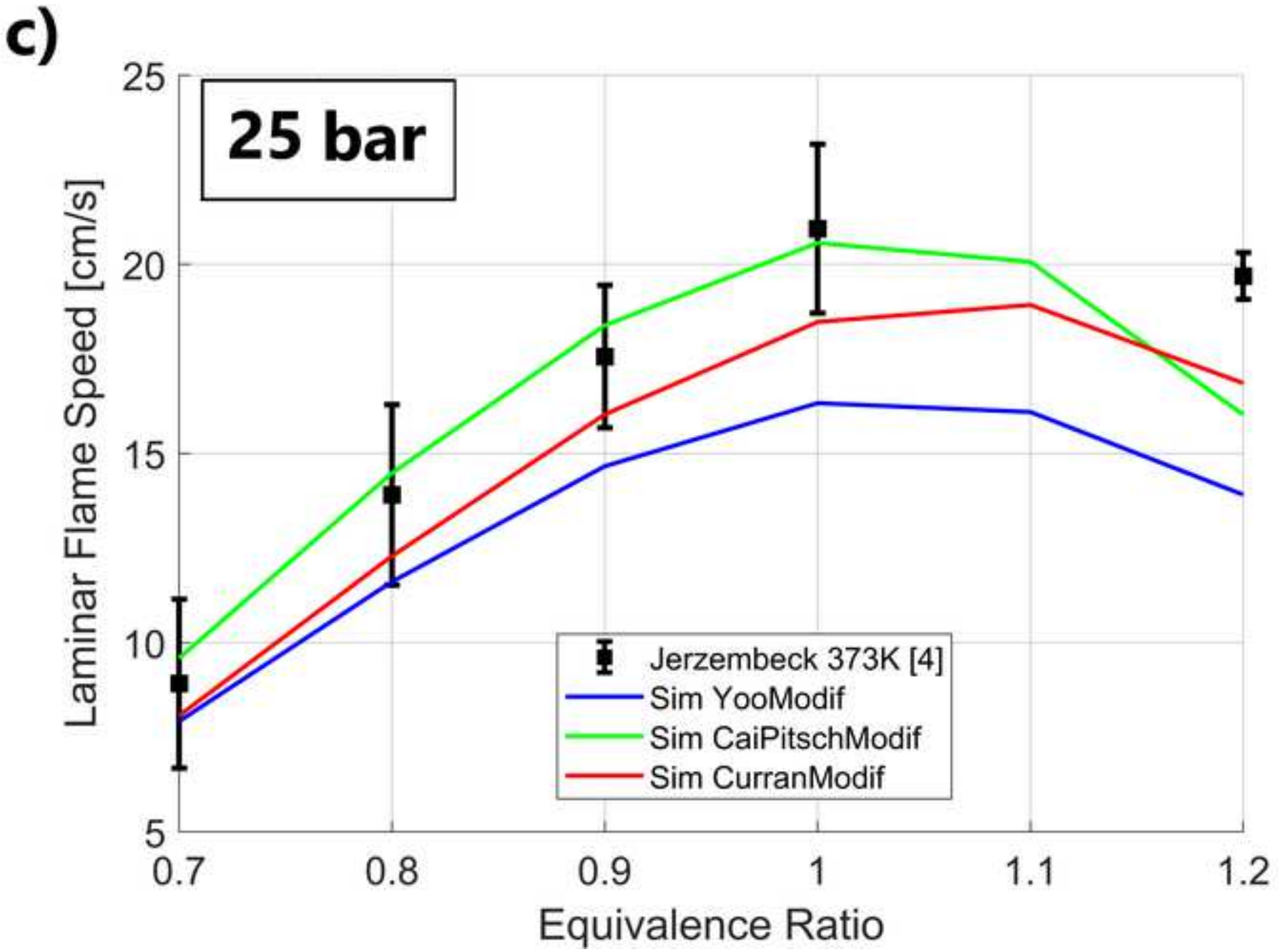

Figure 4

Click here to access/download;Figure;Fig.4.png

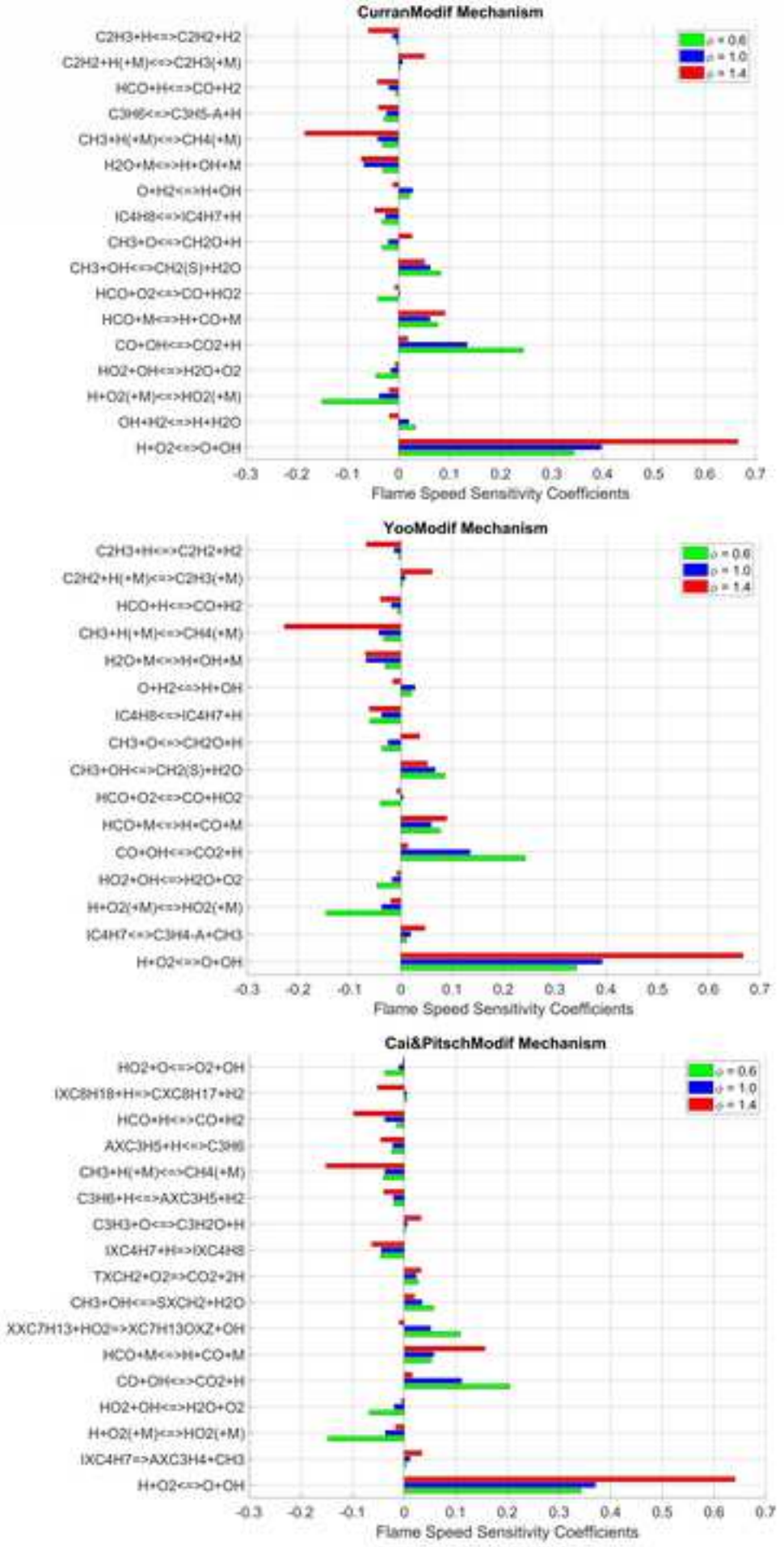

Figure 5a

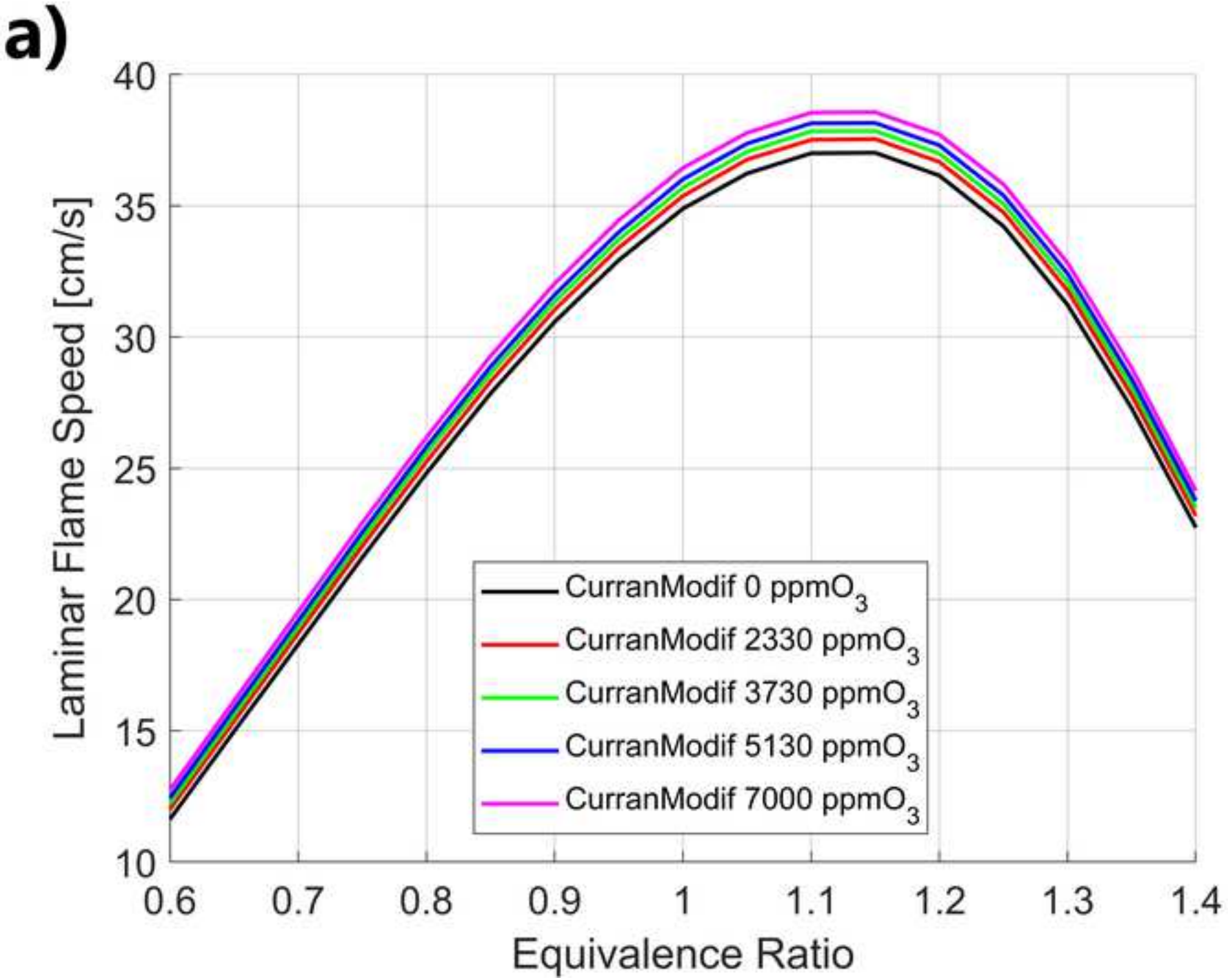

Figure 5b

Click here to access/download;Figure;Fig.5b.png

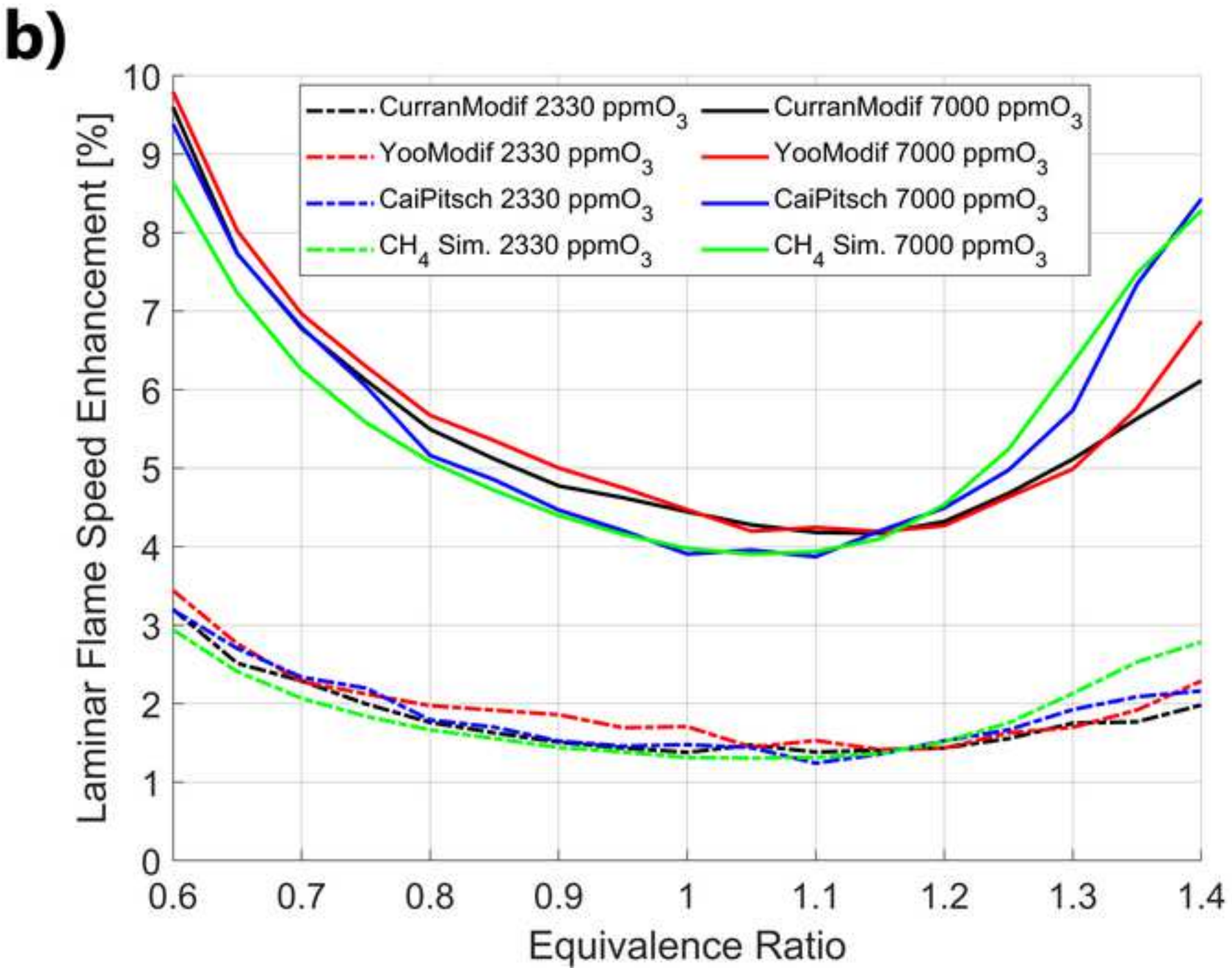

Figure 6a

Click here to access/download;Figure;Fig.6a.png

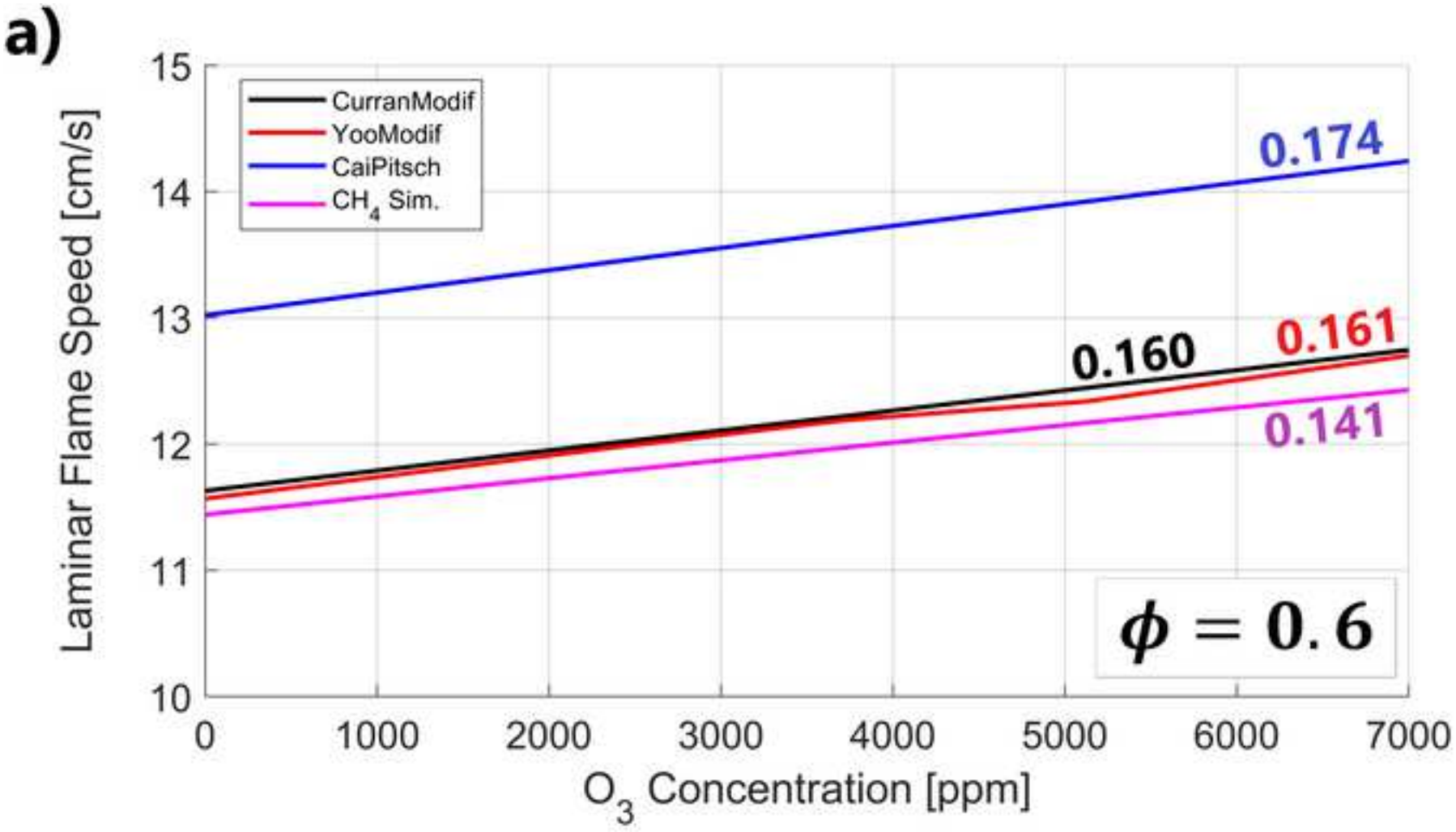

Figure 6b

Click here to access/download;Figure;Fig.6b.png

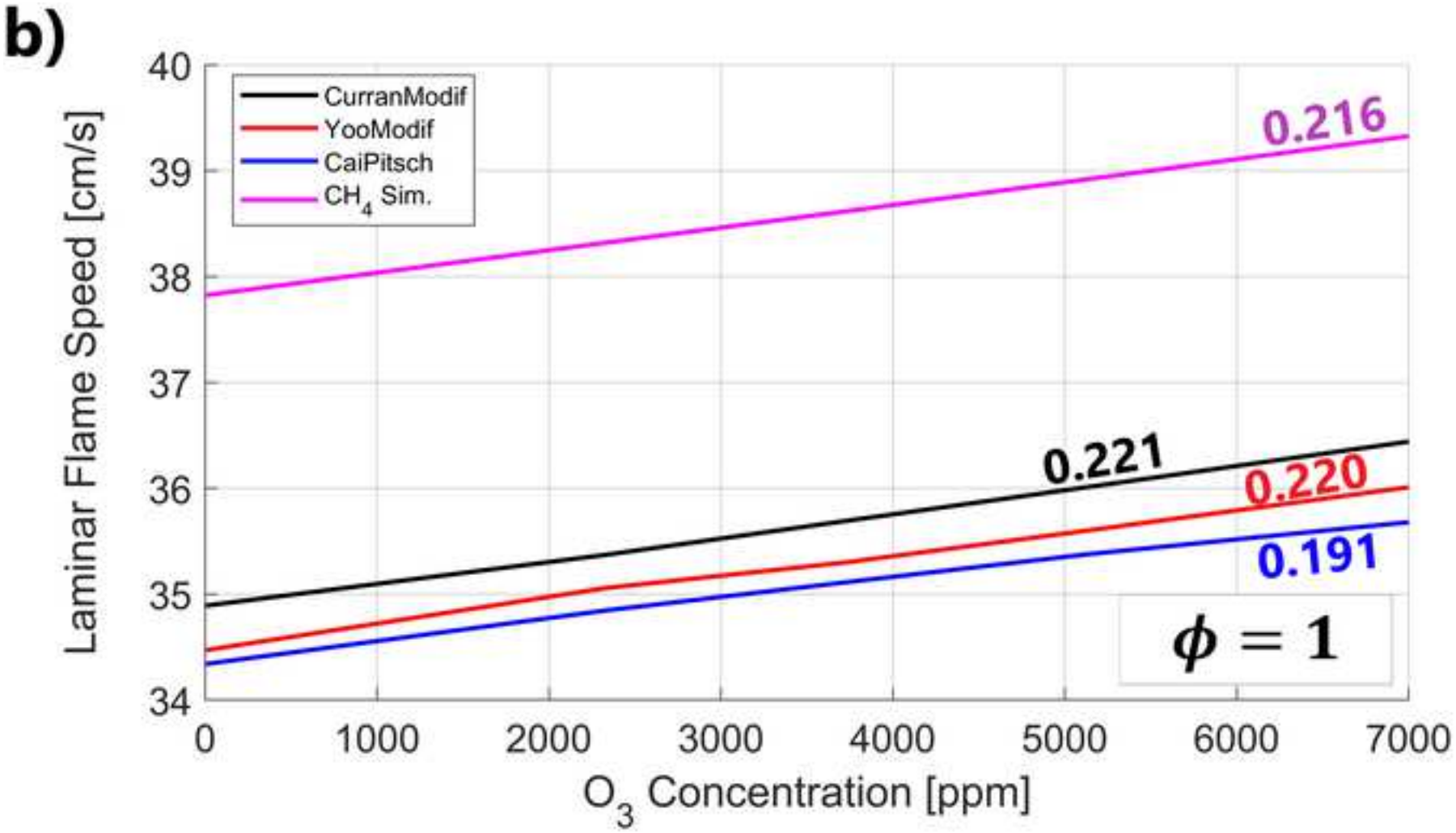

Figure 6c

Click here to access/download;Figure;Fig.6c.png

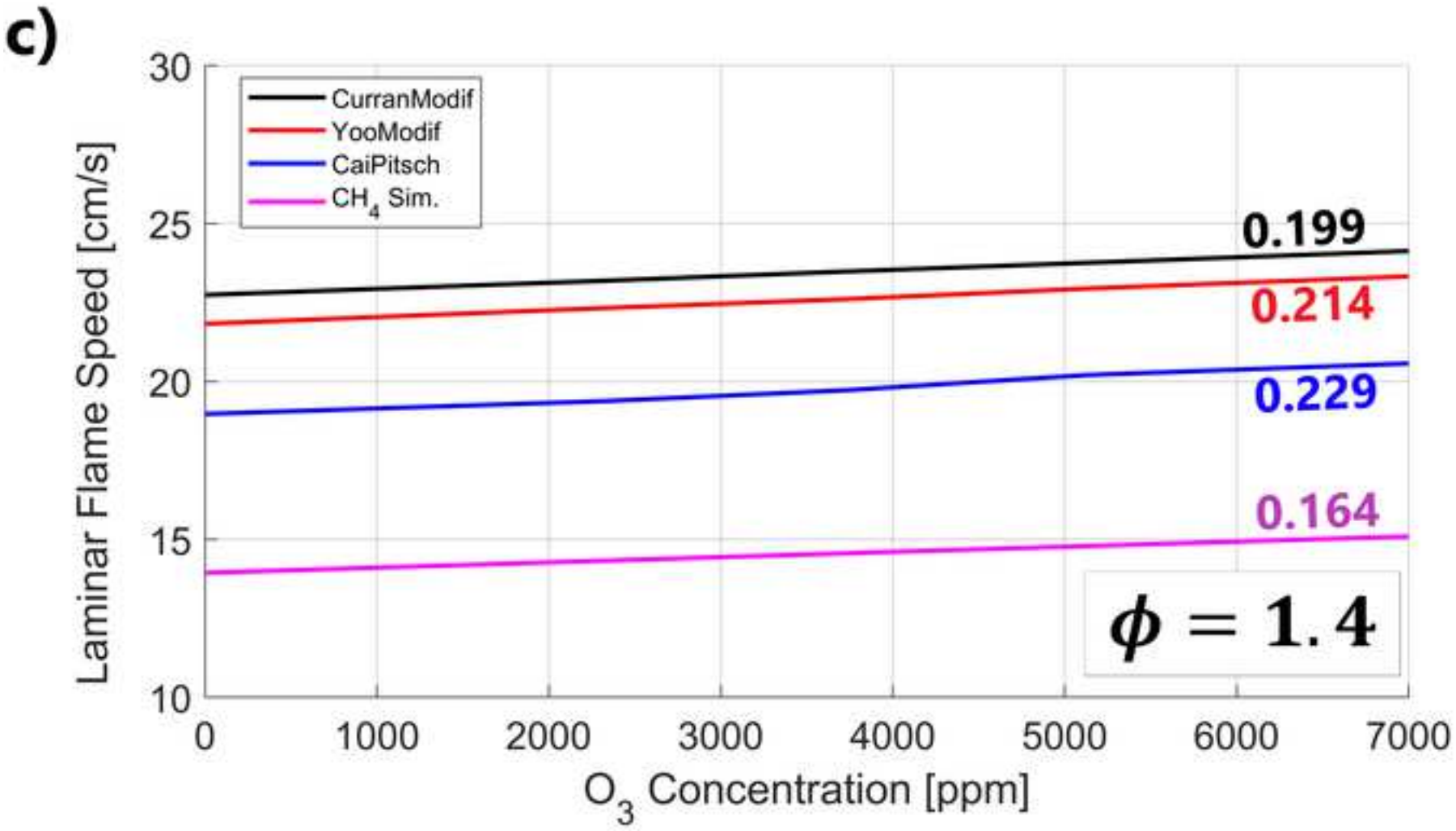

Figure 7a

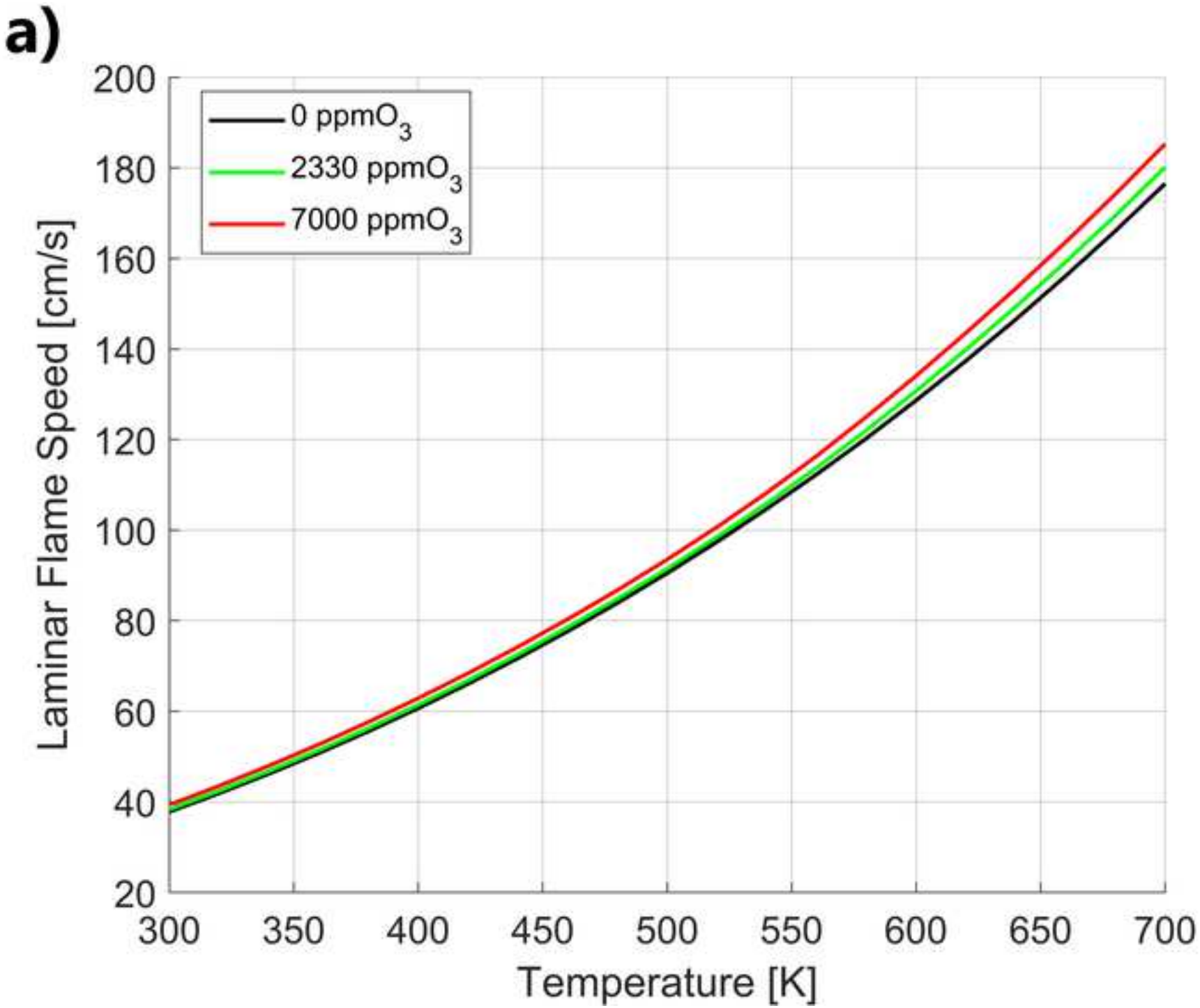

Figure 7b

Click here to access/download;Figure;Fig.7b.png

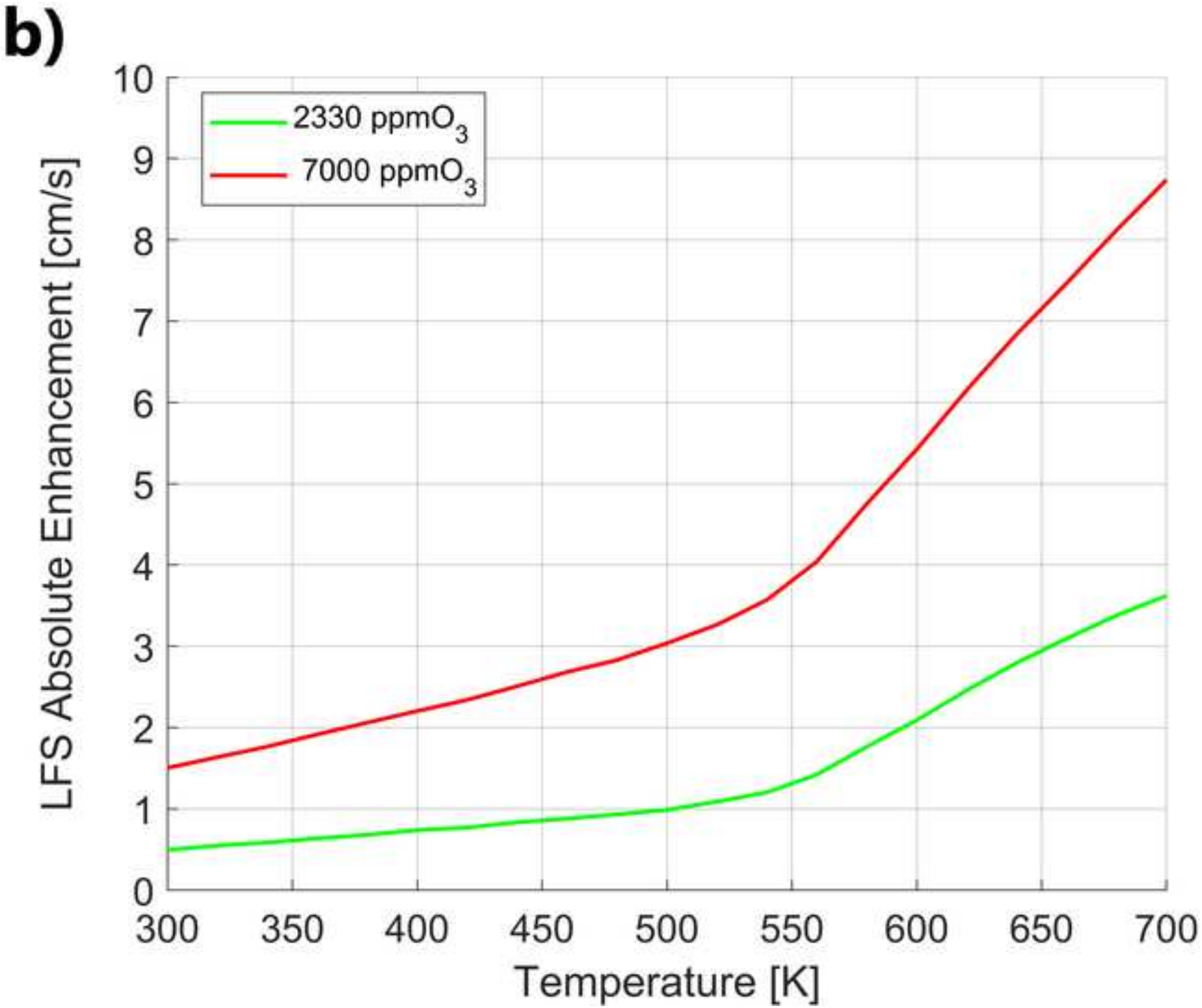

Figure 7c

Click here to access/download;Figure;Fig.7c.png

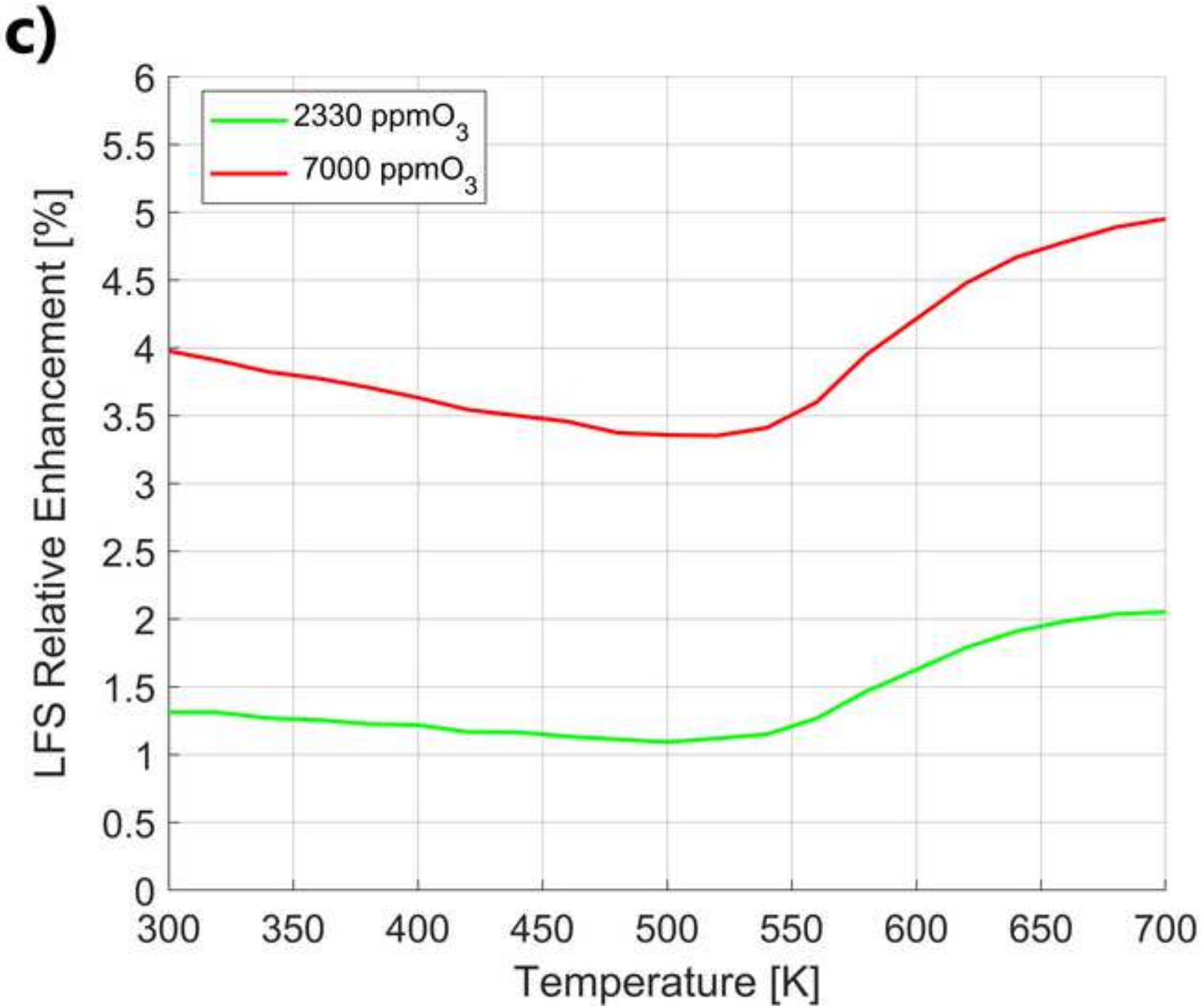

Figure 8a

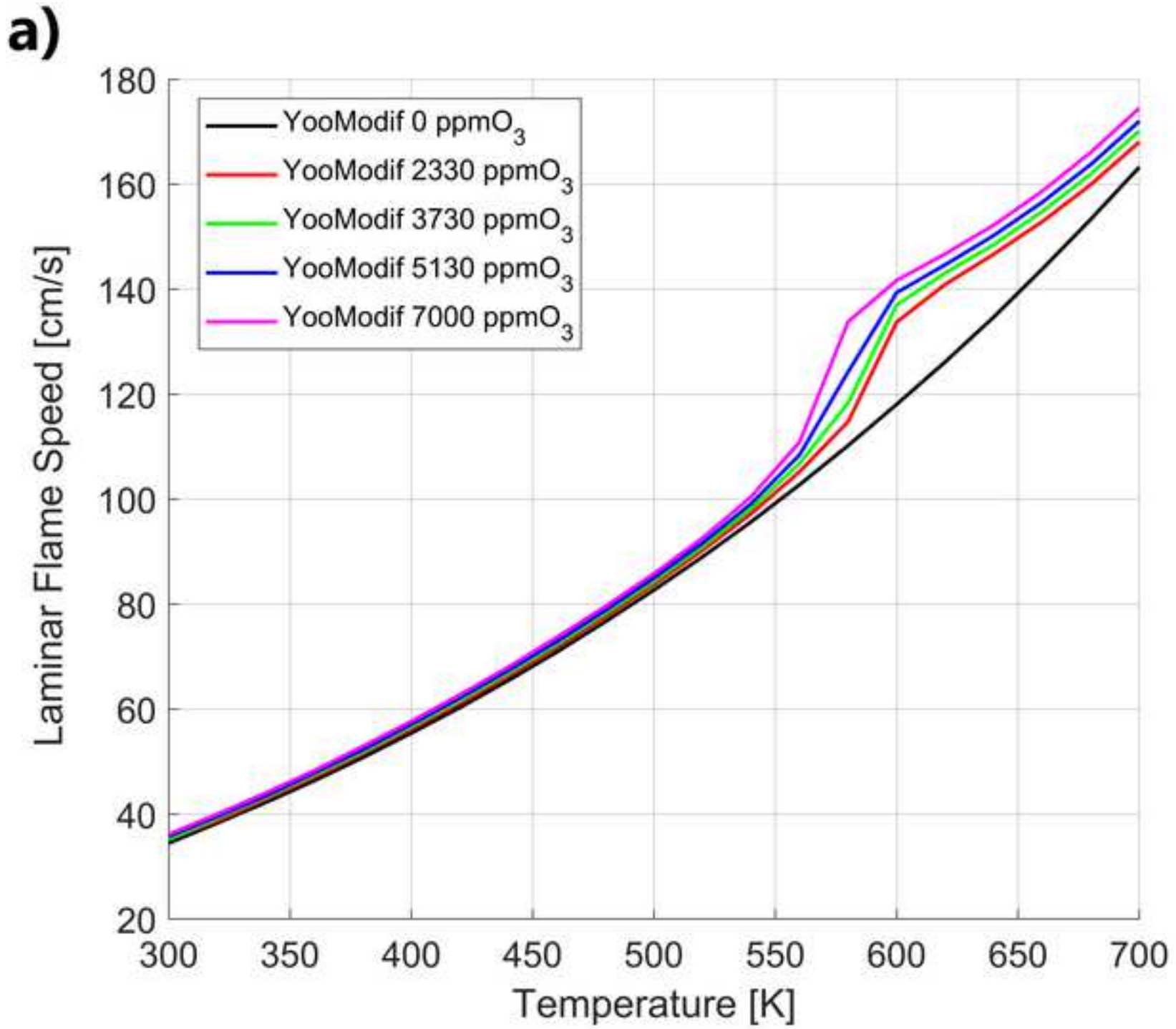

Figure 8b

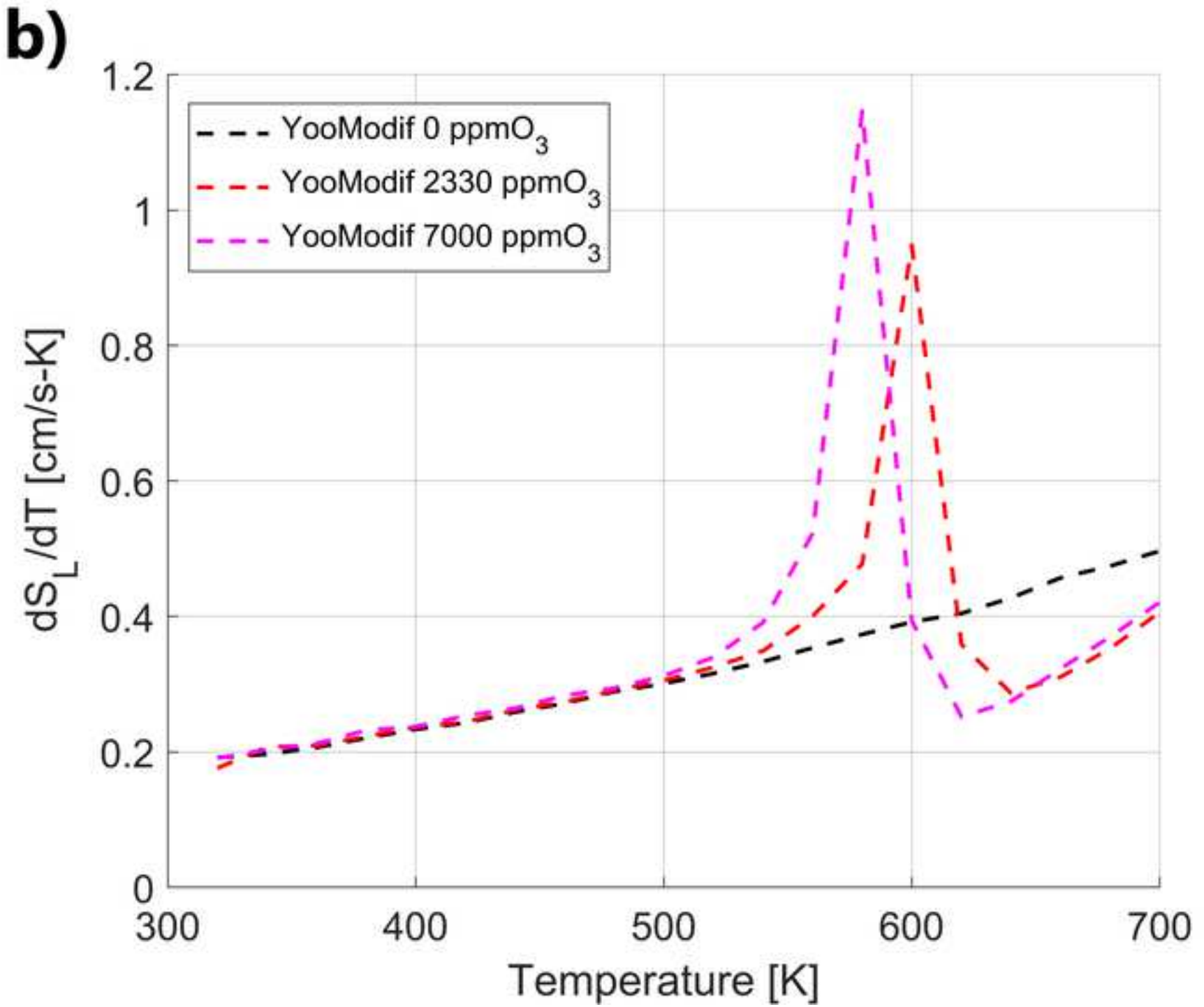

Figure 8c

Click here to access/download;Figure;Fig.8c.png

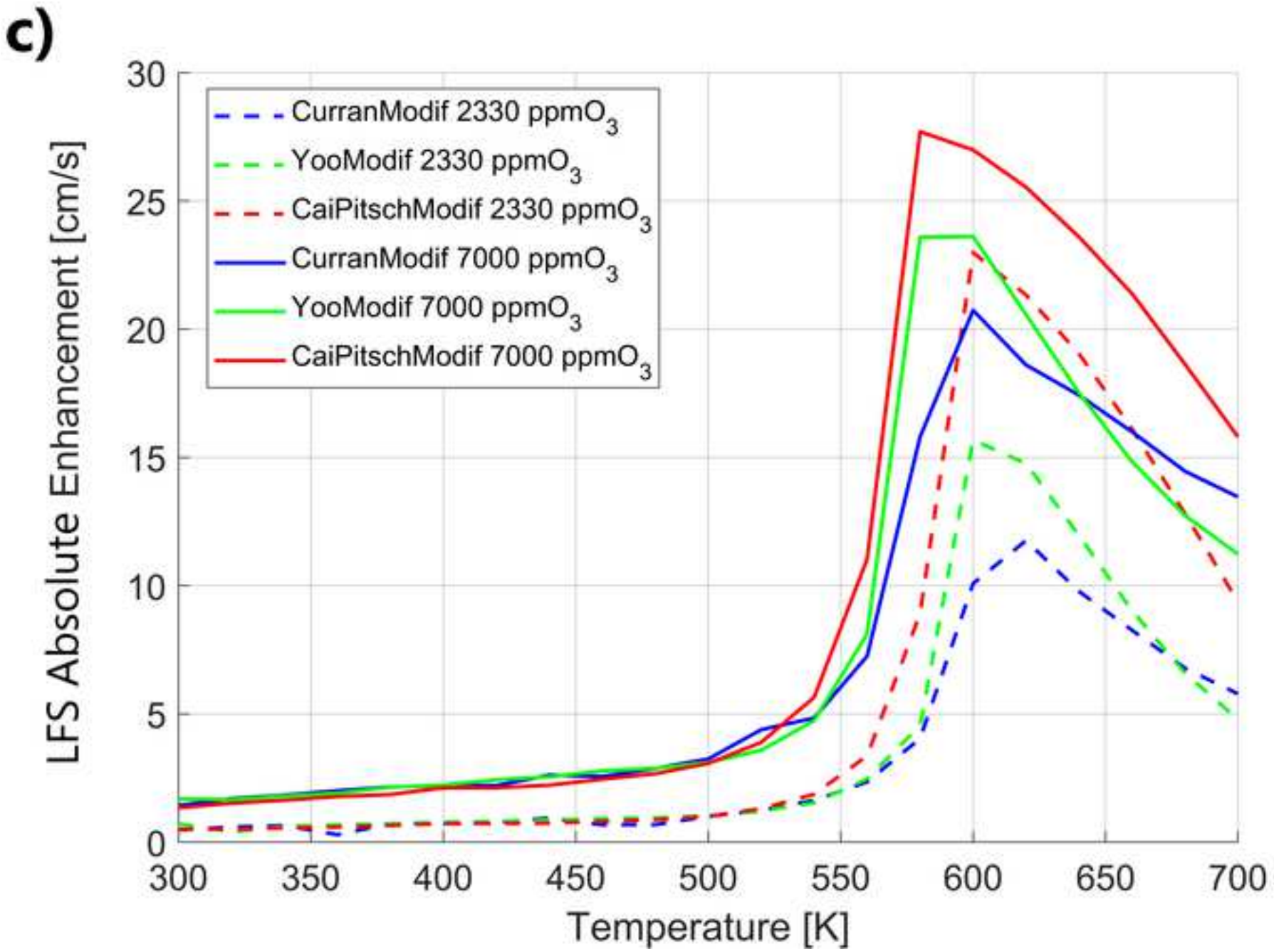

Figure 8d

Click here to access/download;Figure;Fig.8d.png

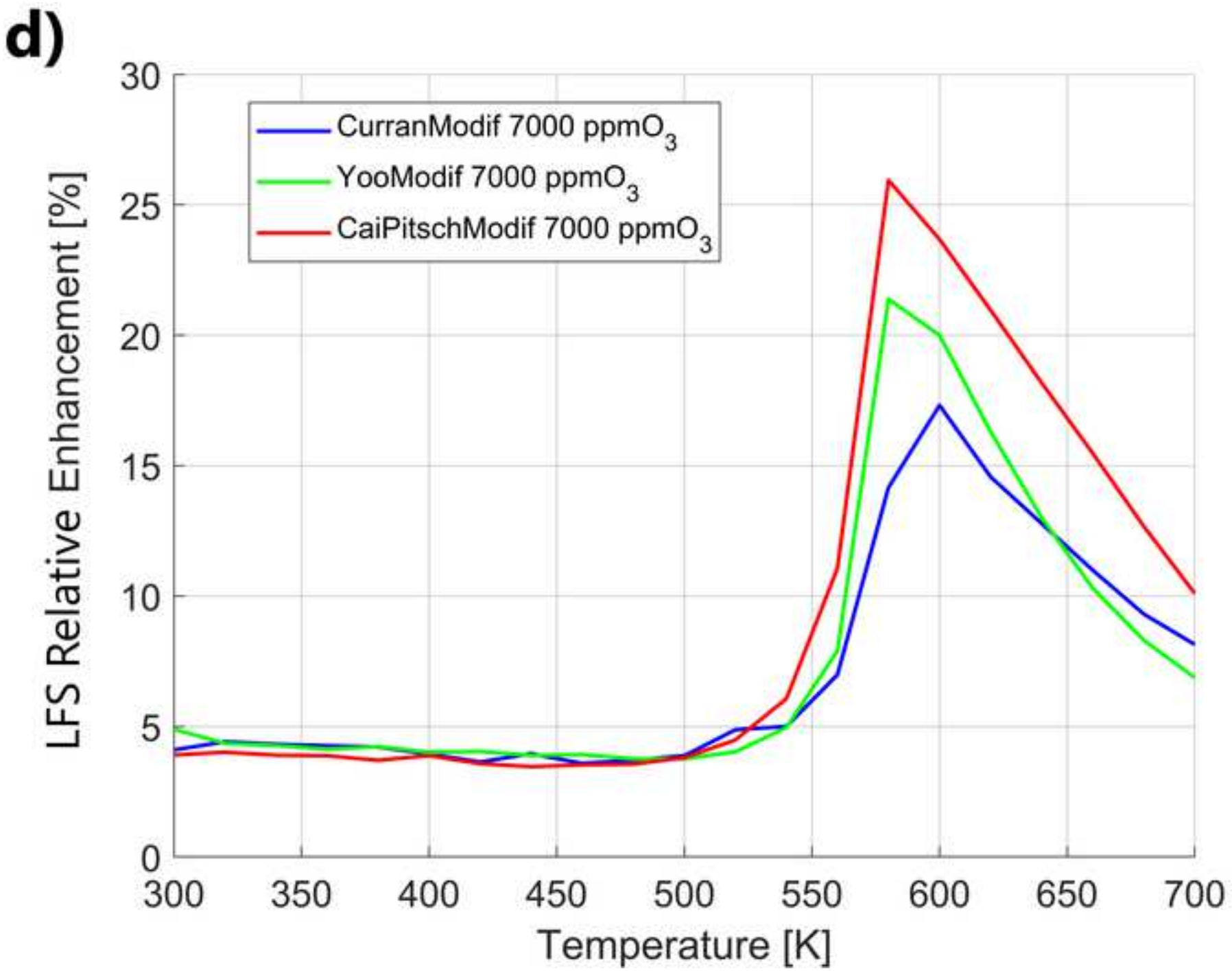

Figure 9a

Click here to access/download;Figure;Fig.9a.png

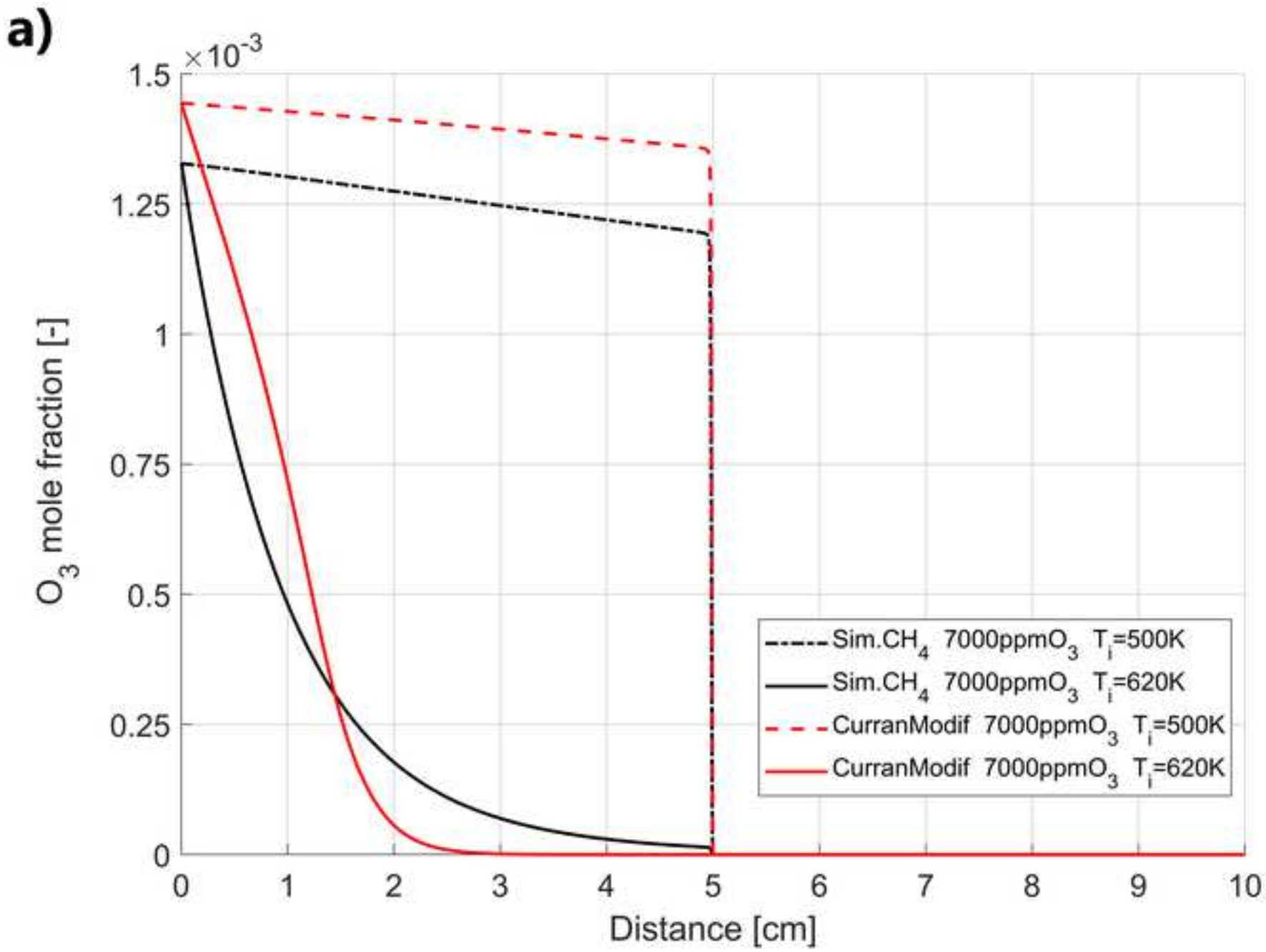

Figure 9b

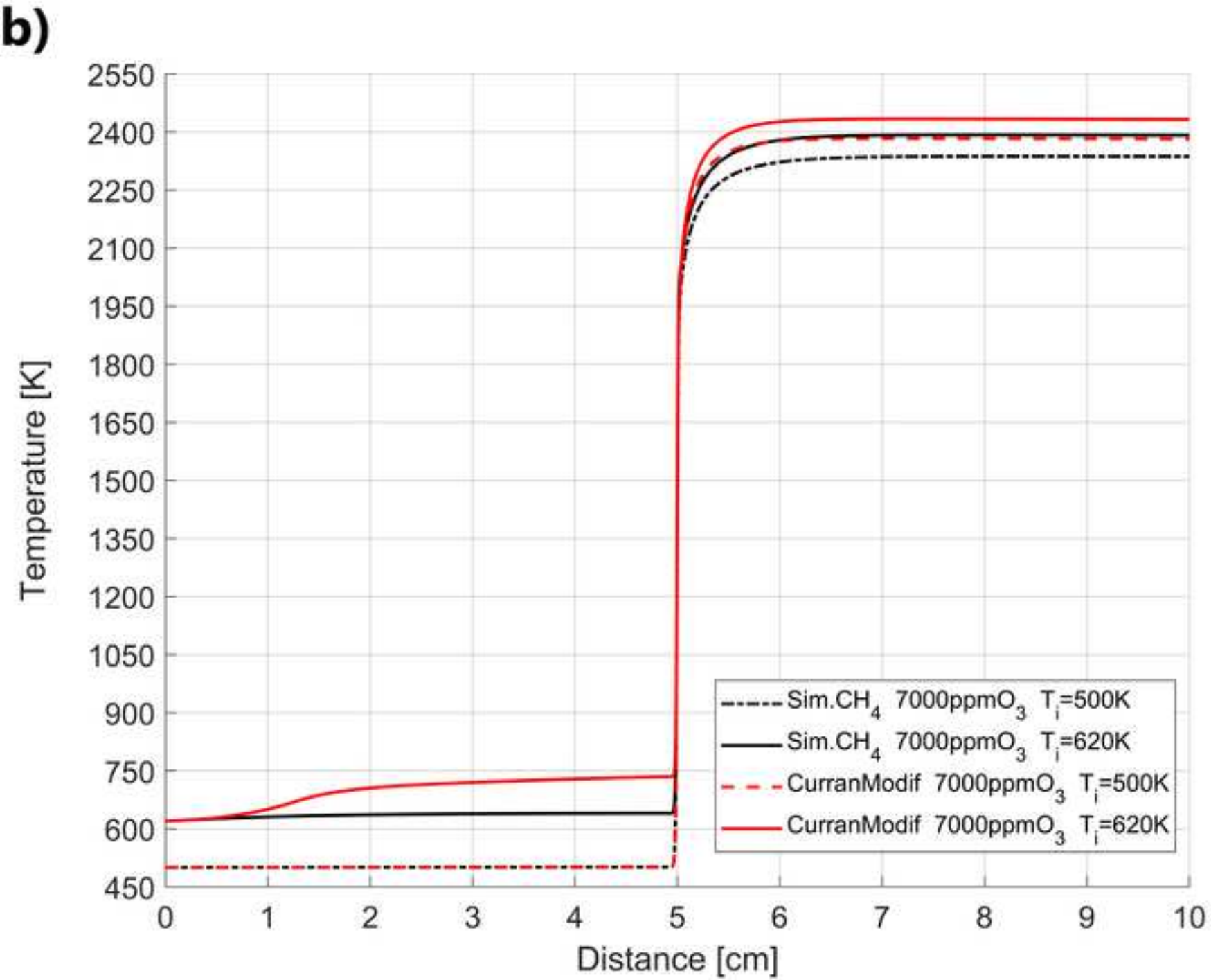

Figure 9c

Click here to access/download;Figure;Fig.9c.png

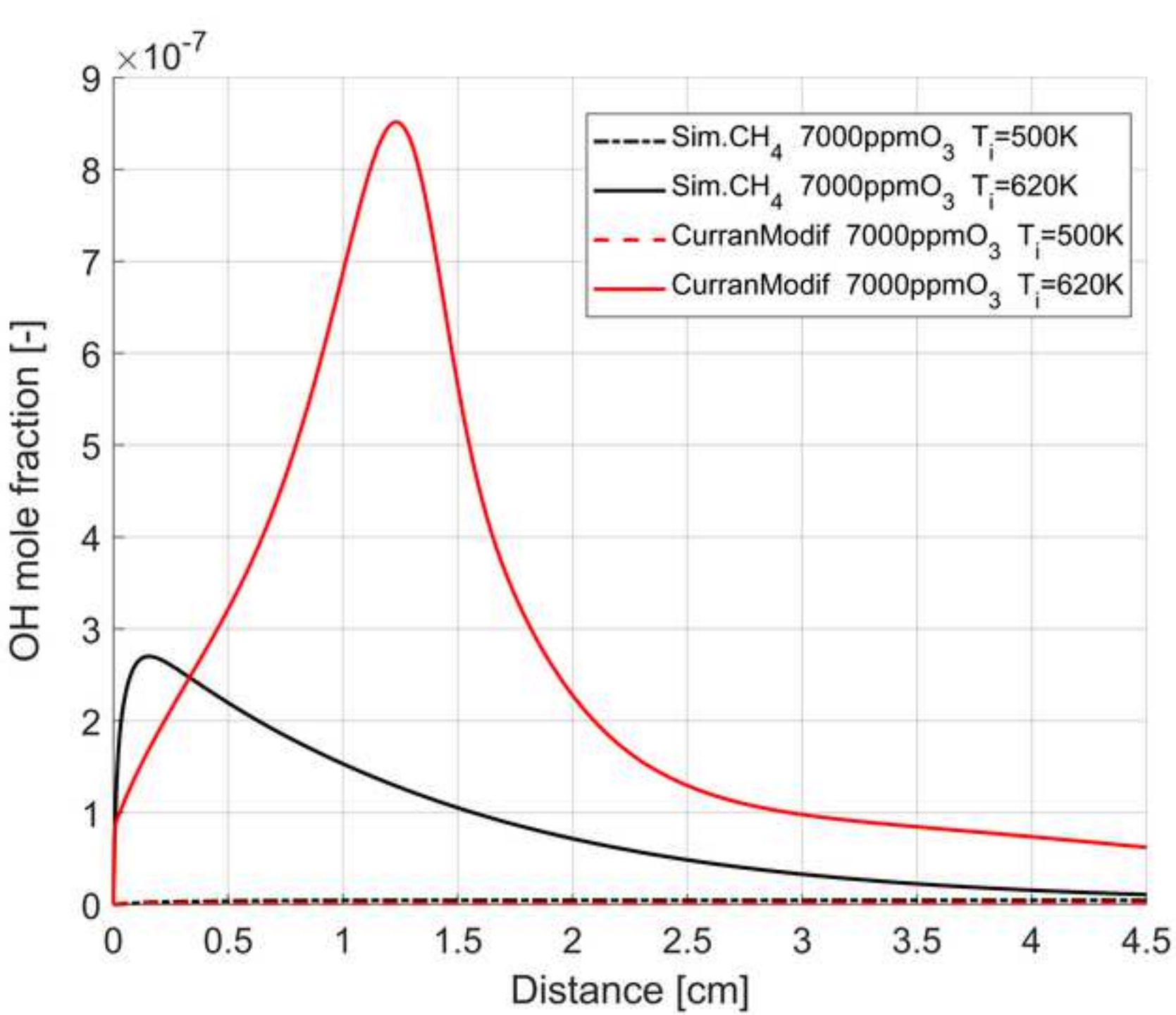

Figure 10a

Click here to access/download;Figure;Fig.10a.png

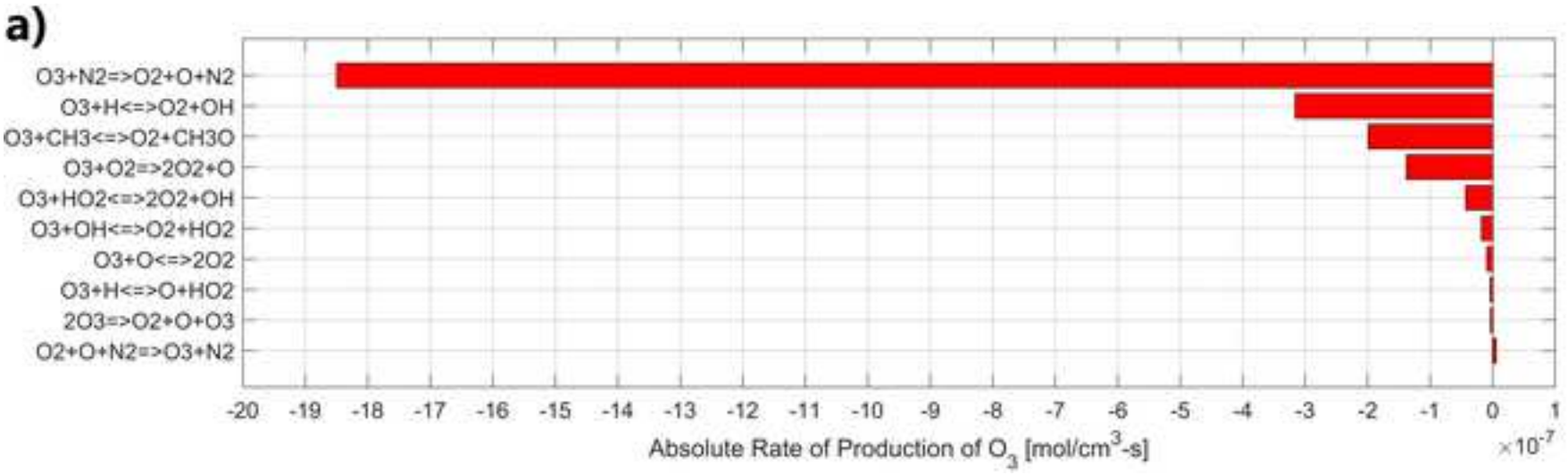

Figure 10b

Click here to access/download;Figure;Fig.10b.png

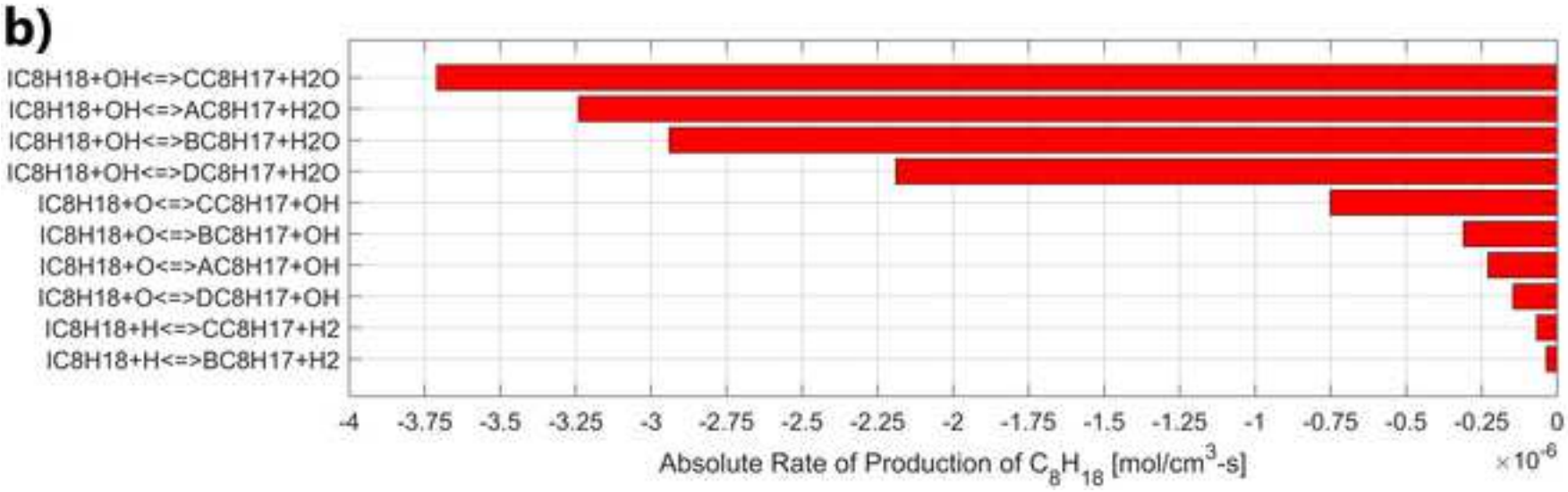

Figure 10c

Click here to access/download;Figure;Fig.10c.png

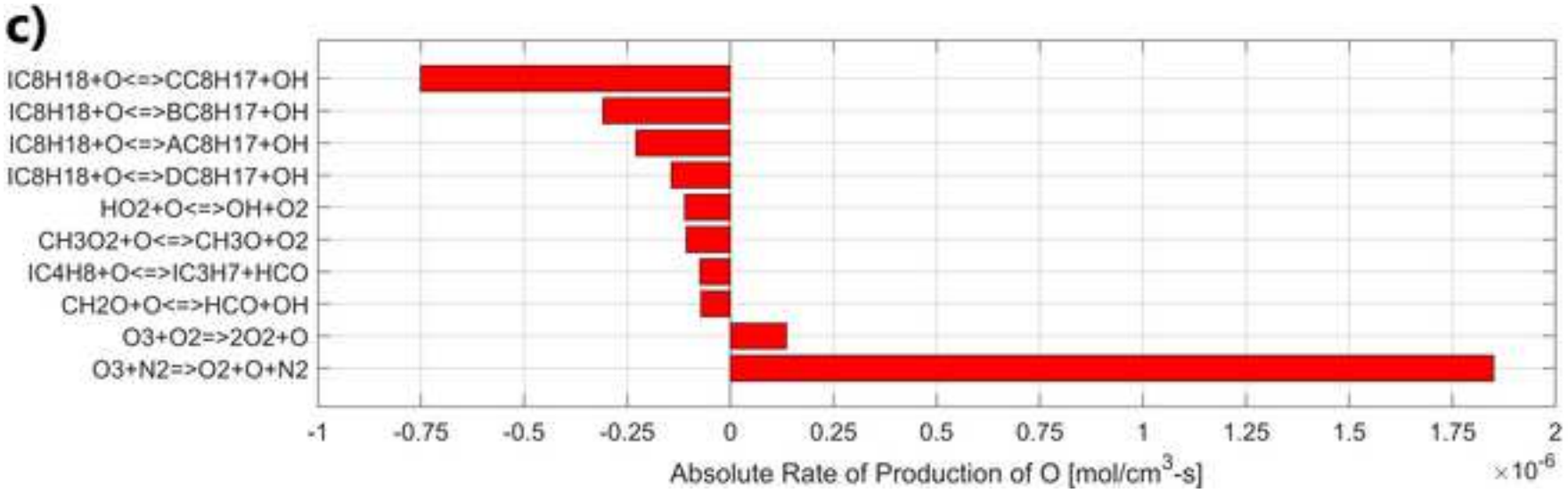

Figure 10d

Click here to access/download;Figure;Fig.10d.png

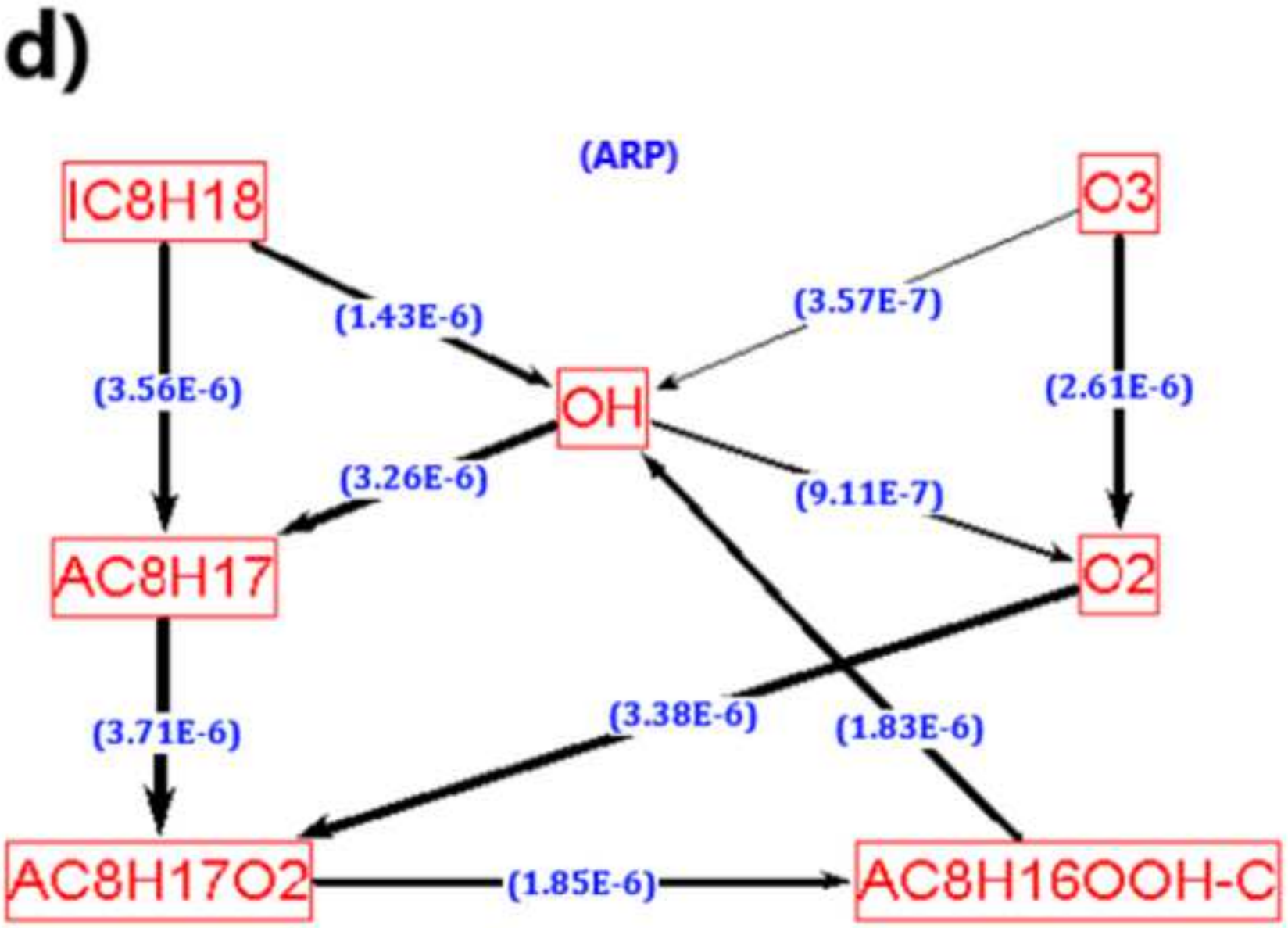

Figure 10e

Click here to access/download;Figure;Fig.10e.png

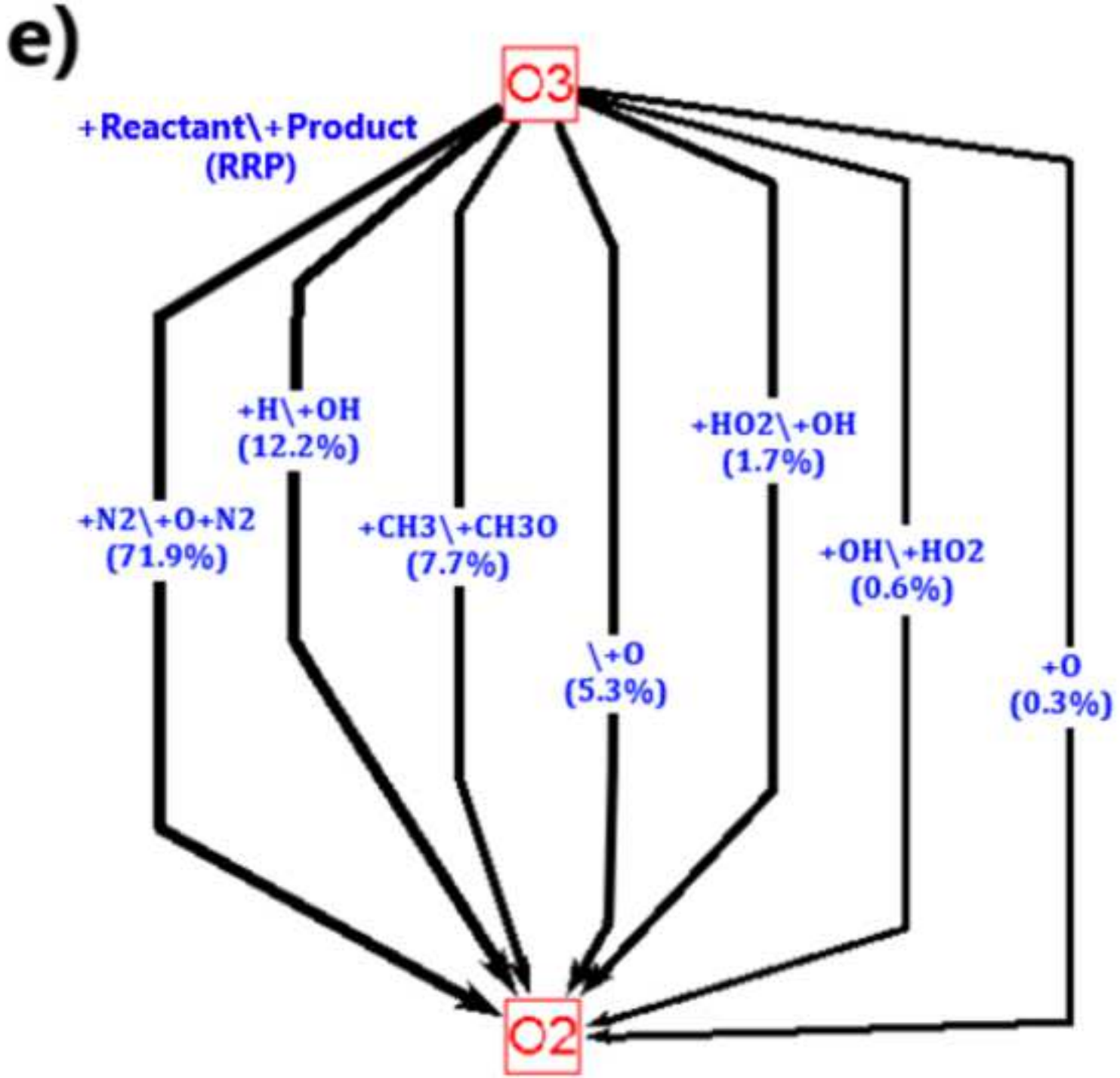

Figure 11a

Click here to access/download;Figure;Fig.11a.png

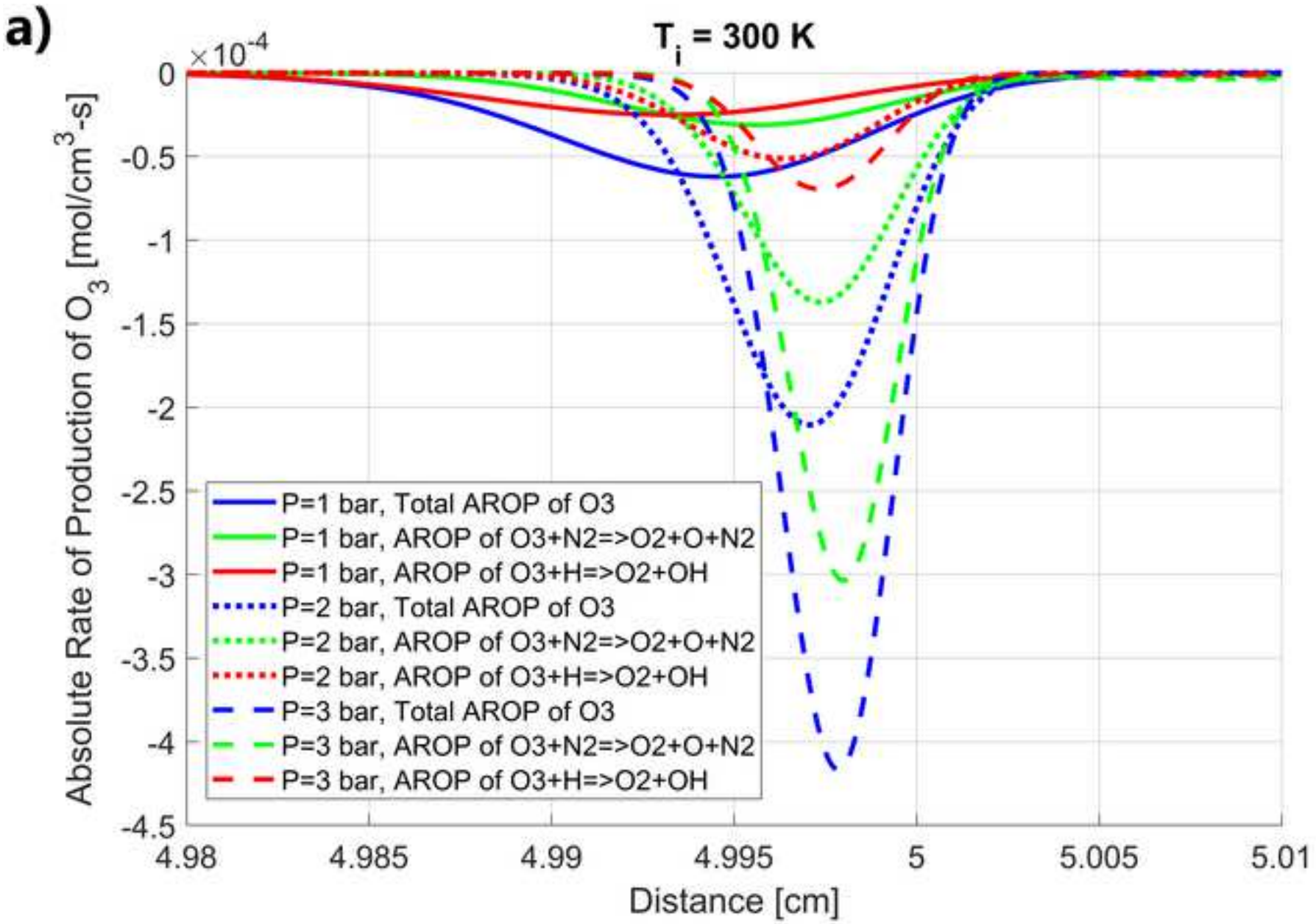

Figure 11b

Click here to access/download;Figure;Fig.11b.png

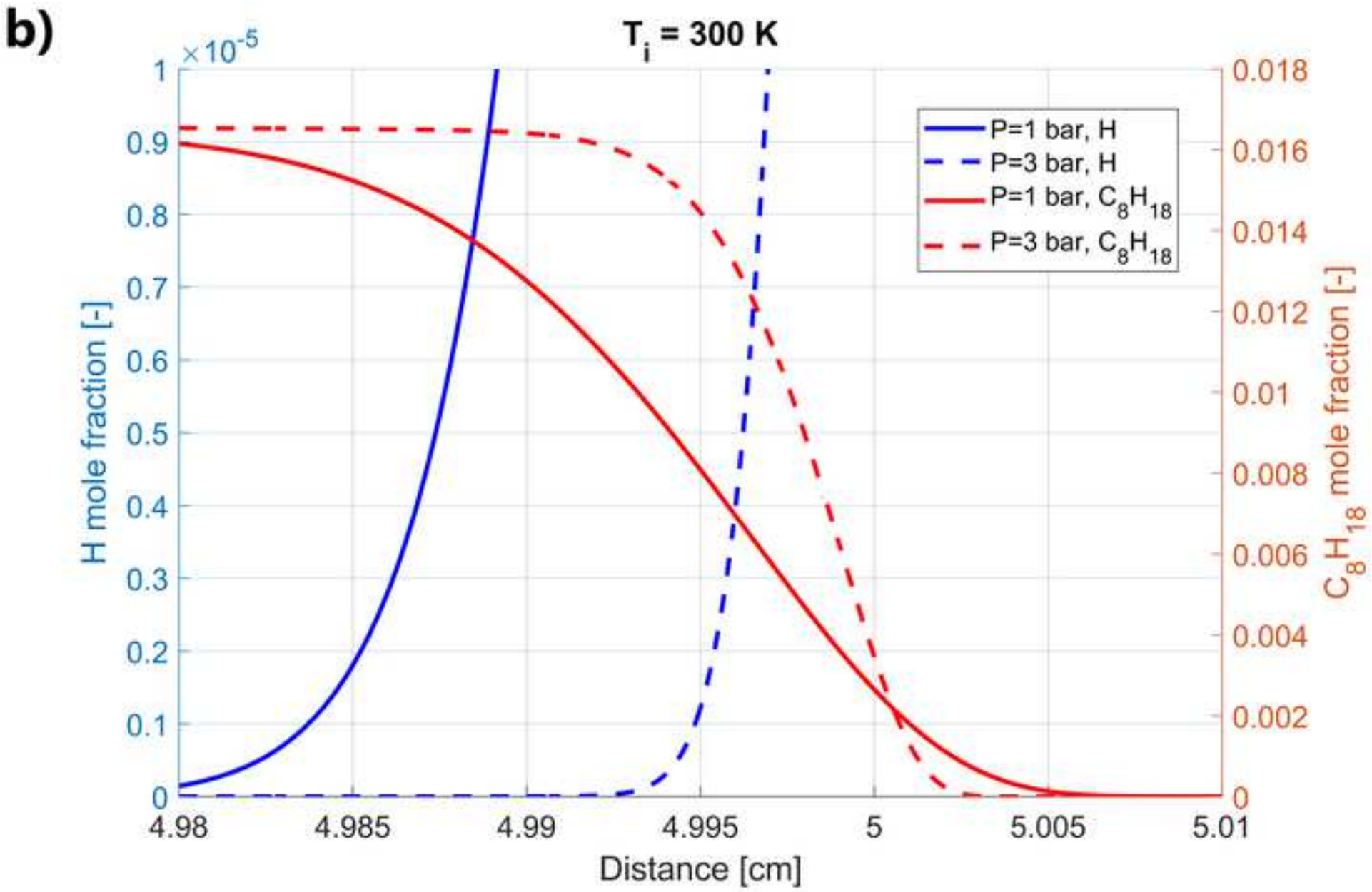

Figure 11c

Click here to access/download;Figure;Fig.11c.png

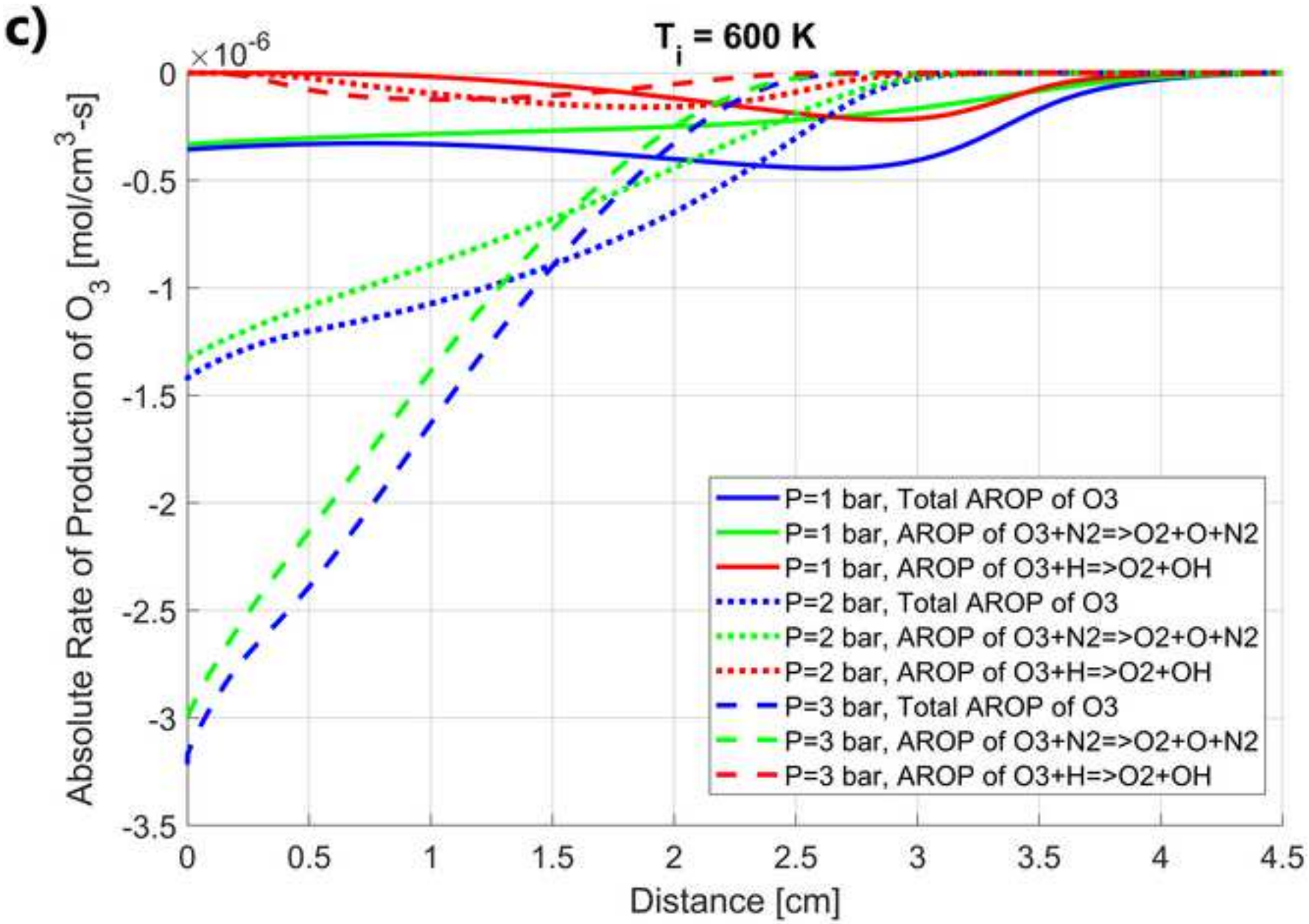

Figure 11d

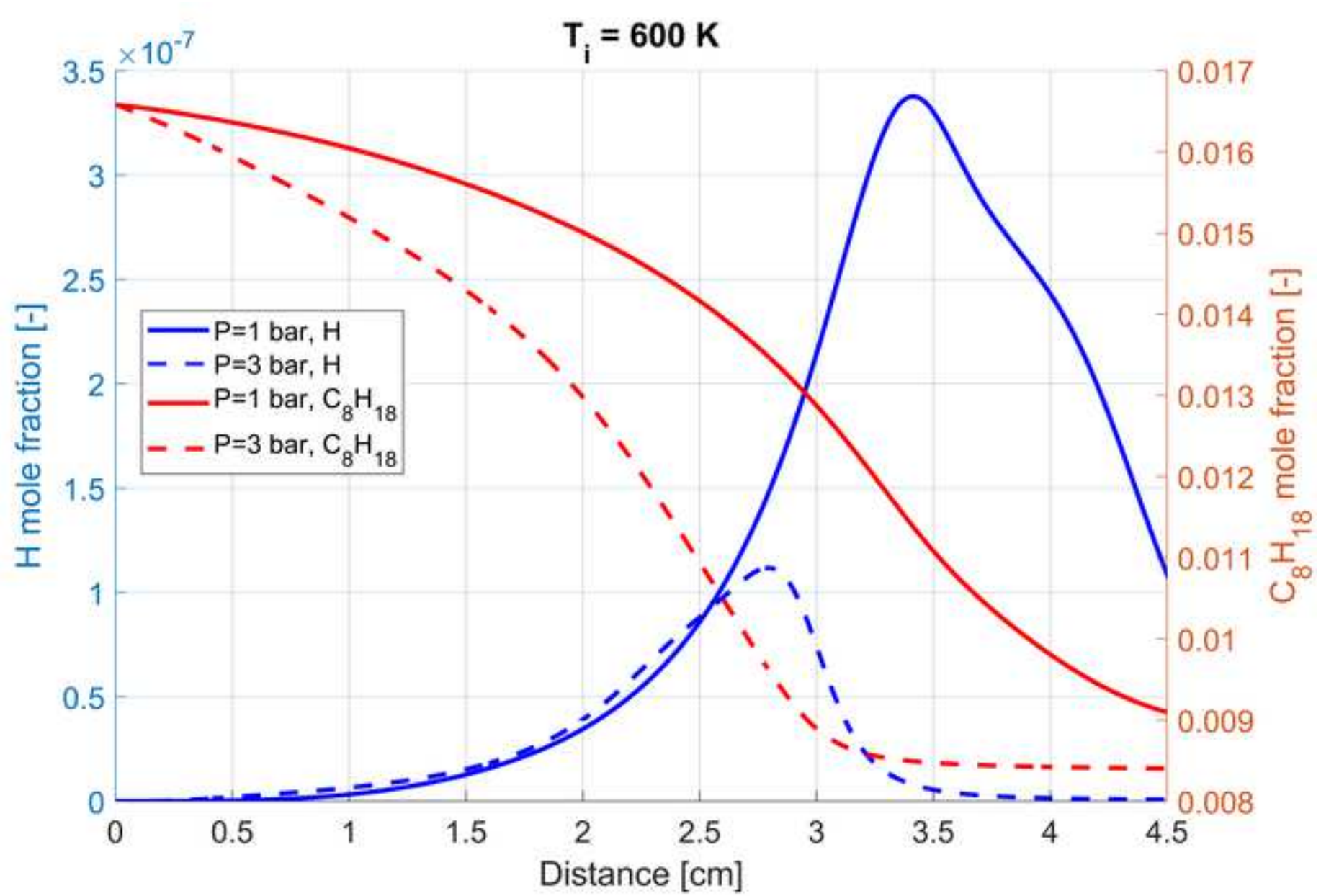

Figure 12

Click here to access/download;Figure;Fig.12.png

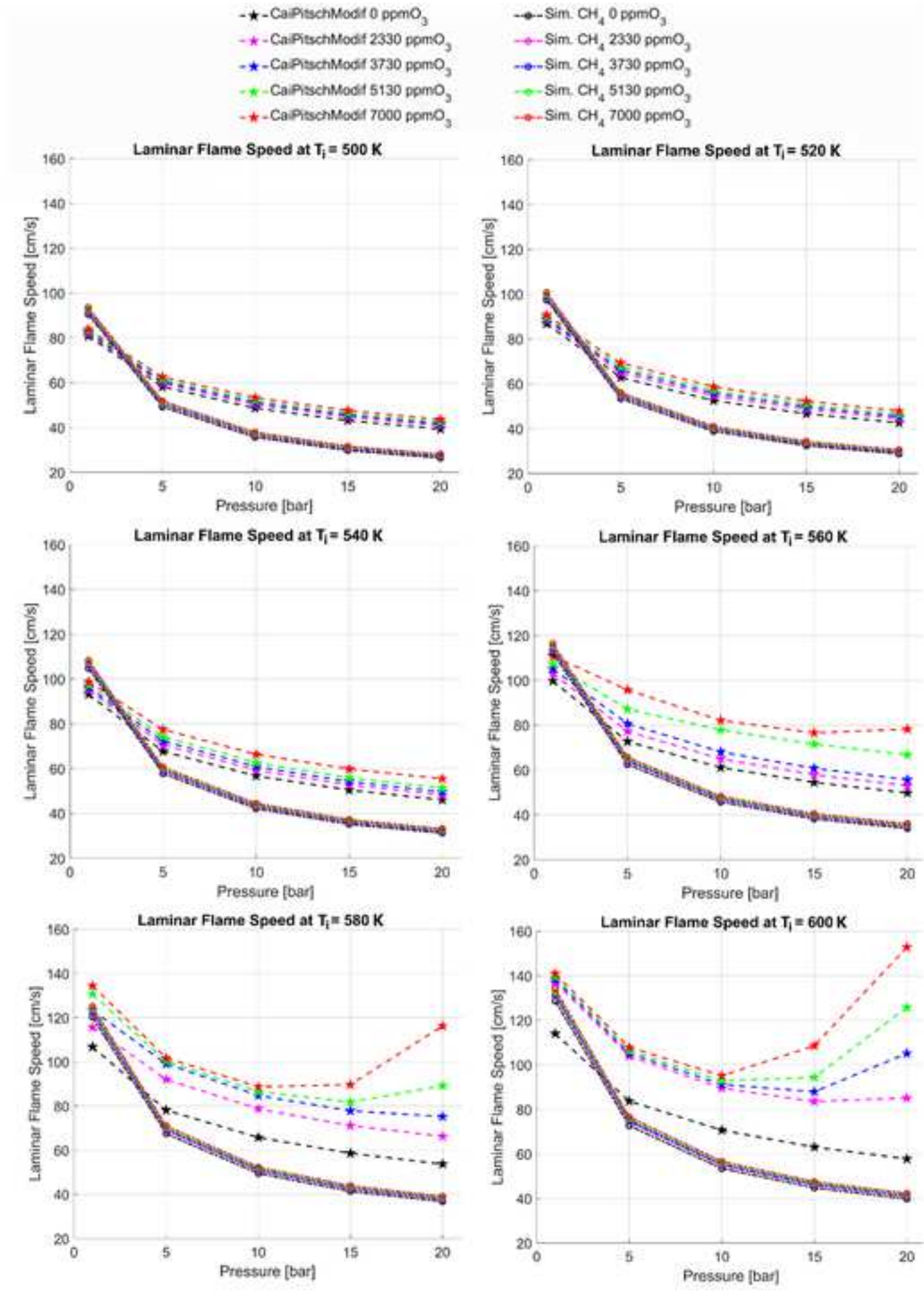

Figure 13

Click here to access/download;Figure;Fig.13.png

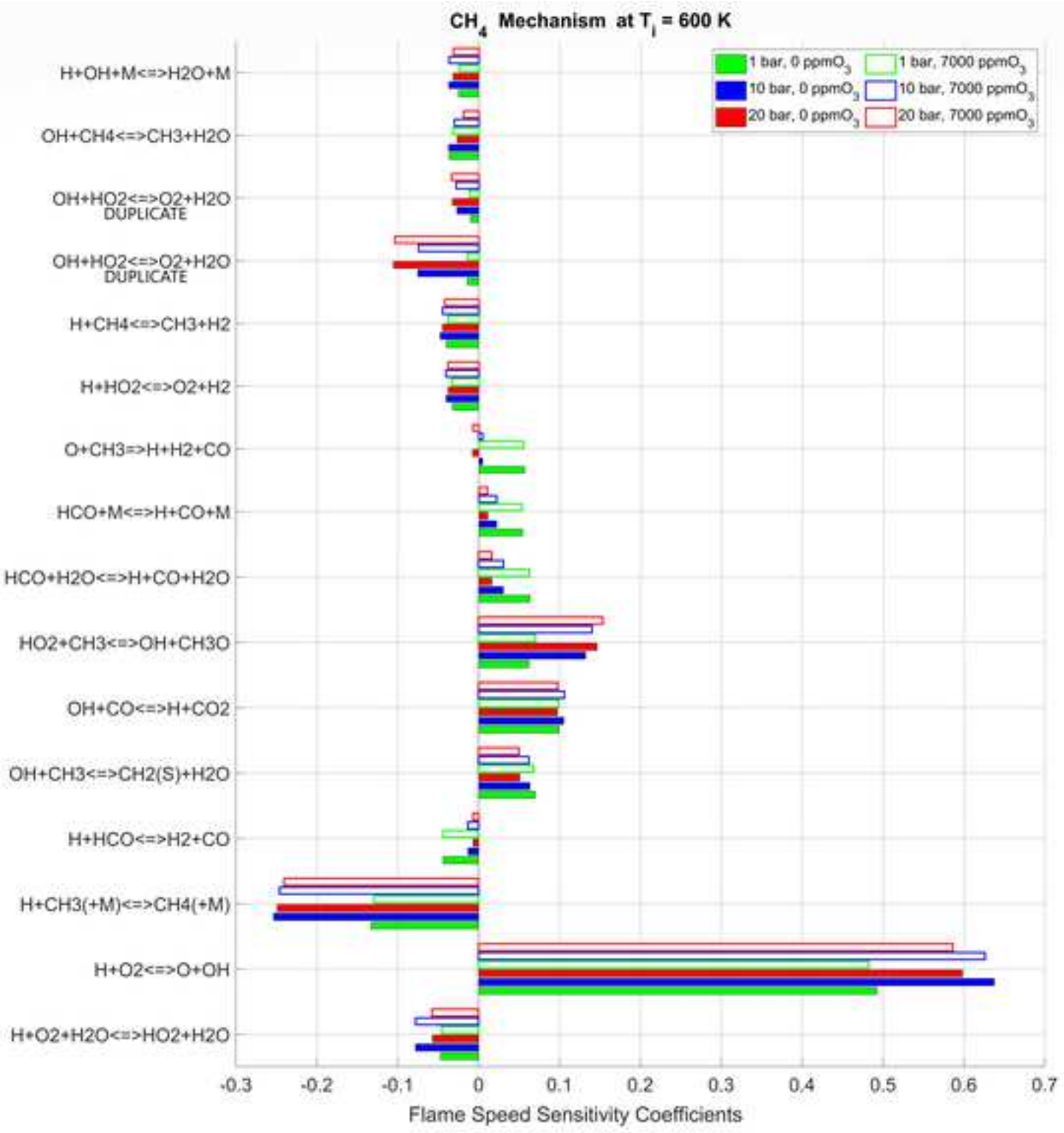

Figure 14

Click here to access/download;Figure;Fig.14.png

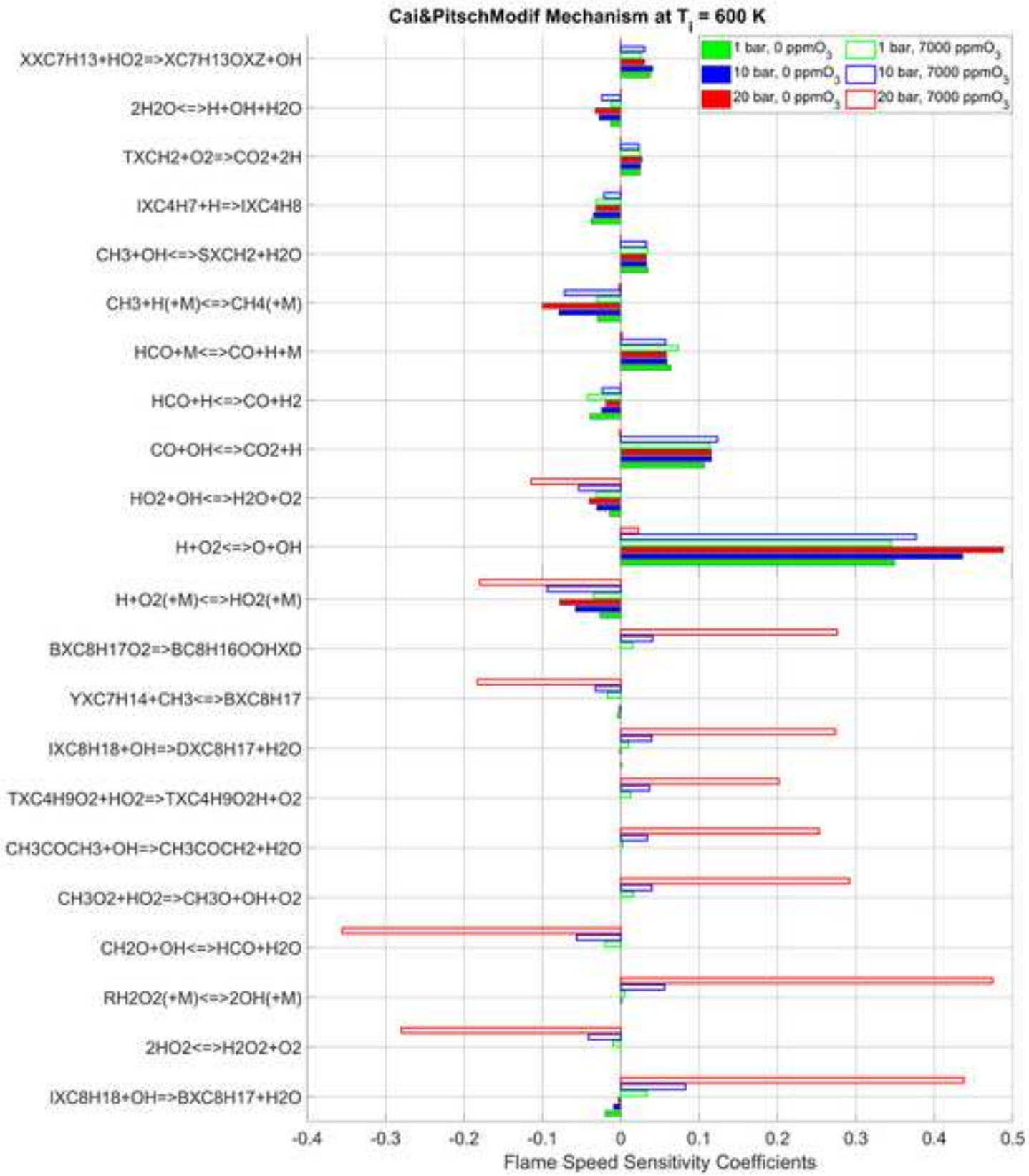

Declaration of interests

☑ The authors declare that they have no known competing financial interests or personal relationships that could have appeared to influence the work reported in this paper.

☐The authors declare the following financial interests/personal relationships which may be considered as potential competing interests: